REPRODUCTION AND EARLY LIFE OF THE HUMBOLDT SQUID

A DISSERTATION
SUBMITTED TO THE DEPARTMENT OF BIOLOGY
AND THE COMMITTEE ON GRADUATE STUDIES
OF STANFORD UNIVERSITY
IN PARTIAL FULFILLMENT OF THE REQUIREMENTS
FOR THE DEGREE OF
DOCTOR OF PHILOSOPHY

Danielle Joy Staaf
August 2010

I certify that I have read this dissertation and that, in my opinion, it is fully adequate in scope and quality as a dissertation for the degree of Doctor of Philosophy.

William Gilly, Primary Adviser

I certify that I have read this dissertation and that, in my opinion, it is fully adequate in scope and quality as a dissertation for the degree of Doctor of Philosophy.

Mark Denny

I certify that I have read this dissertation and that, in my opinion, it is fully adequate in scope and quality as a dissertation for the degree of Doctor of Philosophy.

George Somero

Approved for the Stanford University Committee on Graduate Studies.

Patricia J. Gumport, Vice Provost Graduate Education

This signature page was generated electronically upon submission of this dissertation in electronic format. An original signed hard copy of the signature page is on file in University Archives.

Abstract

Dosidicus gigas, the Humboldt squid, is endemic to the eastern Pacific, and its range has been expanding poleward in recent years. It is a voracious predator of small fish and invertebrates and prominent prey for large fish and mammals, including humans. Very little is known about Humboldt squid reproduction, development, and early life stages. To study the behavior, including dispersal capabilities, of paralarval *D. gigas*, I analyzed video of animals swimming in the laboratory, and determined that paralarvae are active swimmers that engage in hop-and-sink behavior. Control of the mantle aperture allows them to engage in slow swimming, in which water is leaked through the mantle aperture, and fast jetting, in which the mantle aperture is tightly closed and all water is expelled through the siphon—as is typical of adult jetting. A theoretical model of squid swimming was built to study the importance of aperture control during the jet cycle. This model predicts that active reduction of the aperture during jetting increases hydrodynamic efficiency, and that squid of large sizes can constrain the risk of embolism by increasing aperture size and decreasing jet frequency to values comparable to empirical measurements.

Connectivity among populations of *D. gigas* throughout the range of this species was assessed with a population genetic approach, in which *D. gigas* was compared to the co-occurring squid *Sthenoteuthis oualaniensis*. In *D. gigas*, only two weakly differentiated populations were evident, with a biogeographic break at 5-6° N. I uncovered four deeply divergent clades in *S. oualaniensis*, including one which aligns with previous descriptions in the literature of *Sthenoteuthis* sp. nov. Breaks between clades of *S. oualaniensis* also occurred at 5-6° N.

Range overlap between these two species occurs in the eastern tropical Pacific (ETP), a region both are believed to use as spawning grounds. I looked for paralarvae of *D. gigas* and *S. oualaniensis* in surface and subsurface net tows taken in the ETP from 1998 to 2006, and found that abundance was much greater in surface than subsurface tows. I then used a Generalized Linear Model approach to assess the importance of *in situ* oceanographic variables as predictors of paralarval incidence.

Sea surface temperature was found to be a strong predictor of incidence in both surface and subsurface tows, with the probability of paralarval capture rising monotonically from near zero at 15 °C to 0.9 at 30 °C.

The apparent lack of paralarvae at surface temperatures below 15 °C raises a question of whether *D. gigas* can spawn in the temperate and even subpolar waters of its expanded range. I conducted *in vitro* fertilization studies and found the optimal temperature range for successful laboratory development of *D. gigas* is 15-25° C.

Acknowledgements

Many squid were sacrificed for this research, and I only hope that the science presented here will serve to make the world a better place for their descendants, as well as my own.

For support and guidance over the last six years I am grateful to all my mentors, especially my advisor, William Gilly. I've learned so much from six hilariously unpredictable years in his lab. Mark Denny was an endless source of advice and encouragement, and conversations with George Somero continually invigorated my work. Collaborating with John Field has always been an education and a pleasure. Rob Dunbar served as a kind and thoughtful committee chair.

I truly don't know what would have become of this thesis if not for my labmates. Ashley Booth and Julie Stewart, with their boundless generosity and good humor, made the lab a place to call home. Lou Zeidberg gave freely of his time, supplies, and sarcastic wit, and Charles Hanifin dispensed tall tales and scientific wisdom. Alex Norton has been rooting for me since day one, and Carl Elliger was always happy to process "just one more sample." Zora Lebaric was my lab mother, and Judit Pungor my new little lab sister.

Hopkins Marine Station is such a character that I want to thank it as one entity, but the individuals who make it run deserve personal mention. Judy Thompson, Doreen Zelles, Chris Patton, John Lee, Freya Sommer, Joe Wible, and Jim Watanabe have all solved problems and opened doors for me. Equally worthy of gratitude is our umbilical cord to main campus, the wonderfully friendly and competent biology student services staff: Valerie Kiszka, Jennifer Mason, and Matt Pinhiero.

Eternal thanks go to all my fellow grad students, with whom I have laughed, cried, ranted and celebrated. Monthly progress meetings with Cheryl Logan kept me motivated, and spontaneous field trips with Alison Haupt always improved my mood and perspective.

For taking me to the Monterey Bay Aquarium at a malleable age, and for their subsequent tolerance of pet octopuses, I am grateful to my parents, Ben and Sue

Shulman. A special shout-out to my father for learning to scuba dive just so I would have a buddy. To my older brother Michael, whom I've always looked up to, even when we were the same height, and to his lovely wife Megan, thanks for getting your PhDs so I had to get mine.

To my in-laws--Carmen, Carl, Diana and Clint--thanks for adopting me so readily, and being so understanding of my tilting at the PhD windmill for the entire time you've known me.

That also goes for my husband. Anton, this thesis is for you.

Table of Contents

List of Tables

List of Figures

Chapter 1
Introduction

They look like aliens.

Remarkable growth rates and abundance throughout the world's oceans lend additional fascination to the early life stages of squids (Cephalopoda: Teuthoidea). Squids are broadly divided into the primarily nearshore Myopsida and the mostly oceanic Oegopsida. Myopsids are more tractable study organisms and consequently provide most of our knowledge of squid biology, including reproduction and development (Gilbert et al. 1990). Much less is known about oegopsids. *'Our almost complete ignorance of the eggs and early larval stages of oegopsid squids is the most extraordinary omission in our knowledge of cephalopod biology.'* Clarke made this assertion over 40 years ago (1966), and information concerning the spawning and early life of these oceanic cephalopods remains sparse (see reviews: Young et al. 1985a, Boletzky 2003). The omission is distressing, as oegopsid squid are tremendously important players in open ocean ecosystems, providing protein to predators from larval fish to sperm whales.

Among oegopsids, the family Ommastrephidae is of particular interest. Ommastrephid squid dominate the diets of many marine megafauna and support the world's largest cephalopod fisheries, which have been expanding as fish stocks decline (Caddy and Rodhouse 1998). Unfortunately, management of these fisheries is challenged by limited ecological knowledge, particularly regarding questions of reproduction and early development.

The largest invertebrate fishery in the world (818,000 tonnes in 2006 and 670,000 tonnes in 2007, ftp://ftp.fao.org/fi/stat/summary/a1e.pdf) targets the largest ommastrephid species, *Dosidicus gigas* Orbigny (1835), commonly known as the Humboldt or jumbo (flying) squid. For the past few decades, artisanal and commercial fisheries for this species have been growing off the Pacific coasts of Mexico and South America (Markaida et al. 2005).

Eastern Pacific waters from 30° N to 25° S comprise the historical range of *D. gigas* (Nigmatullin et al. 2001). However, this range has recently expanded poleward in both northern and southern hemispheres (Figure 1-1). *D. gigas* has been resident in the submarine canyon system associated with Monterey Bay (37° N) since the 1997-1998 El Niño (Zeidberg and Robison 2007), and individuals have been reported from as far north as south-east Alaska (59° N) (Cosgrove 2005, Wing 2006, unpublished data). Sport fishing boats in California can now rely on "squid trips" to tide them over during the slow winter months when other targeted species are not available.

The ecological role of *D. gigas* in the California Current is still not fully understood, but clearly differs from that in subtropical Mexican waters. In both regions, adult Humboldt squid are prominent prey for large fishes and marine mammals (Klimley et al. 1993, Abitia-Cardenas et al. 2002, Rosas-Aloya et al. 2002, Ruiz-Cooley et al. 2004, Barlow and Forney 2007, Vetter et al. 2008, Preti et al. 2008). However, in the Gulf of California, *D. gigas* consumes an enormous quantity of small mesopelagic fish, crustaceans and squids (Markaida and Sosa-Nishizaki 2003), whereas in the California Current of central California *D. gigas* feeds not only on these organisms but also at a higher trophic level, preying heavily on a variety of larger neritic and pelagic fish (Field et al. 2007).

Broadly speaking, *D. gigas* is a voracious predator on anything small enough to be ingestible, and that limitation is lessened by the ability to reduce large items into bite-sized portions with its sharp beak. The recent range expansion along the Pacific coast of the US and Canada has generated increasing concern that Humboldt squid may have negative impacts on the largest fishery on the US west coast, Pacific hake (*Merluccius productus*), both directly through predation (Zeidberg and Robison 2007) and indirectly through alteration of hake schooling behavior (Holmes et al. 2008, J. Field pers. comm.). *D. gigas* is also known to consume other species of commercial importance, such as the market squid *Doryteuthis opalescens,* the target of California's most valuable fishery, as well as juvenile Chinook and Coho salmon (Field et al. 2007, J. Field pers. comm.).

Although *D. gigas* has been alternating between boon and bane of the California fishing industry for almost a decade, the biological details of the invasion are still frustratingly vague. The squids' presence is seasonal, but difficult to predict. Do they migrate north to feed and south to spawn, as do hake (Bailey et al. 1982)? Or could they be spawning throughout their expanded range? Their participation in a local or regional ecosystem would vary considerably between a scenario in which they are only transiently present as feeding adults and one in which hatchlings and juveniles are also abundant as prey and small predators. As mid-size predators, adult Humboldt squid are a key forage species, transferring energy from lower trophic levels (krill, sardines, hake) to the highest (sperm whales, mako sharks). Spawning shifts the movement of energy in the other direction, providing nutrition to very small predators (larval fish, chaetognaths) in the form of numerous baby squid.

Squids spawn large numbers of eggs enclosed in gelatinous capsules or masses that are usually abandoned by the parents (parental care is known from only a single squid: Seibel et al. 2000). *D. gigas* has the largest potential fecundity measured in any cephalopod, from 5 to 32 million oocytes in a single female (Nigmatullin et al. 1999, Nigmatullin and Markaida 2002). In spawning millions of eggs, of which only a few reach maturity, a single female injects enormous numbers of planktonic predators into the ecosystem. A hatchling of one millimeter can grow to a full-size adult in one to two years (Masuda et al. 1996), a transition that must be fueled by a tremendous quantity of prey.

Little is known, however, about the diet of early life stages of *D. gigas*, and indeed of ommastrephids in general. This is partially due to morphological differences between hatchlings and adults. Hatchling squid possess the standard adult anatomy of mantle, fins, head and arms, but the relative dimensions of these structures are strikingly different from those of adults. In addition, squid often do not hatch with functional feeding tentacles; these grow as the hatchling gradually develops into a juvenile. These anatomical differences have led to use of the term "paralarvae" to refer to hatchling cephalopods, since this taxonomic group has no true larval stages (Young and Harman 1988). During the unique paralarval stage of ommastrephids, called the

rhynchoteuthion, the two tentacles grow first as a single fused proboscis (Figure 1-2), which splits later in development. Use and development of this structure are not well understood (Shea 2005).

Ommastrephid paralarvae are less than a millimeter long at hatching, only half the size of most myopsid paralarvae. Nevertheless, they are fully capable of swimming by jetting (O'Dor et al. 1985), although the extent of their swimming abilities has never been quantified. Small marine larvae have traditionally been viewed as passive drifters, but studies have been accumulating to indicate that some larvae are, instead, strong swimmers capable of exerting behavioral influence over their dispersal (Fisher et al. 2000). Even when larval swimming is not strong enough to overcome horizontal ocean currents, controlled hop-and-sink behavior could be used to move vertically into and out of these currents (Mileikovsky 1973), thus exerting some control over dispersal direction and speed.

Extensive dispersal capabilities in *D. gigas* are suggested by evidence of its range expansion alone. Swimming abilities of paralarvae can only be estimated from laboratory studies, but direct measurements of adult swimming can be taken by tagging individual squid. This work has revealed regular seasonal migrations within the Gulf of California (Markaida et al. 2005) and illustrated the potential to swim from Monterey, California, to Ensenada, Mexico in just 17.5 days (J. Stewart unpublished data).

Dispersal and migration affect population connectivity, a concept of critical importance to fishery management. Fisheries are often regulated locally, yet if geographically distant populations are connected by dispersal and migration, local choices can have impact throughout an organism's range (Caley et al. 1996).

The range and fishery for *D. gigas* overlap with that of another ommastrephid, the purpleback flying squid *Sthenoteuthis oualaniensis* Lesson (1830) (Vecchione 1999). Although not fished nearly as extensively as *D. gigas*, *S. oualaniensis* is of growing commercial interest (Zuyev et al. 2002, Xinjun et al. 2007). The ranges of these two species overlap in the eastern tropical Pacific, but *S. oualaniensis* does not extend into the temperate Pacific and is found across the tropical and subtropical

Pacific and Indian Oceans (Figure 1-1), a region not inhabited by *D. gigas*. This transoceanic range is typical of the subfamily Ommastrephinae, to which both species belong. *D. gigas* is the only ommastrephin with a latitudinally broad yet longitudinally narrow distribution. This feature may be tied to the eastern Pacific's prominent oxygen minimum zone (indicated by the white hashed line on Figure 1-1), a consequence of this region's upwelling-driven high productivity. It is also an area regularly impacted by El Niño events that periodically provide a major environmental perturbation. Both phenomena are expected to have played a role in shaping the evolutionary history of *D. gigas*.

D. gigas and *S. oualaniensis* are both believed to spawn throughout the region of their range overlap in the eastern tropical Pacific, but details remain vague. Reproduction is a challenging topic to study in the open ocean, a vast three-dimensional space with access issues. Mating and spawning themselves are such transitory activities that observations are rare indeed, but they can leave longer-lasting evidence in the form of offspring. Sampling of paralarvae is thus one way to reconstruct a picture of reproduction.

The central Gulf of California has been identified as a spawning ground of *D. gigas* based on the presence of genetically identified eggs (Staaf et al. 2008) and hatchlings (Gilly et al. 2006a). Further south, the eastern tropical Pacific's Costa Rica Dome has revealed a great abundance of rhynchoteuthion paralarvae, leading to the hypothesis that it is a major spawning area for either *D. gigas* or the co-occurring ommastrephid *Sthenoteuthis oualaniensis* Lesson (1830) (Vecchione 1999). Unfortunately, the hatchlings of these two species cannot be reliably distinguished based on morphology (Ramos-Castillejos et al. 2010).

Hatchlings of known parentage can, however, be produced in the laboratory with artificial fertilization, and their development studied in a controlled environment. Looking for paralarvae in the wild permits correlation of abundance with oceanographic variables, but artificial fertilization in the laboratory allows manipulation of some environmental variables as a means of assessing their effects on

development, thereby informing further field studies on where and when to look for spawning events in the wild.

In this thesis, I address the interrelated questions of dispersal, connectivity, reproduction, and development in the Humboldt squid *D. gigas*, touching on *S. oualaniensis* for comparative purposes where data are available. Paralarval swimming behavior and mechanics are presented in Chapter 2, alongside a theoretical model of jet propulsion that can be scaled from a 1-mm paralarvae to a 1-m adult. In Chapter 3, I move from dispersal of individuals to dispersal on an evolutionary timescale with a comparative population genetics study of both species. Having thereby determined who is breeding with whom, I seek in Chapters 4 and 5 to elucidate where reproduction occurs. Chapter 4 covers a ten-year dataset of plankton tows collected in the eastern tropical Pacific by NOAA. Paralarvae of both *D. gigas* and *S. oualaniensis* were identified from these tows, carrying interesting implications for the reproductive biology and early life history of these two closely related species. Chapter 5 provides results from artificial fertilization, indicating the range of temperatures at which *D. gigas* can successfully develop, to assess the possibility of spawning in the California Current.

When I began work on my thesis, egg masses of *D. gigas* had never been observed either in nature or in captivity. In 2006, I was on a research cruise in the Gulf of California when a group of divers discovered the first naturally deposited egg mass of *D. gigas*. Also on this cruise, and on a subsequent cruise in 2007, adult female *D. gigas* spawned egg masses in captivity on the ship. I recorded information on all the egg masses, reared samples of the eggs to hatching, and studied the development and behavior of the hatchlings. I published my results in the Journal of the Marine Biological Association of the United Kingdom with S. Camarillo-Coop, S. Haddock, A. Nyack, J. Payne, C. Salinas-Zavala, B. Seibel, L. Trueblood, C. Widmer, and W. Gilly as co-authors (Staaf et al. 2008). The paper can be found in the Appendix of this thesis, reprinted with permission from Cambridge University Press.

1.1. Figures

Figure 1-1. *Dosidicus gigas* and *Sthenoteuthis oualaniensis* species ranges illustrating the region of overlap (adapted from Roper et al. 1984). Eastern Pacific oxygen minimum zone (OMZ) is shown by a hashed white line, indicating 20 μM dissolved oxygen at 300 m depth (data from the National Oceanographic Data Center's World Ocean Atlas 2005

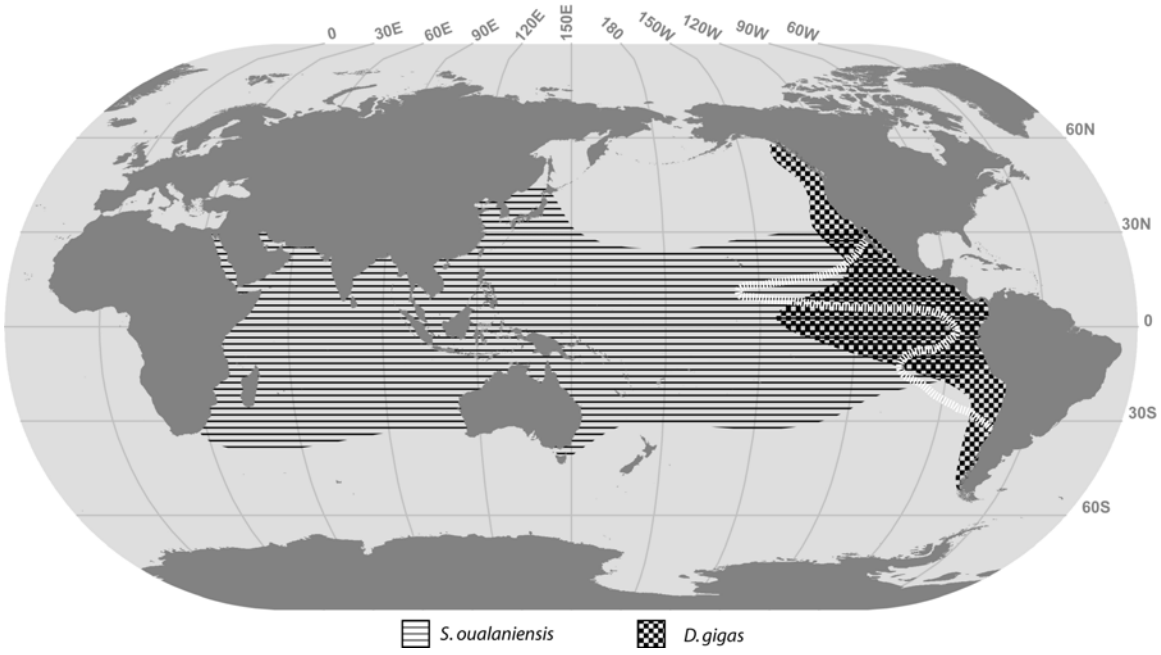

Figure 1-2. Rhynchoteuthion paralarva of *Dosidicus gigas* produced by artificial fertilization (techniques described in Chapter 5). Scale bar is approximately 1 mm.

Chapter 2
The littlest squid: Low Reynolds numbers and funnel aperture modification

2.1. Abstract

Adult oceanic squid are the biggest jet propellers in nature, but as paralarvae they are some of the smallest. In this study I explore the behavior and kinematics of locomotion in 1-mm paralarval squid, the smallest yet to be studied. They swim with hop-and-sink behavior, and can engage in fast jets by reducing the mantle aperture. I go on to explore aperture effects in a theoretical model of jet propulsion as it scales from the smallest (1 mm) to the largest (1 m) squid (and a hypothetical 10 m squid). I find that shrinking the funnel aperture during a mantle contraction increases efficiency but ultimately limits squid size by increasing stress in mantle muscles. These results indicate that the smallest squid is limited by its muscular capabilities and speed of contraction. A very large squid must contract more slowly than its maximal ability--or adjust the funnel during a powerful contraction--to maintain stress within maximal muscle tolerance.

2.2. Introduction

Marine larvae tend to propel themselves either with ciliary activity or muscular undulation of the body or fins. Jet-propelled squid paralarvae are a striking exception. Jet propulsion in paralarvae, as in adult squid, is accomplished with contractions of circular muscle fibers of the mantle. Water is expelled from the mantle through a muscular funnel, which can be angled to direct the jet and therefore the direction of swimming (Figure 2-1). Due to the energetic losses of accelerating a relatively small jet of water to high speeds, as well as the costly refilling period, during which there is no active thrust, squid jet propulsion is inherently inefficient in comparison to undulatory locomotion in fish (O'Dor and Webber 1986, 1991).

Adult squid supplement jet propulsion with undulatory activity of the fins, but the relatively tiny fins of paralarvae provide little to no thrust (Hoar et al. 1994). These

small jet propellers also face the challenges of operating at low Reynolds numbers, where viscosity dominates over inertia. In this realm, gliding is nearly impossible, especially during the refilling period.

These and other intriguing factors have stimulated studies on the mechanics of paralarval jet propulsion, but work has been limited to a few species. Escape responses, the characteristic fast jets of squid, have been analyzed in embryonic and hatchling *Doryteuthis opalescens* (Gilly et al. 1991). More recently, Bartol et al. (2009) have discovered that paralarval *Doryteuthis pealeii* make use of complex hydrodynamics in the jet wake to significantly increase propulsive efficiency.

Both of the above species, along with most other small squid selected for study of swimming kinematics, belong to the nearshore loliginid group of squids, as these are the species that are generally most feasible to maintain and breed in culture. Meanwhile, locomotion in oceanic squid remains largely a mystery. Ommastrephid hatchlings, for example, are only half the length of loliginid hatchlings, and hatch at a less developed stage. However, they are active swimmers immediately upon hatching (O'Dor et al. 1986, Staaf et al. 2008).

Ommastrephid squid are of particular interest. At less than a millimeter mantle length (ML), their hatchlings may be the smallest squid in existence, but they can exceed 1 m in ML as adults. In general, squid face a range of Reynolds numbers from ~1 as paralarvae to ~10^8 as the largest adults (Bartol et al. 2008), and a question arises as to how the same jet propulsion mechanism can be utilized at all sizes? Adults, as previously mentioned, can supplement jet propulsion with fin undulation, but during fast escape jets, critical to a squid's survival, the fins are wrapped around the body and do not contribute to propulsion (O'Dor 1988a).

Jet propulsion in squid is an inherently unsteady swimming technique, consisting of separate contraction and refilling phases. At Reynolds numbers approximately > 1000, inertia from the contraction phase can continue to carry the squid forward during the refill phase by gliding, so that it gets the advantage of burst-and-coast swimming technique. But in the low Reynolds number regime, continuous swimming is better than burst-and-coast (Weihs 1974). Indeed, burst-and-coast

swimming is nearly impossible at low Reynolds numbers. Paralarvae stop moving almost immediately after they stop jetting; accordingly, they exhibit more frequent contractions than adults (Preuss et al. 1997, Thompson and Kier 200).

Jet frequency is only one of several features that scale with body size in squid. Overall shape of the mantle also changes, such that paralarvae are shorter and wider than adults, which may aid in stabilization in the absence of fins that can perform this role (Hoar et al. 1994). Adult squid are longer and thinner, a more streamlined shape that aids in gliding.

In addition to allometric scaling of body size, the area of the funnel aperture relative to body size is larger in paralarvae than in adults. Because the muscular funnel is under the squid's control, just like the mantle, the size of the funnel aperture is of particular interest in regard to the scaling of jet propulsion with body size. Unfortunately, its contribution to locomotion is difficult to quantify and consequently has been largely ignored (O'Dor and Webber 1991).

A few empirical studies, however, hint at the importance of the funnel in controlling jet propulsion. At high speeds, an adult *Illex illecebrosus* (an ommastrephid squid) increases speed by increasing intramantle pressure, which may in turn be caused by restricting the funnel aperture through muscular contraction (Webber and O'Dor 1986). Control of the funnel aperture has also been observed or suggested in paralarvae of various species (O'Dor 1988, Bartol et al. 2001b, Anderson and DeMont 2005). However, no one has incorporated this feature into a theoretical framework of squid jet propulsion.

In this chapter, I present empirical results on the swimming behavior and mechanics of paralarval Humboldt squid, *Dosidicus gigas*, and describe a novel mechanism for restricting the flow between mantle and head, which functionally affects jetting in the same way as does active control of the funnel aperture. Finding the importance of aperture control at this size, I incorporate aperture control into a theoretical model of jet propulsion that can be scaled over three orders of magnitude from the tiniest hatchling to a large, powerful adult. Extrapolation of this model to even larger squid is also considered.

2.3. Methods

2.3.1. Animal collection

Paralarvae of *Dosidicus gigas* were obtained from a naturally deposited egg mass collected in the Guaymas Basin of the Gulf of California, Mexico on 21 June 2006 (Staaf et al. 2008). Filming of these paralarvae occurred 3-6 days after hatching.

Hatchlings were also obtained from *in vitro* fertilization, using gametes collected at Cordell Bank, California on 13 November 2007 and in Half Moon Bay, California on 11 January 2009. Artificial fertilization techniques were those described in Chapter 5. Filming of these paralarvae occurred 1-10 days after hatching.

2.3.2. Video recording

Paralarvae were observed in still water in either a rectangular 1 L acrylic aquarium or a thinner viewing chamber (72 x 47 x 7 mm). Black backgrounds were placed behind both chambers to enhance visibility of the nearly transparent paralarvae.

Standard 30-frames-per-second videos were taken with a Sony DCR-TRV70 mini-DV camcorder (Sony Electronics, San Diego, USA). Selected sequences that covered a range of swimming movements were captured with Adobe Premier 5.0 (Adobe Systems Incorporated) and exported as frames into ImageJ (NIH, http://rsb.info.nih.gov/ij) to analyze the dynamics of mantle contraction and speed of swimming.

For high-speed video, individual paralarvae were placed in 50 mm Petri dishes underneath a dissecting microscope. A high-speed Photron FASTCAM-512PCI camera (Photron, San Diego, USA) under computer control was mounted on the microscope and used to film, select and extract video clips. Video was taken at either 125 or 250 frames per second; both sampling rates provided sufficient resolution to observe details of the fastest jets.

Eleven sequences of 30fps video and sixteen sequences of high-speed video were extracted and analyzed. Sequences were chosen based on the paralarva being in focus and, in the case of the 1L aquarium, at least several body lengths away from the

walls. The narrowness of the viewing chamber prevented assessment of the paralarva's distance from the walls, and in the case of the Petri dishes, avoiding wall effects was not possible.

Ambient temperature during the video trials ranged from 18-20° C, comparable to the temperatures *D. gigas* paralarvae would likely experience in the wild and well within the range of optimum temperature for development (see Chapter 5).

2.3.3. Kinematic measurements

Both 30 fps and 125-250 fps video clips were analyzed frame by frame with ImageJ. In each frame, I measured mantle width at the widest part of the mantle, approximately one-third of the mantle length from the head, and dorsal mantle length. Mantle aperture width, the opening of the mantle just behind the head, was also measured in the high-speed video. As the squid's exact distance from the camera could not always be determined, especially in the 1 L aquarium, dorsal ML was used to normalize all measurements. ML is invariable due to the stiffening presence of the pen (Zeidberg 2004).

Minimal mantle width was calculated by dividing the narrowest normalized mantle width (MW) in each clip by the maximal normalized MW measured in that clip. Mantle aperture width was divided by the head width so that a value of 1 would indicate seal between the head and mantle, and any value larger than 1 would indicate leakage around the head through the mantle opening.

Swimming speed was measured as the number of mantle lengths traveled per second, based on frame rate. Contraction time was determined by counting the number of frames between the fully expanded mantle and the minimal mantle width, and dividing this by frame rate. Mantle contractions were counted in each clip, and the rate of mantle contraction, or jet frequency, was calculated as the number of mantle contractions per second.

2.3.4. Modeling

A model of squid jet propulsion was built in Matlab (MathWorks, Inc., Natick, MA, USA), using three primary hydrodynamic components--thrust, drag, and effective mass--to calculate a swimming squid's speed, intramantle pressure, and whole-cycle efficiency. We considered only swimming in the posterior direction (i.e., in the direction of the fins), and squid movement in this direction is considered to be in the positive direction.

For most model runs, the squid was assumed to be neutrally buoyant and therefore its density was set to seawater density. However, to model the direct vertical jetting of paralarvae, squid density was set to 1055 kg/m^3 (O'Dor 1988). Gravitational force was subtracted from thrust.

Thrust, T, the rate at which fluid momentum is expelled, was calculated from the velocity of the jet relative to the squid, u_j, the density of the expelled fluid (seawater), ρ, and the area of the aperture through which the jet is expelled, A. Note the absolute value of one of the u_j terms:

$$T = -\rho A |u_j| u_j \qquad (1)$$

Thrust always acts on the squid in the direction opposite to that of the jet (angular aiming or rotation of the funnel is not considered in this model). If u_j is in the negative direction, water and momentum are being expelled, and this propels the squid forward. If u_j is positive, water is being drawn in to the mantle cavity, which pulls the squid in the opposite direction.

Jet velocity was calculated from the aperture area and the rate of change of volume inside the squid.

$$u_j = \left(\frac{1}{A}\right)\left(\frac{dV}{dt}\right)$$

During mantle contraction, volume decreases, and dV/dt and u_j are both negative--in the opposite direction of squid movement. During refilling, these parameters are positive.

Drag, F_d, is highly dependent on Reynolds number, Re. For Re ≤ 1, drag can be calculated directly from the mantle radius, r, mantle length, L, seawater dynamic viscosity, μ, and squid speed, S, relative to the stationary water (Happel and Brenner 1965).

$$F_d = \frac{8\pi\mu S\sqrt{\left(\frac{L^2}{4} - r^2\right)}}{\left(t_0^2 + 1\right)\coth^{-1}\left(t_0\right) - t_0} \tag{2}$$

where t_0 is defined as

$$t_0 = \frac{1}{\sqrt{1 - \left(\frac{2r}{L}\right)^2}}$$

For Re > 1, F_d can be calculated from the squid's speed, the mantle radius, and the coefficient of drag, C_d.

$$F_d = -\frac{1}{2}\rho S|S|C_d\pi r^2 \tag{3}$$

For Re > 1000, C_d is dependent only on the squid's mantle radius and length, and an empirically calculated constant, $C_f = 0.004$ (Hoerner 1965):

$$C_d = 0.44\frac{2r}{L} + 2C_f\frac{L}{r} + 4C_f\sqrt{\frac{2r}{L}} \tag{4}$$

For intermediate Re, between 1 and 1000, drag is not well described by simple theory. For this range, we calculated C_d by interpolating with a cubic spline between Re = 1 (back-calculating C_d from F_d from equation 2) and Re = 1000 (from equation 4), and used this value in equation 3.

Effective mass, M_{eff}, is the sum of the squid's mass and the added mass of water around the squid as the squid is accelerated. Following Lamb (1932) we calculated these terms as:

$$M_{eff} = \rho V + \rho V\left(\frac{a}{2-a}\right) \tag{5}$$

where a is the aspect ratio of the prolate ellispoid:

$$a = \left(\frac{1-e^2}{e^3}\right)\ln\left(\frac{1+e}{1-e} - e\right)$$

and e is the eccentricity, calculated from mantle radius and length:

$$e = \sqrt{1-\left(\frac{2\mathrm{r}}{L}\right)^2}$$

Acceleration of the squid was calculated from thrust, drag, and effective mass, and integrated numerically over time with a fourth-order Runge-Kutta routine (Jameson et al. 1981) to give squid velocity.

$$\frac{dS}{dt} = \frac{\left(T + F_d\right)}{M_{eff}} \tag{6}$$

We considered intramantle pressure to come from two sources: directly from the squeeze of contracting mantle muscle and indirectly from viscous effects as water

is forced through the funnel aperture. Pressure from thrust, P_T, can be calculated from the momentum and the Bernoulli equations, as in Anderson and DeMont (2000), to be a function of thrust and aperture area:

$$P_T = \frac{T}{2\mathrm{A}}$$

Pressure from viscous effects, P_μ, is dependent on the dynamic viscosity of seawater, μ, the aperture radius r_a, and the rate of flow. We calculate rate of flow as volume change inside the mantle, dV/dt. The following relationship is given by Happel and Brenner (1965):

$$P_\mu = -\frac{\kappa\mu\dfrac{dV}{dt}}{r_a^3}$$

where κ is a constant determined by the Re of flow through the aperture. Happel and Brenner (1965) provide a theoretical value of 3 for Re less than approximately 3, which we used our calculations.

The two pressure terms summed give total intramantle pressure:

$$P = \frac{T}{2\mathrm{A}} - \frac{\kappa\mu\dfrac{dV}{dt}}{r_a^3} \qquad (7)$$

Pressure can then be used to calculate stress in the mantle muscle, as the force that pressurizes water in the mantle cavity must be counteracted by an equal force stressing in the mantle itself. Pressure acts over the cross-sectional area of the mantle cavity, which is $2rL$ if we assume the mantle is a simple cylinder. Stress acts over the cross-sectional area of the mantle muscle, which is $2wL$, where w is the thickness of the mantle. We can therefore set:

$$P(2rL) = \sigma(2wL)$$

which can be simplified to produce an equation for stress:

$$\sigma = \frac{Pr}{w} \tag{8}$$

Our final calculation concerns efficiency. Considerable ink has been expended over the question of how to measure this. We follow Anderson and Grosenbaugh (2005) in considering hydrodynamic efficiency, η, to be useful power divided by total power, where total power is useful power plus wasted power. Useful power is jet thrust multiplied by squid speed, and wasted power comes from the kinetic energy left in the wake by the jet that did not impart thrust to the squid.

Kinetic energy is determined from mass and velocity. The mass of fluid in the jet over a given time is determined by the absolute value of jet velocity, aperture area, and fluid density:

$$\rho A|u_j|$$

The velocity of this mass relative to still water is given by the difference between jet velocity and squid velocity, so wasted power due to kinetic energy is

$$\frac{1}{2}\rho A|u_j|(u_j + S)^2$$

We thus arrive at an equation for efficiency:

$$\eta = \frac{T|S|}{|TS| + \frac{1}{2}\rho A|u_j|(u_j + S)^2} \tag{9}$$

The absolute values are assigned such that efficiency is positive when the squid is moving forward, and negative if it is being forced backward (e.g., during refilling). Note that when $u_j = -S$, no momentum is left in the wake, and jetting is 100% efficient. In our model, η was summed over ten jet cycles to cover the change in efficiency as the squid gets up to speed from a starting velocity of zero.

Mantle contraction and refilling were effected by linearly varying r, the mantle radius, from a maximal value at the beginning of contraction to a minimal value at the beginning of refill. The choice of maximal and minimal values is explained in the next section.

To study the importance of aperture control, aperture radius (and therefore area) was either kept constant throughout the jetting cycle, or followed the mantle radius in varying linearly from its maximum at the beginning of contraction to its minimum at the beginning of expansion.

Figure 2-2 illustrates the model output for 10 jet cycles of a 1 mm ML squid with constant aperture radius.

2.3.5. *Parameterization*

To evaluate the scaling of jet population with size, we provided the model with mantle length only. This simplified the analysis, allowing us to focus on size by maintaining consistent relationships between morphological parameters. We used the regression equations of Stevenson (1996) for mantle radius, mantle thickness, and funnel radius, all of which vary allometrically with mantle length. Jet frequency as a function of mantle length was calculated by O'Dor (cited in Stevenson 1996). The regression equations are plotted on a log-log scale in Figure 2-3, along with measurements gleaned from the literature, taken by the author, and provided by W. Gilly (unpublished data).

The degree to which mantle diameter decreases during contraction is itself somewhat size-dependent, reportedly ranging from 40% (hatchlings) to 20% (adults) in *Doryteuthis opalescens* (Gilly et al. 1991) and 40% (hatchlings) to 30% (adults) in

Sepioteuthis lessoniana (Thompson and Kier 2001). However, we chose to set the decrease in mantle width to a constant value for all squid sizes to simplify our model. We used the most commonly reported value across a range of species, which is a 30% reduction from fully expanded to fully contracted (Packard 1969, Gosline and Shadwick 1983, Gosline and DeMont 1985, Preuss et al. 1997).

We did not attempt to model the distinctive characteristics of escape jets, which include hyperinflation of the mantle (e.g. Thompson and Kier 2001) and retraction of the head into the mantle (e.g. Packard 1969). These features increase the total volume of water expelled from the mantle, and escape jets are therefore likely to present both increased velocity and intramantle pressure when compared to our modeling of regular jets.

Mantle thickness as calculated from the regression in Figure 2-3D was adjusted slightly for use in our model. For equation (8), we are only interested in one component of the mantle: the circular muscle, which acts to squeeze the water inside the mantle. Circular muscle makes up the majority of the mantle, about 91% of total volume. The remainder of the mantle is taken up primarily by radial muscle, with collagen fibers forming as little as 0.2% of the total mantle by weight (Gosline and Shadwick 1983, Gosline and DeMont 1985). We therefore adjusted the allometric mantle thickness by a factor of 0.91.

Each jetting cycle consists of a period of contraction, during which the mantle radius decreases, and a period of refilling, during which the mantle radius increases. Thompson and Kier (2001) present data showing the time spent in contraction is roughly equal to that spent in refilling, but more often contraction is seen to be briefer than refill. Bartol et al. (2009) report a contraction period that lasts 23% of the total jet period. Anderson and Grosenbaugh (2005) report the jet period taking 31% and the refilling period 46% of each cycle, with the remaining 23% spent in opening and closing the funnel, and not categorized as either jetting or refilling. O'Dor (1988b) reports a total cycle length of 1.5 s, with refilling beginning after 0.6 s, which would give a 60:40 refill:contract ratio. The ratio is likely dependent on both size and species of squid, as larger squid and those species which spend more time gliding extend the

time between contractions (refilling period). We chose to use the 60:40 ratio in our model, to incorporate a marginally, not drastically, shorter contraction period, as indicated by a review of the literature.

The final parameter of concern is the size of the aperture through which the jet flows. In our model, this "aperture size" is the whole area through which water can flow at any given time. During the refilling phase of the jet cycle, it includes both funnel and mantle openings. We used a constant aperture area during refilling of twice the funnel area (Anderson and Grosenbaugh 2005), which was in turn calculated from funnel radius based on the regression in Figure 2-3C.

During the contraction phase of the cycle, the mantle opening is closed by one-way valves on either side of the head, and water flows only through the funnel. In the simplest version of the model, funnel area is held constant throughout contraction at the size determined by the regression in Figure 2-3C. This is considered the "maximal funnel area." In order to investigate the effect of dynamic control of the funnel during jetting, we added a layer of complexity whereby the funnel radius is set to the maximal value at the beginning of a contraction and reduces over the course of the contraction to 50% of the maximal value. This is referred to as "variable funnel area." For comparison purposes, we also ran with the model with the funnel radius set to a constant 50% of the maximal value, referred to as "minimal funnel area." The value of 50% was chosen arbitrarily to represent a significant, but not total, closure of the funnel, as values for this parameter are not available from the literature.

2.4. Results

2.4.1. Behavior

Paralarvae demonstrated a variety of swimming behaviors, categorized as maintenance jetting, slow jetting, and fast single jets. Maintenance jetting consisted of individual jets that just counteracted the rate of sinking (-0.46 ± 0.02 cm/s, N = 3), thereby maintaining the paralarva's vertical position in the water column. During this behavior, the distance the animal moved up during each jetting period was roughly equal to the distance it moved down during each refilling period. Jetting frequency

during maintenance jetting was 2.13 ± 0.44 Hz (N = 3). If not actively swimming, paralarvae always sank.

Slow jetting consisted of prolonged periods of repeated jetting, usually vertical, during which velocities exceeded the passive sinking rate and reached maximal measured speeds of 0.51 cm/s (approximately 5 ML/s). Periods of slow jetting thus moved the animal upward, often to the water surface. These periods were usually followed by periods of sinking that lasted much longer than a single refilling period and during which no active swimming was observed. This behavior resembled the hop-and-sink behavior described for other negatively buoyant zooplankton (Haury and Weihs 1976).

Fast single jets were individual jets that launched the animal out of the field of view, and appeared to be similar to the "escape jets" of adult squid. The maximal speed measured in one of these jets was 2.34 cm/s (approximately 23 ML/s).

The dominant swimming direction was vertical, although paralarvae showed the ability to change direction extremely rapidly. Occasionally, they would engage in circular jetting, a period of several fast jets which departed notably from the standard jet-and-sink behavior. The direction of swimming during circular jets was always fins-first, and these episodes bore no resemblance to the circling behavior used by paralarval *Doryteuthis opalescens* to orient to their prey (Chen et al. 1996). Both circular jetting and fast single jets could represent escape behavior, although they often occurred without any startling stimulus that was obvious to the observer.

Paralarvae also demonstrated a distinctive pulsing behavior with high contraction frequency (4.5 ± 0.84 Hz, N = 3); the maximal frequency measured was 5.4 Hz. During these episodes they neither sank nor moved an appreciable distance, and displayed almost no oscillatory up/down motion.

2.4.2. Kinematics

Representative traces are shown in Figure 2-4 from 30 fps (A) and high-speed (B) video. Normalized mantle width is shown in both panels, and normalized mantle aperture is shown for the high-speed trace. Closure of the mantle aperture can be seen

to precede contraction of the mantle itself, presumably forcing water to be expelled through the funnel alone, rather than "leaked" through the mantle opening. Selected video frames from a single contraction are shown in Figure 2-4C to illustrate closing of the mantle aperture around the head.

When all 30 fps jets were analyzed together, including both slow jetting and fast single jets, the squid's velocity showed a slight relationship (Figure 2-5A, R^2 = 0.23) with minimal mantle width, which ranged from fully expanded (1.0) to fully contracted (0.4). Faster jets, as one might expect, occur when the mantle contracts to a smaller diameter, thereby expelling more water. However, it also clear that fast single jets can occur over the entire range of mantle contraction.

Although I attempted to quantify the speed of individual contractions by counting the number of frames from expanded to contracted, standard video sampling of 30 fps was too slow, and most images were extremely blurry. Therefore, I chose to consider rate of mantle contraction by counting the number of contractions over a longer period of time. Of course it is not possible to assess this statistic for individual jets, so data in Figure 2-5B were derived only from slow jetting sequences. The R^2 value of 0.45 indicates a relationship between slow jetting speed and frequency, consistent with the idea that hatchlings increase the rate of mantle contraction in order to move faster.

Measurements of fast single jets were made with high-speed video sampling. Figure 2-6 shows that contraction time, minimal mantle width, and mantle aperture width are all negatively correlated with squid velocity.

For mantle aperture width, two clusters of data appear (Figure 2-6C). It seems like a binary rather than a continuous variable--either the paralarvae let water leak out around their heads, behaving more like a jellyfish than a squid, or they clamp down their mantle and expel water only through the funnel. "Sealed" jets are clearly the faster ones.

The statistics package R (R Development Core Team, 2005) was used to create a generalized linear model (GLM) for squid velocity with contraction time, minimal mantle width, and mantle aperture width. An ANOVA run on this model showed that

only aperture width was a significant predictor of velocity ($p < .001$). Further statistical analysis confirmed that the most robust model of squid velocity uses a single binary "leaky or sealed" variable. A model including contraction time, minimal mantle width, and aperture width as a continuous variable had an Akaike Information Criterion (AIC) of 102, while a model including time, minimal mantle width, and aperture width as a binary variable had an AIC of 95, and a model with only binary aperture width had an AIC of 92 (lower AICs indicate a better fit).

2.4.3. Model

Specific model simulations were run for 1-mm paralarvae to compare with empirical results. A "leaky" paralarva, with the aperture area constant throughout the jetting cycle, reaches maximal speeds of about 0.4 cm/s, while an aperture-controlling paralarva can reach up to 2 cm/s. With the effects of gravity included, and arbitrary control of jetting frequency instead of using the regression, I found that an aperture-controlling paralarva contracting at about 3 Hz exactly holds its position in the water, neither rising nor sinking. This value is close to, but higher than, that measured during maintenance jetting (2.13 ± 0.44 Hz, $N = 3$).

Iterating the model simulation over all sizes of squid, and extracting the maximal velocity, efficiency, and maximal stress for each size resulted in the plots in Figure 2-7. Curves for constant maximal and constant minimal funnel area during contraction, as well as variable funnel area, are plotted. A constant large aperture results in slow swimming and low stress in the mantle, while a constant small aperture results in fast swimming and high stress in the mantle. A variable aperture strikes a balance in speed and stress, while sharply increasing efficiency.

However, Figure 2-7C raises an interesting question. Muscle cannot generate endlessly increasing stress. The maximal isometric tension of striated muscle is 3-5 x 10^5 N/m^2 (Alexander and Goldspink 1977), and isotonic contraction, when the muscle is actually shortening, as during mantle contraction, must be less than isometric. In squid, Gosline and Shadwick (1983) have estimated that the muscle tension needed for 100% utilization efficiency of circular mantle muscle is $2x10^5$ N/m^2, and O'Dor

(1988) suggests that $2.4x10^5$ N/m^2 is the most reasonable estimate of maximal stress in these muscles.

If we draw a line across Figure 2-7C at $2.5x10^5$ N/m^2, it seems that, during contraction with a variable aperture area, small squid would be underutilizing their muscle, while large squid appear to be exceeding the stress their muscle can withstand. In order to further investigate this question, we altered the model to maintain stress at a constant $2.5x10^5$ N/m^2, and back-calculated the necessary parameter adjustments to keep it that way. We investigated two possible parameter adjustments separately: jet frequency and aperture size.

Figures 2.8 and 2.9 compare the previously presented model output, in which funnel area and jet frequency respectively vary according to the regression equations in Figure 2-3, to a "constant-stress" model in which funnel radius (Figure 2-8) or jet frequency (Figure 2-9) are controlled to produce a stress of $2.5x10^5$ N/m^2. The first panel (A) in each figure indicates the funnel radius or jet frequency that is necessary to produce this stress, while panels B and C show the impact on maximal velocity and efficiency.

From these figures, it can be seen that a 1-mm squid must either reduce its funnel radius to 0.015 mm (about 20% of the maximal radius predicted by regression) or increase its jet frequency to more than 100 Hz to obtain a stress of $2.5x10^5$ N/m^2. A 1 m squid must either increase its funnel radius to 2 cm (about twice the maximal radius predicted by regression) or decrease its jet frequency to once every 8 s for the same result.

2.5. Discussion

2.5.1. Behavior of Humboldt squid paralarvae

The locomotory behavioral repertoire discussed in this study is a subset of the behaviors described in adult squid. Hunt et al. (2000) described four distinct speeds of adult *Doryteuthis opalescens* swimming: Hovering, Gliding, Slow Swimming, and Jetting. The fins and the jet are used in the first three, while only the jet is used in the fourth. *D. gigas* paralarvae exhibit two of these four: Hovering (maintenance jetting)

and Jetting (including slow and fast jetting). In paralarvae, the fins were not well controlled and appeared to have no real effect on movement. Both *D. opalescens* adults (Hunt et al. 2000) and *D. gigas* paralarvae were able to reverse course by flipping the funnel 180 degrees.

Pulsing was an interesting additional behavior. During these episodes, the minimal relative mantle width was 0.6-0.7, roughly comparable to what was seen in jetting (Figure 2-5). Since the paralarvae did not propel themselves either forward or backward, the water expelled during these contractions must have been largely leaked through the mantle aperture, rather than expelled solely through the funnel. Pulsing may be similar to predatory behavior described by Preuss et al. (1997) for hatchling *Doryteuthis opalescens*, in which attacks on *Artemia* were sometimes prefaced by frequent mantle contractions (exceeding 5 Hz).

It has been suggested that the swimming abilities of paralarvae could be used to effect diel vertical migrations, allowing the paralarvae to sink to deeper depths during the day to avoid visual predators (Staaf et al. 2008). These authors calculated that a paralarval migration of 15 m would take less than 1 hour at the observed swimming speed of 0.5 cm/s, and as the hatchling squid grew, the extent of this diel migration could increase to that of adults

Vertical swimming could also be used to move in and out of currents as the squid grows, in order to move from prime paralarva habitat into prime juvenile habitat. Alternatively, vertical movements on the order of tens of meters would be sufficient to allow the squid to move across the thermocline or to position itself at a depth corresponding to a subsurface chlorophyll maximum. Such an area might also be a good feeding area, whether the paralarvae eat dissolved or particulate organic matter, phytoplankton or small zooplankton.

Regular vertical excursions followed by sinking could result in significant energetic savings, as has been demonstrated for other negatively buoyant zooplankton (Haury and Weihs 1976). Hop-and-sink behavior has been reported in other cephalopod paralarvae (Boletzky 1974, O'Dor 1988a, Zeidberg 2004) and may well be an adaptation to save energy.

Two factors are needed to calculate whether hop-and-sink behavior saves energy in any particular situation: the ratio of swimming speed to sinking speed, and α, the ratio of frontal areas presented in the two modes. The swimming:sinking speed ratio reported for paralarval ommastrephids is in the range of 1 (Staaf et al. 2008) to 2 (O'Dor et al. 1986). Paralarvae in laboratory observations sink in the direction of the arms, and the arms (sinking) are less streamlined than the mantle tip (swimming upward), so the value of α must be greater than 1. Furthermore, the mantle narrows during swimming. Packard (1969) reports that the mantle width of fresh hatchlings (*Loligo vulgaris*) reduced from 2.1 to 1.3 mm during a jet, which would correspond to an α of 2.6. According to the predictions of Haury and Weihs (1976, Figure 2-2), a speed ratio of 1-2 and an α of 2-3, such as calculated here for *D. gigas* paralarvae, are within the parameter space for energy savings.

2.5.2. Kinematics of Humboldt squid paralarvae

In studies on the swimming kinematics of *Lolliguncula brevis*, Bartol et al. (2001) found that the smallest size class, 1-2.9 cm ML, increases jet frequency and speed without changing mantle contraction amplitude, while larger squid do the opposite: to increase speed, they alter mantle contraction to expel greater volumes of water in a given time. Our very small *D. gigas* paralarvae alter their slow jetting speed primarily by varying jet frequency, like small *L. brevis*, although very small *D. gigas* do appear to contract to a slightly smaller minimal width for faster jets, unlike small *L. brevis* (Figure 2-5).

In contrast to the frequency-dependent control of slow jetting, I found that faster jets correlated most closely with smaller mantle aperture (Figure 2-6), and fast jetting thus appears to rely on closing the mantle aperture to increase thrust (Figure 2-6). Because of the difficulty of observing the funnel in video of very small squid, we do not know whether they are able to control the funnel aperture itself, but they can clearly alter the total aperture through which water flows by sealing the anterior edge of the mantle around the head (Figure 2-4). This study is the first to report such behavior.

Figure 2-6, and the linear regressions therein, suggest that increasing mantle contraction time and degree of contraction may assist with increasing jet velocity, but they appear to be of secondary importance. Such correlations make intuitive sense. If contraction time decreases, water is expelled in less time, and if the minimal mantle width decreases, a greater volume of water is expelled in a given time. In either case, dV/dt, u_j, and thrust would all be increased. These findings seemingly contradict the results of Bartol et al. (2009), who found that contraction time *increased* with increasing velocity. These authors suggest that an increased contraction time would expel a greater volume of water. However, this would only be the case if an increase in contraction time were accompanied by a decrease in minimal mantle width, which was not measured by these authors. More data, at a greater range of speeds, are needed to resolve this discrepancy. It is possible that taxonomic differences in velocity modulation exist between the paralarvae of different species.

One might legitimately query whether there is any advantage to leaking water through the mantle opening, rather than concentrating all expelled water through the funnel. O'Dor and Webber (1991) point out that, "*Once the mantle becomes an integral part of the jet engine it is impossible to breathe without moving nearly half of the body mass.*" In the case of *D. gigas* paralarvae, the wide aperture between the head and mantle to some extent uncouples the jet engine from respiration needs, and the low-pressure flow through the leaky head-mantle aperture is more like that in a jellyfish than in an adult squid. Sealing the mantle around the head leads to high-pressure "squid-like" propulsion.

2.5.3. Ontogeny of jet propulsion

Hydrodynamic efficiency of jetting is a matter of considerable biological relevance to squid. More efficient swimming requires less energy, allowing the squid to allocate more resources to growth or reproduction. The high metabolic rates typical of squid are generally attributed to the relative inefficiency of jet propulsion (O'Dor and Webber 1986), which adult squid mitigate somewhat with the use of fins.

Paralarval squid do not have this luxury, and furthermore, jet propulsion itself is less efficient for smaller squid.

Calculated efficiency at very small sizes is not much above 10%, increasing as the squid grows until it levels off at around 1 cm at 40% (Figure 2-7). This is precisely the size at which Yang et al. (1986) observed juvenile *Doryteuthis opalescens* develop the ability to hold a swimming position and begin schooling behavior. A certain hydrodynamic efficiency may be a necessary prerequisite for the more complex swimming behaviors required to maintain a school.

We calculate that small squid would have to jet with a biologically unrealistic frequency (100 Hz) to reach maximal muscle stress (Figure 2-9), but the frequency predicted for a large squid to limit maximal stress (once every 8 s) is quite relevant. Tag data of 75 cm *D. gigas* suggests active jetting once every 8-9 seconds (L. Zeidberg pers. comm.), a frequency which places these squid just at the 2.5×10^5 N/m^2 limit. A further "safety valve" may be present in the funnel aperture, as the few measured funnel radii of large squid are larger than regression predictions (Figure 2-3, see also Stevenson 1996). In fact, the funnel radius of a 78-cm ML adult D. gigas was measured at 3 cm, comfortably above the 2 cm needed by the model to limit stress at 2.5×10^5 N/m^2 (Figure 2-8).

Maximal jet speed increases with squid size when measured in absolute terms (m/s, Figure 2-7A), but when measured relative to body size (ML/s, Figure 2-10) we see a different story. By the time a squid reaches 3 mm in length, the model predicts that both maximal speed and average speed begin to *decrease* relative to body size. Slower relative speeds in larger animals have also been seen in jet-propelled jellyfish, and attributed to a size-dependent decrease in jet frequency (McHenry and Jed 2003). Jet frequency also decreases with size in squid (Figure 2-3D), and our results on maximal mantle stress suggest that large squid may jet at frequencies even lower than those predicted by the regression (Figure 2-9A). Thus, the speeds attained by larger squid are likely limited by the capabilities of mantle muscle, although altering the funnel aperture can change the size at which this becomes a concern (2-20 cm, Figure 2-7C).

2.6. Acknowledgements

Great thanks are due to Mark Denny, who worked patiently with me on all the math and modeling. Lou Zeidberg and Kevin Miklasz both shared their knowledge of and enthusiasm for locomotion in numerous brainstorming sessions. Ian Bartol kindly provided advice and feedback.

2.7. Figures

Figure 2-1. Diagram of jet propulsion in squid indicating refilling and contraction phases of the jet cycle. During refilling, water enters through openings around the head. During contraction, these openings are closed and water is expelled through the funnel.

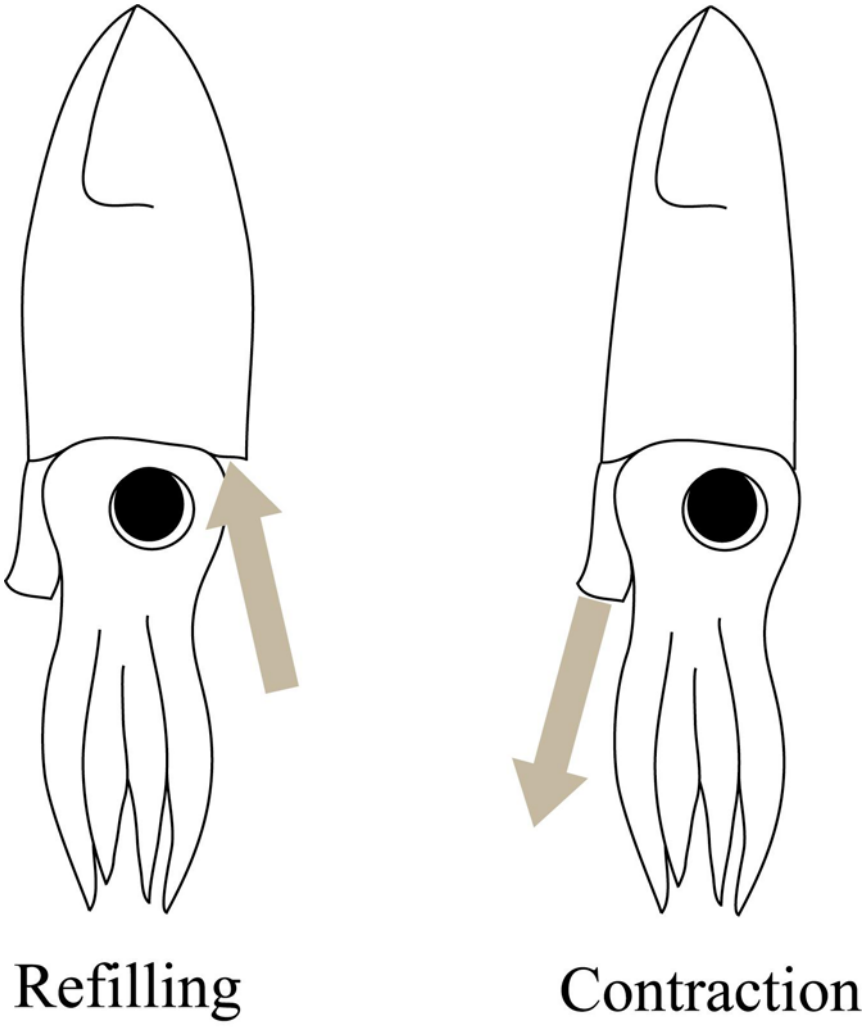

Figure 2-2. Theoretical jet propulsion by a 1-mm ML squid swimming for 10 cycles of contraction and refilling. A) Squid velocity, B) propulsive efficiency, and C) stress in the mantle muscle.

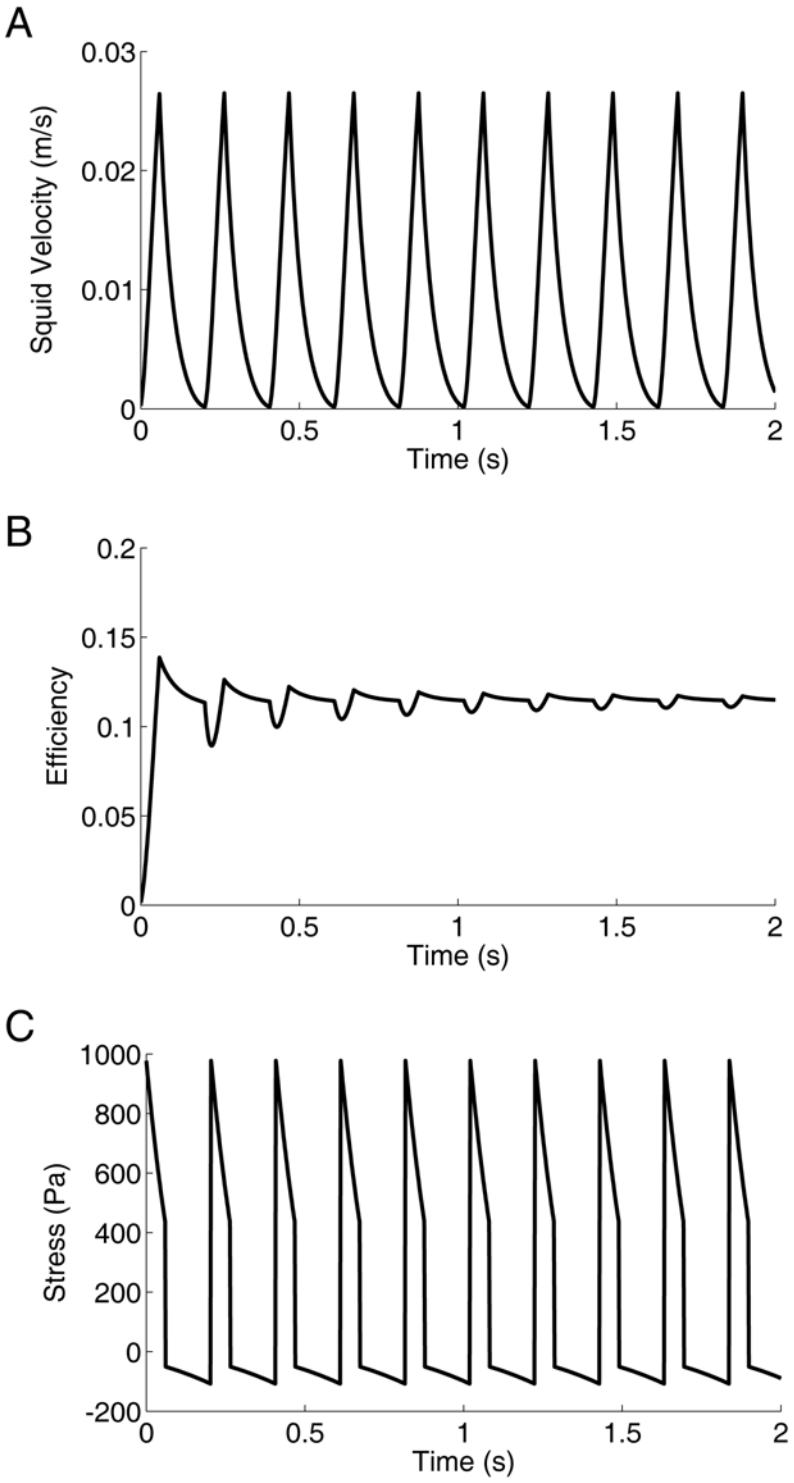

Figure 2-3. Allometric growth of squid. Regressions between A) mantle width, B) mantle thickness, C) funnel radius and D) jetting frequency and mantle length calculated by Stevenson (1996) based on empirical values (not shown here). Black circles represent additional data points gleaned from the literature (Gosline and Shadwick 1983, O'Dor 1988, Preuss et al. 1997, Bartol et al 2001, Anderson and Grosenbaugh 2005, Bartol et al 2009, unpublished data).

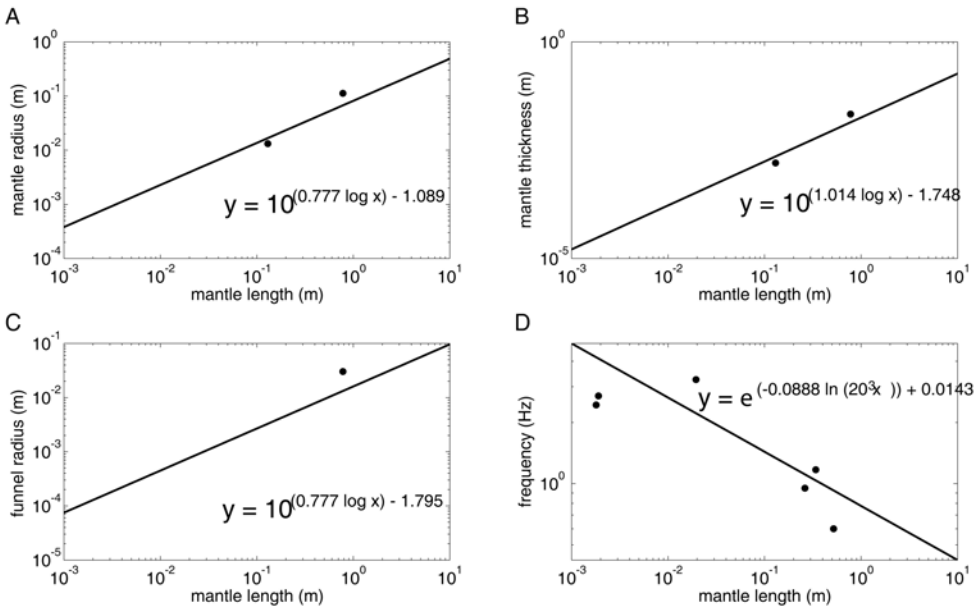

Figure 2-4. Representative traces of A) normalized mantle width from 30 fps and B) mantle width and mantle aperture from high-speed video. Closure of the mantle aperture can be seen in panel B and is illustrated with video frames in panel C.

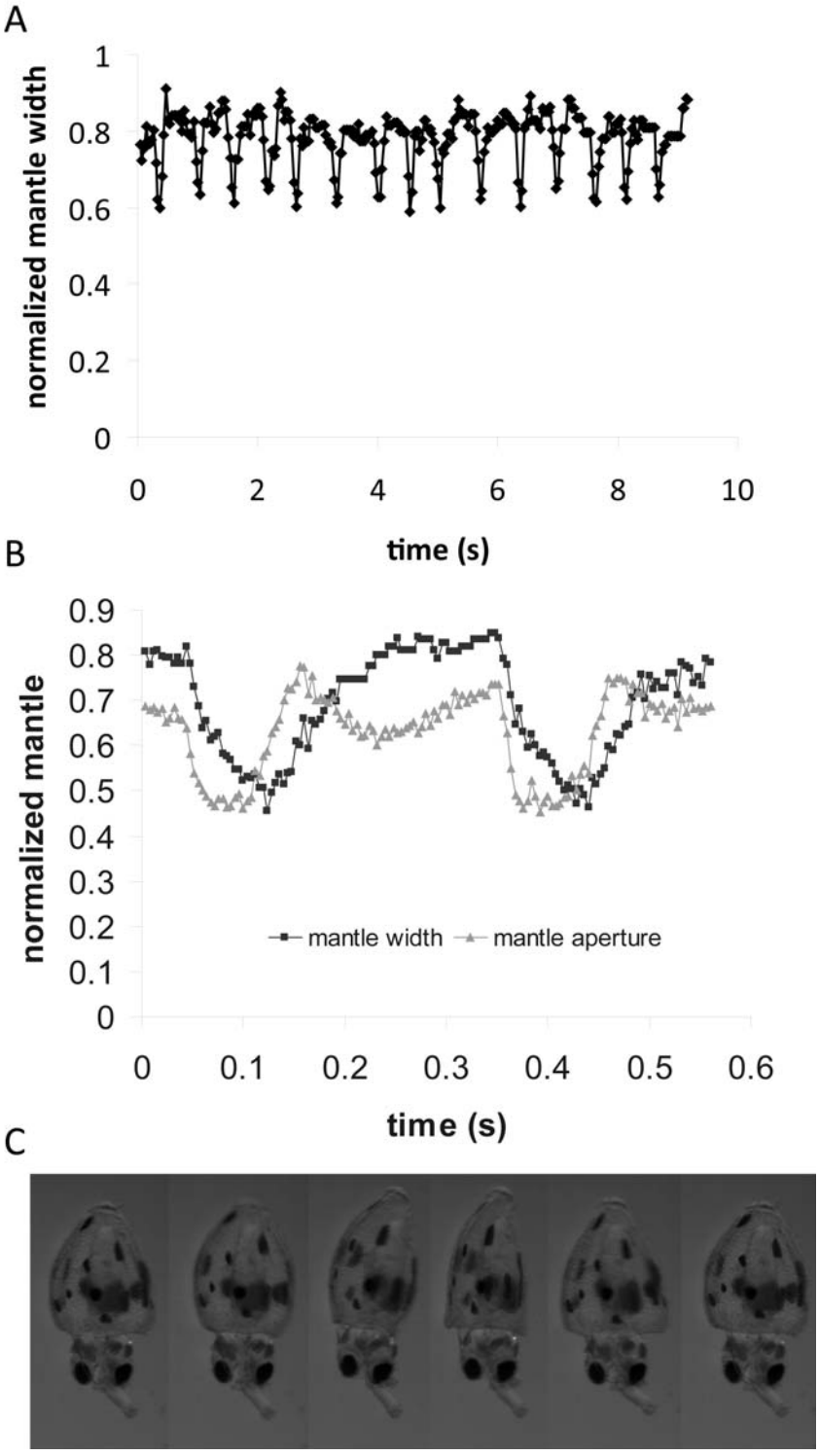

Figure 2-5. Kinematics of paralarval *Dosidicus gigas* swimming from 30fps video clips. A) Velocity plotted against the minimal mantle width (ratio of fully contracted to fully expanded mantle, smaller numbers indicate more contraction), and B) frequency of contraction--single fast jets excluded, as frequency cannot be calculated.

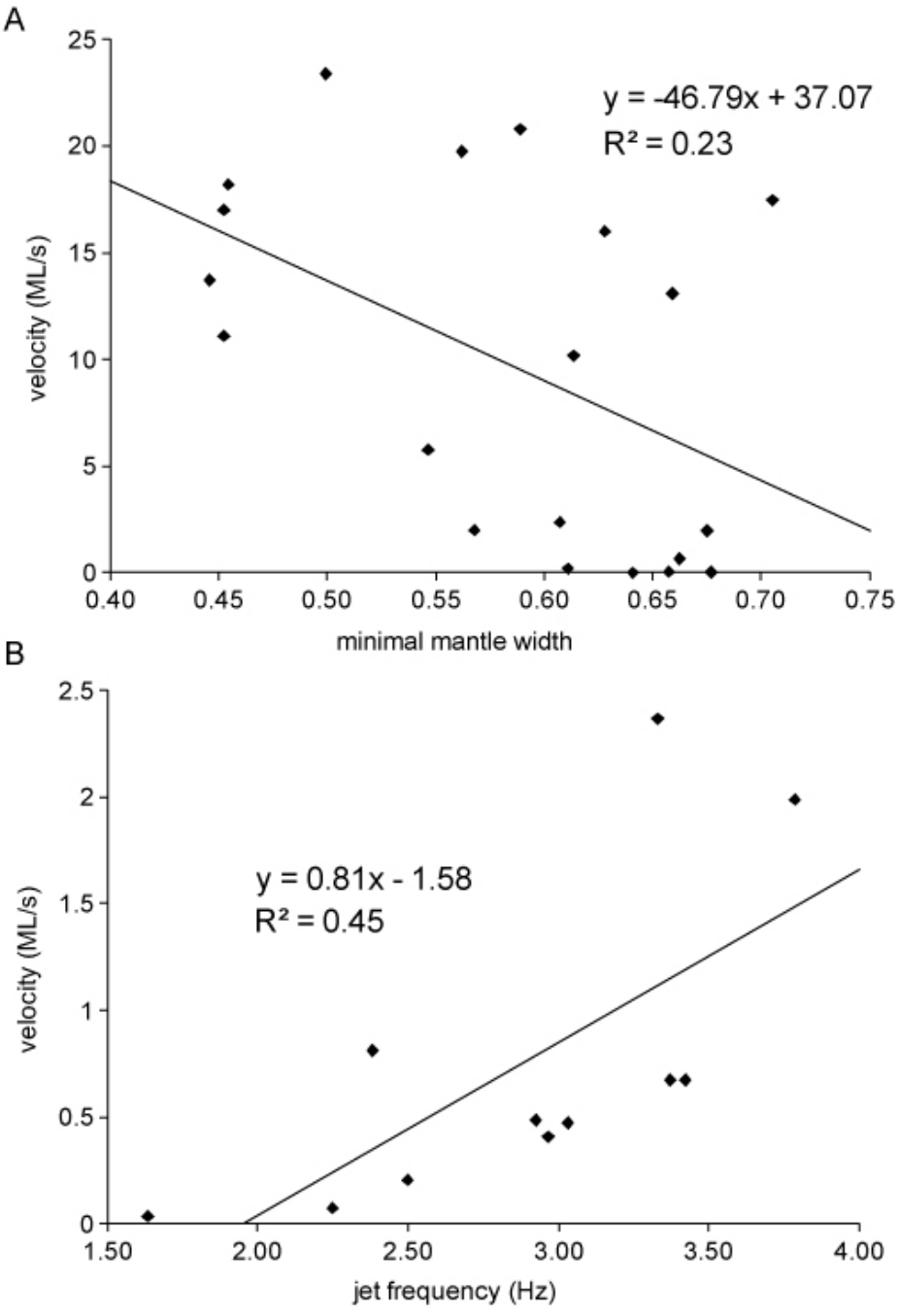

Figure 2-6. Kinematics of paralarval *Dosidicus gigas* swimming from high-speed video clips. A) Velocity plotted against minimal mantle width, B) contraction time, and C) aperture closure.

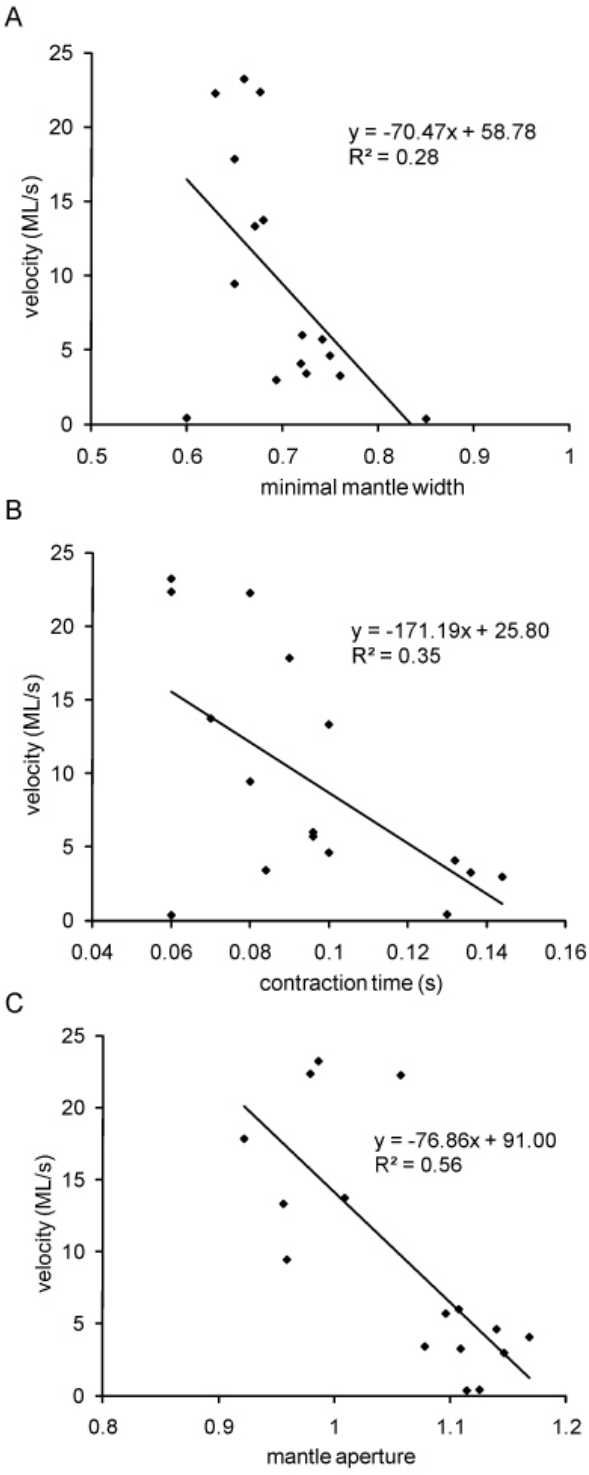

Figure 2-7. Ontogenetic scaling of squid jet propulsion and the effect of jet aperture area. Theoretical results for A) maximal squid velocity at the peak of a single jet, B) hydrodynamic efficiency after 10 jet cycles, and C) maximal stress on the mantle muscle at the peak of a single jet. Models with a constant small aperture area (dotted line), a constant large aperture area (dashed line), and a dynamically varying aperture area (solid line) are shown. A horizontal gray line in panel C indicates a maximal muscle stress of 2.5×10^5 N m^{-2}. Mantle lengths at which this stress is reached for each of the three models are given in gray.

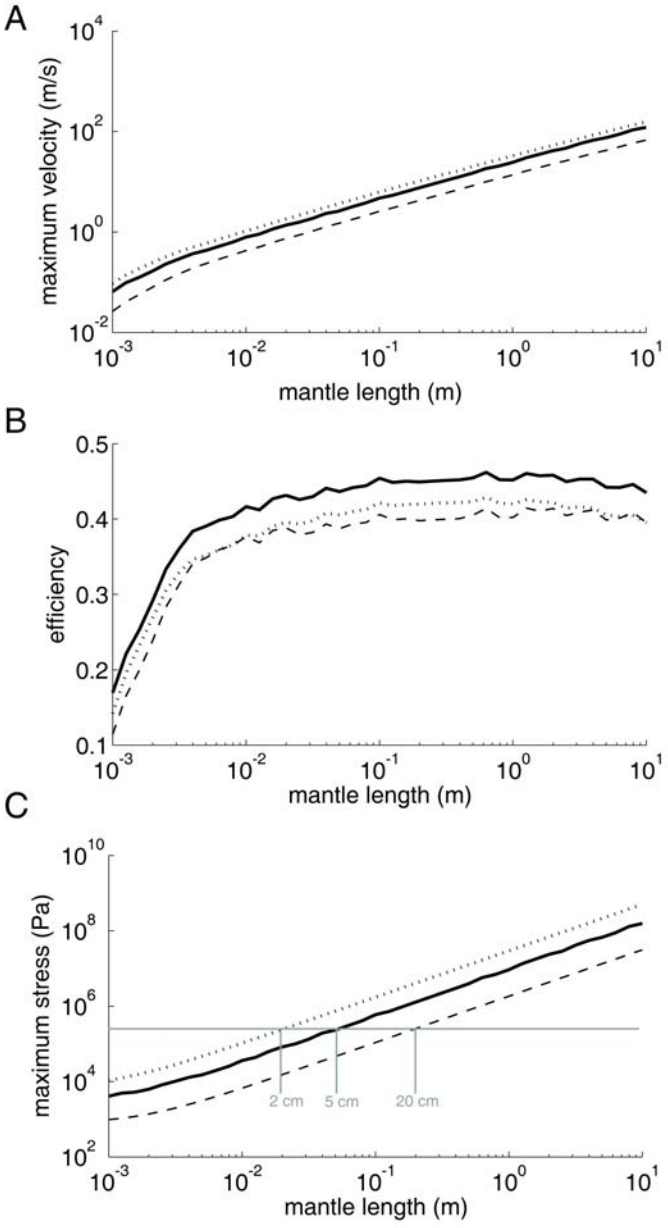

Figure 2-8. Ontogenetic variation in jetting when variables are set by regressions with a dynamically varying aperture (solid lines) compared to when funnel radius is controlled to maintain a constant stress (dotted lines). A) Funnel radius that results in a constant value for stress of 2.5×10^5 N m^{-2}. Theoretical results of using this aperture radius for B) maximal squid velocity at the peak of a single jet and C) hydrodynamic efficiency.

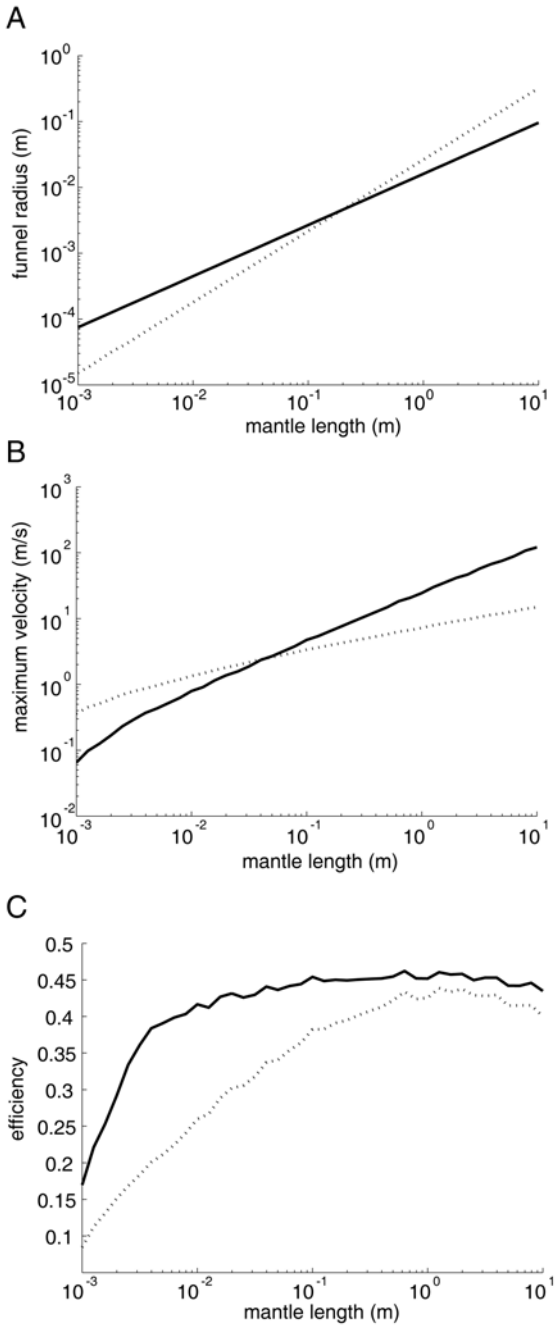

Figure 2-9. Ontogenetic variation in jetting when variables are set by regressions and stress is variable (solid lines) compared to when jet frequency is controlled to maintain a constant stress (dotted lines). A) Jet frequency that results in a constant value for stress of 2.5×10^5 N m^{-2}. Theoretical results of using this jet frequency for B) maximal squid velocity at the peak of a single jet and C) hydrodynamic efficiency.

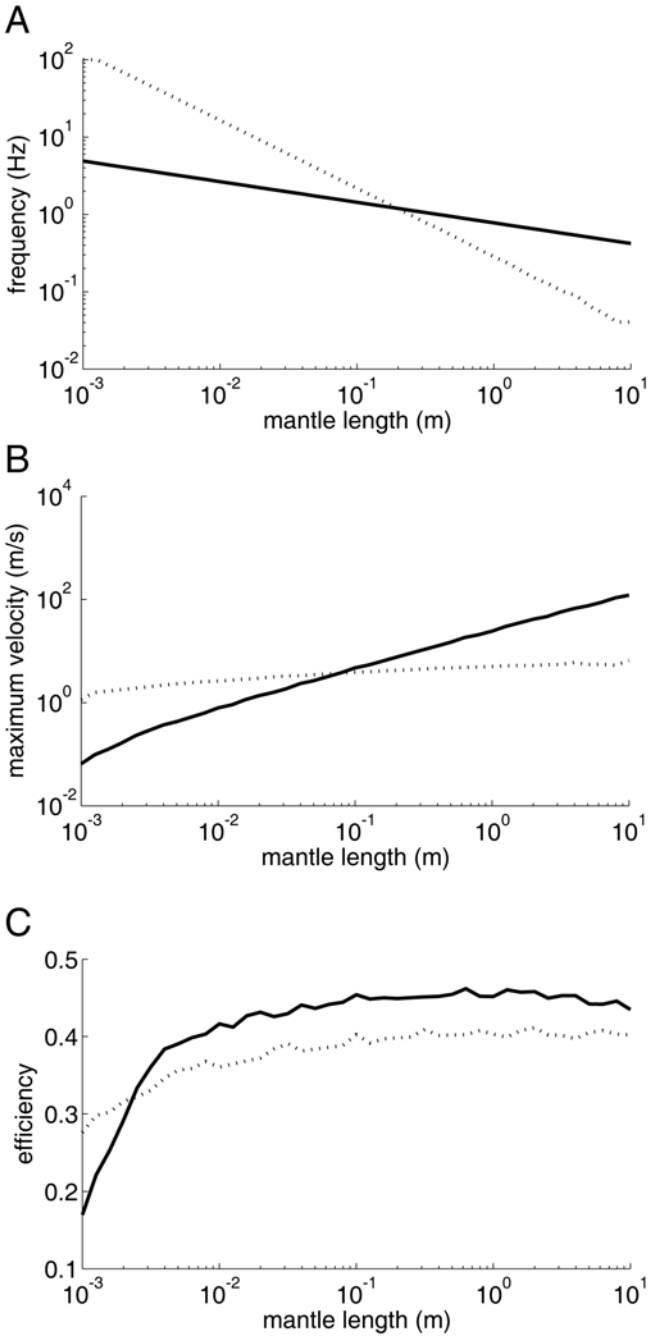

Figure 2-10. Maximal squid velocity (ML/s) at the peak of a single jet (solid line) and mean squid velocity (ML/s) averaged over 10 jet cycles (dotted line). Values calculated from a theoretical model of jet propulsion over squid sizes ranging from 1mm to 10m ML.

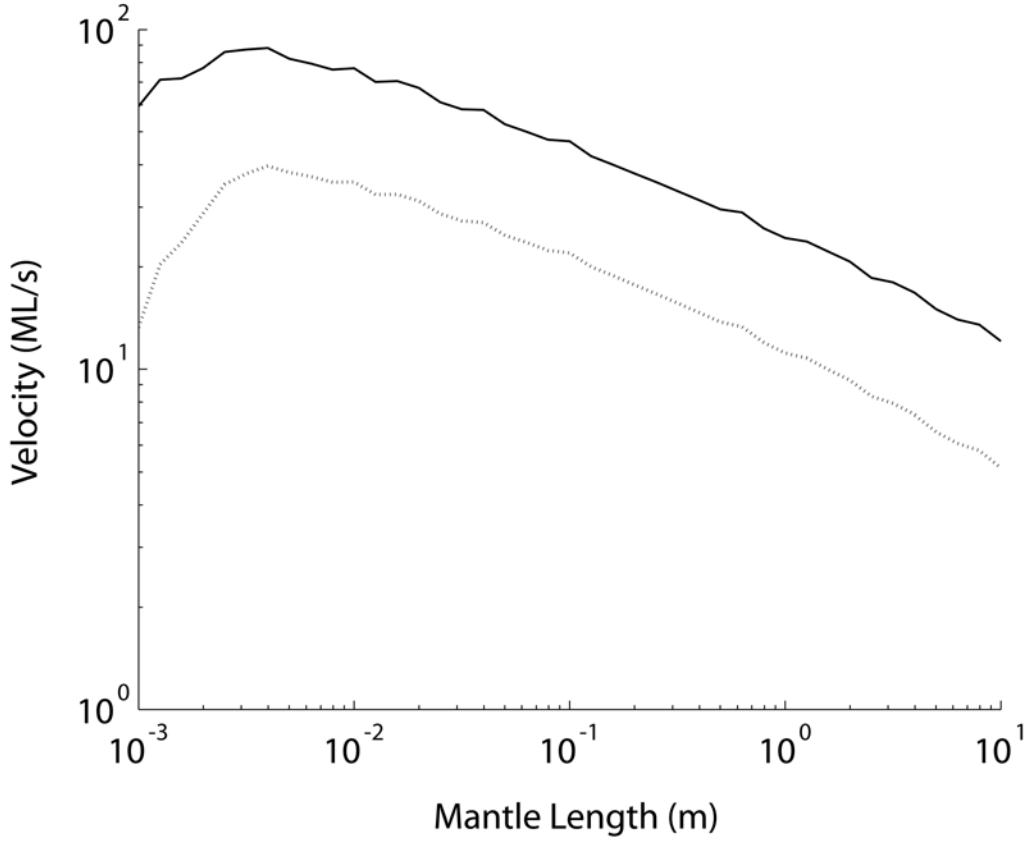

Chapter 3

Divergent cousins: Population structures of ommastrephid squid in the eastern Pacific

3.1. Abstract

Dosidicus gigas and *Sthenoteuthis oualaniensis* (Teuthoidea: Ommastrephidae: Ommastrephinae) are abundant, ecologically important squid that co-occur in the eastern tropical Pacific. Little is known about the genetic basis of population structure in either species, although the presence of two species within *S. oualaniensis* has been suggested. We report here on a comparative population genetic study of *D. gigas* and *S. oualaniensis* using the mitochondrial marker NADH dehydrogenase subunit 2. Despite the high potential for dispersal in these active swimmers, both species exhibit a distinct biogeographic break at 5-6° N. *S. oualaniensis* contains multiple deeply divergent, geographically segregated clades, whereas *D. gigas* shows only mild divergence between Northern and Southern hemisphere populations. We suggest that dispersal and genetic mixing across the eastern tropical Pacific may be impeded by both oceanographic and ecological factors.

3.2. Introduction

Three different forms of *Dosidicus gigas* have been recognized based on mantle length (ML) at maturity (Nigmatullin et al. 2001, Table 3-1). The "medium" size-at-maturity form occurs across the entire species range. A "small" size-at-maturity form is thought to be limited to equatorial waters, and the northern and southern peripheries of the species range are inhabited by a "large" size-at-maturity form which can exceed 100 cm ML. Tagging studies on large individuals of the third form have revealed that they make extensive use of the prominent oxygen minimum zone (OMZ) in the eastern Pacific. This zone provides a refuge from predators that cannot tolerate hypoxia and also appears to be a favored hunting area of large *D. gigas* (Gilly et al. 2006b). Similar data are not available for smaller individuals.

Nigmatullin et al. (2001) suggested that the three size-at-maturity forms may be incipient species, or at least distinct stocks. However, other researchers have proposed separating *Dosidicus gigas* into only two stocks, one "northern" and one "southern," based on migration patterns rather than size-at-maturity (Wormuth 1976, Nesis 1983, Wormuth 1998, Clarke and Paliza 2000).

Sthenoteuthis oualaniensis also comprises multiple forms (Nesis 1983, Dunning 1998) (Table 3-1), varying both in size-at-maturity and in the possession of a distinctive large dorsal photophore. A middle-sized "typical" form with the photophore is found throughout the species range and co-occurs with *Dosidicus gigas* in the eastern tropical Pacific. Equatorial waters of the Indian and Pacific (10-15° N to 10-15° S) are inhabited by an "early maturing" dwarf form that lacks the dorsal photophore and may constitute a separate, as yet undescribed, species (Clarke 1965, Nigmatullin et al. 1983a, Nesis 1993).

In the western part of the species range, detailed studies have revealed greater complexity. The middle-sized and dwarf forms may each contain two groups with distinct morphologies, and the middle-sized form can have two different sizes at maturity (Nesis 1993). Perhaps most striking, a giant form of *Sthenoteuthis oualaniensis* was documented in the western Indian Ocean north of 15-17° N (Nesis 1993). Like the large form of *Dosidicus gigas*, this giant *S. oualaniensis* is associated with a prominent oxygen minimum zone. Snÿder (1998) suggested this form may arise through phenotypic plasticity, a feature that may facilitate best use of available resources associated with the OMZ. Alternatively, Zuyev et al. (2002) proposed that the various forms of *S. oualaniensis* are indicative of active sympatric and allopatric speciation facilitated by the high fecundity and rapid generational turnover common to all ommastrephid squid.

Indeed, variation in size at maturity within both *Sthenoteuthis oualaniensis* and *Dosidicus gigas* has been attributed at different times and by different researchers to genetic substructure or phenotypic plasticity. Genetic assertions remain speculative, however, due to limited molecular studies. The only molecular work on *S. oualaniensis* used allozymes from Indian Ocean samples to support the hypothesis that

the dwarf photophoreless form is a separate species, while suggesting that middle-sized and giant forms might be considered "local groups" (Yokawa and Jerez 1999). As for *D. gigas*, isozyme analysis indicated that the three size groups from Peruvian waters belong to a single population (Yokawa 1995). Sandoval-Castellanos et al. (2007) distinguished northern and southern genetic populations of *D. gigas* with randomly amplified polymorphic DNA from eight near-shore sites from approximately 30° N to 35° S. However, these authors (Sandoval-Castellanos et al. 2010) did not find further support for the north-south structure in cytochrome b sequences.

In this study, we present a comparative genetic analysis of *Dosidicus gigas* and *Sthenoteuthis oualaniensis* using mitochondrial sequence data from specimens collected throughout their region of range overlap (Figure 1-1), as well as the recent northward expansion of *D. gigas*. We aim to test the hypothesis that different size-at-maturity forms comprise genetically distinct units and to look for biogeographic patterns in the genetic structure of these two species. This study presents the first genetic analysis of *S. oualaniensis* in the eastern Pacific Ocean and the first genetic sampling of *D. gigas* throughout its range.

3.3. Methods

3.3.1. Sample collection

Tissue samples were taken from 802 individuals of *D. gigas* collected between 1999 and 2008 from 53 locations throughout this species' range (Supplemental Table 1). 107 individual samples of *S. oualaniensis* were collected from 40 locations between 2003 and 2007 in the central and eastern Pacific (Table 3-3).

Squid were obtained by jigging, from beach strandings, with dip nets (small juveniles), or in bongo net tows (paralarvae). Either muscle or gill tissue was sampled for molecular work. Small pieces of gill (~0.5 cm^3) were dissected and preserved in 90% ethanol. Muscle samples were taken from adults and juveniles by cutting 1-2 cm of tissue off an arm tip with subsequent preservation in 70% ethanol. In some cases, the entire animal was frozen, and the arm tip sampled at a later date. Small paralarvae

were used in their entirety for DNA extraction; only the posterior part of the mantle of larger paralarvae was used.

Dorsal mantle length was measured for adult squid from a subset of the geographic locations sampled. Sex and sexual maturity of these specimens were visually assessed (Lipiński and Underhill 1995). Mantle length and sexual maturity from a subset of specimens were used to identify forms for each species as described in Table 3-1.

3.3.2. DNA isolation, PCR amplification and sequencing

DNA was extracted, typically from about 25 mg of tissue, using the Qiagen DNeasy Tissue/Blood Kit. The quality and quantity of DNA was not affected by the type of tissue or length of time that the sample was kept frozen or in ethanol. However, we did find that carcasses in Baja California Sur, México, that remained at ambient air temperatures in excess of ~30°C without preservation for more than ~6 hours tended to yield degraded DNA. The concentration for use as a PCR template was adjusted to an A_{260} of about 0.05-0.2.

The complete mitochondrial genomes of four individuals (one *D. gigas*, three *S. oualaniensis*) were sequenced using PCR primers designed from highly conserved regions of tRNA sequences of related species (Yokobori et al. 2004) with additional specific primers designed as required from sequences already obtained. PCR amplifications were carried out using TAKARA ExTaq HS DNA polymerase in 50 µl volumes, using 1 µl of template according to the manufacturer's recommendations. Extension times were 3-4 min, depending on amplicon length. PCR products were purified by use of the Qiagen Qiaquick Kit or with the Machery Nagel Nucleospin Extract II Kit. Sequence data were obtained using an ABI PRISM 3100 genetic automatic sequencer and Big Dye v. 1.3 dye terminator chemistry. Sequencing primers are shown in Supplemental Tables 2-11. Sequence analysis and assembly were completed in Gene Works v. 2.0 (Intelligenetics, Inc.) or Sequencher v. 4.7 (Gene Codes Corporation).

Sequencing for population genetics used three markers: 1) cytochrome c oxidase subunit 1 (COI), 2) a non-coding region (NCR2) located between tRNA-Glu and cytochrome c oxidase subunit 3 (COIII, copy 1), and 3) the NADH dehydrogenase subunit 2 (ND2) region. For reasons described below, analysis in this paper is focused on ND2.

A 658 Nt fragment (exclusive of primers) of COI was generated using the forward primer LCO1490 (Supplemental Tables 2,5) and reverse primer HCO 2198 (Suppl. Tables 3,6) for both species (Folmer et al. 1994). PCR of the NCR2 (558 Nt in *D. gigas*, and 563 Nt in *S. oualaniensis*) marker was performed with the forward primer DGEF (both species; Suppl. Tables 2,5) and the reverse primers SqCO3R (both species; Suppl. Tables 3,6) and RSqI (*S. oualaniensis*; Suppl. Table 6). PCR of the ND2 marker (1041 Nt) was performed with the following primers: SqSF forward (both species; Suppl. Tables 2,5), DCOR2 reverse (*D. gigas*; Suppl. Table 3), SCOR reverse (*S. oualaniensis*; Suppl. Table 6).

PCR amplification for these regions used 2.5 units of Biolase DNA polymerase (Bioline USA, Inc.) in 100µl volumes using 1 µl of template with 2 mM $MgCl_2$, 200µM dNTPs, and primers at 250 nM. After 7 min at 94 °C the reactions were subjected to 40 cycles of 94 °C (10 sec), 46 °C (30 sec), a gradient of 6 °C/sec to 72 °C, and 72 °C (1.00 min) followed by a final extension of 7 min at 72 °C. Sequencing of purified PCR products used the amplification primers.

The complete mitochondrial genome of *D. gigas* was deposited in GenBank (accession number NC009734). Complete mitochondrial genomes of three major clades of *S. oualaniensis* were also stored in GenBank: Typical (NC010636), Equatorial (EU660577), and Eastern Typical (EU658923) (see Results for explanation of clades). The three mitochondrial markers, ND2, COI, and NCR, are included in these complete genomes. Several additional *D. gigas* ND2 sequences have also been deposited (accession numbers FJ153071, FJ153073, FJ153075, and EF025502).

3.3.3. Analysis

The mitochondrial genomes of both *D. gigas* and *S. oualaniensis* contain duplicated regions that include genes for cytochrome c oxidase subunits 1-3, tRNA-Asp, ATP synthetase subunits 6 and 8, as well as a long non-coding region (NCR) of about 565 nucleotides. Thus, analyses of COI and NCR markers suffer from the complications associated with duplicate copies. In addition, the NCRs of *D. gigas* and *S. oualaniensis* contain numerous insertions and deletions as well as AT-rich regions of variable length, features that complicate analysis.

Therefore, for the purposes of this study, we chose to focus on the gene NADH dehydrogenase subunit 2 (ND2) that occurs as a single copy in both species, obviating the need for concern over which copy is being amplified and sequenced. Although we present results only from ND2, our preliminary analysis of a subset of COI sequences confirmed the patterns reported here (data not shown).

Maximum likelihood phylogenetic trees were constructed for both *S. oualaniensis* and *D. gigas* in PhyML (Guindon and Gascuel 2003). The search started with a neighbor-joining tree, used the nearest-neighbor interchange (NNI) search method, optimized both topology and branch lengths, and computed aLRT for branch support. One sequence of each species was used as outgroup for the other. Optimal nucleotide substitution models for maximum likelihood were calculated with AIC in jMODELTEST (Posada 2008) (TrN + I for *D. gigas* and TIM + I for *S. oualaniensis*; Rodríguez et al. 1990, Tamura and Nei 1993). As TIM is not implemented in PhyML, the next best option, GTR + I, was used for *S. oualaniensis*.

Due to the large size of the *D. gigas* sample set (N=802), bootstrapping attempts proved excessively time-intensive, and as obvious clades were not present, we chose not to pursue this avenue. For *S. oualaniensis*, in which clear clades were present, clade support was assessed with 1000 bootstrap replicates. Arlequin was used to calculate average pairwise genetic distances between and within the clades, by calculating the number of (corrected average) pairwise differences and dividing this by the total number of loci (1027).

Pairwise genetic distances between the 57 sampled locations for *D. gigas* were calculated as Slatkin's linearized pairwise F_{st} (Slatkin 1995) with Arlequin. Locations with fewer than 15 individuals that were within 6 degrees of each other, and did not have a significant ($p < 0.05$) pairwise F_{st}, were pooled. The Baja California area (32-22°N) was more densely sampled than the remainder of the study area and different criteria were used for pooling in this region. A large number of samples were taken in 1999, after the strong 1997-98 El Niño. These were kept separate from the remaining samples, taken in 2004-2006. Any 2004-2006 locations within 2 degrees of each other that did not have a significant ($p < 0.05$) pairwise F_{st} were pooled. This resulted in a total of 23 pooled samples (Table 3-2).

Hierarchical AMOVA (Weir and Cockerham 1984, Weir 1996) analysis on this pooled *D. gigas* dataset was performed in Arlequin using the K2P substitution model (Kimura 1980) and 1000 permutations. Details are presented in the Results. Having discerned two distinct populations, we used the Isolation with Migration (IM) computer program (Hey and Nielson 2004) to fit the data to a coalescent model of two populations diverging from one ancestral population and exchanging migrants. Due to the large number of samples, the program did not converge with the complete dataset, so the program was run on four random subsamples of 50 sequences from each population (N and S, total 100). We assigned broad prior distributions based on preliminary trial runs, and implemented Metropolis coupling with 30 chains and a geometric heating model with parameters of 0.8 and 0.9. We used a burn-in period of 200,000 steps and ran the program for 5,000,000 steps, recording results every 100 steps. The HKY mutation model was used, as it is the only model appropriate for mitochondrial data implemented in IM. This program estimates the effective population sizes (female only, as the data are mitochondrial) of the Northern population, the Southern population, the ancestral population, the migration rates from North to South, from South to North, and the time since divergence, all scaled to the neutral mutation rate.

Mitochondrial mutation rates for cephalopods are not available, so we followed Donald et al. (2005) in using a molluscan range from 0.7% (gastropod *Tegula*,

Hellberg and Vaquier 1999) to 2.4% (arcid bivalves, Marko 2002). The IM estimate of time since divergence is given in generations, but the generation time of *D. gigas* is approximately one year (Markaida et al. 2004), so no arithmetic was necessary to convert from generations to years.

Degree of association between genetic distance and geographic distance in *D. gigas* was quantified with a Mantel test (Mantel 1967, Sokal and Rohlf 1995), implemented in Arlequin. Pairwise genetic distances were calculated as Slatkin's linearized pairwise F_{st} (Slatkin 1995). Geographic distances were calculated from latitude and longitude with the Geographic Distance Matrix Generator (Ersts 2009), which assumes the earth is a sphere and uses great circles to calculate distance. This method does not take coastlines into account, such that the distance between two points on opposite sides of the Baja Peninsula is the overland route, which is clearly not available to a traveling squid. As this is of primary concern in the Baja region, and pairwise comparisons between Pacific Baja samples and Gulf Baja samples showed no significant differences (see Results), we accept the approximation.

3.4. Results

3.4.1. Dosidicus gigas

AMOVA analysis of the dataset gave a significant ($p<0.05$) F_{st} of 0.05161, indicating some partitioning of genetic variation between samples. Pairwise genetic distance plotted against geographic distance (Figure 3-3) gave an r^2-value of 0.3148, which was significant according to a Mantel test. This could indicate an isolation-by-distance pattern of genetic variation.

However, pairwise F_{st} values between samples showed that the samples from the five southernmost sampling sites were significantly different from most of the other samples, and not significantly different from each other (Table 3-4). This suggested that the driving force behind the significant F_{st} of the overall dataset was a simple North-South divergence. Indeed, an AMOVA analysis of either the Northern samples alone or the Southern samples alone gave a non-significant F_{st} value (Northern: -0.00456, Southern: 0.00950, $p>0.05$). Imposing a two-group geographic

structure on the dataset (Figure 3-1) and implementing a hierarchical AMOVA resulted in a significant F_{ct}, assigning 11.05% of genetic variation to variability between these two groups.

IM divergence time estimates ranged from 133,000 ± 12,000 (for a mutation rate of 0.7%) to 39,000 ± 3,000 (for a mutation rate of 2.4%) years b.p. (mean ± standard deviation, based on averaging the four subsampled runs).

Overall, the sequence data contained 422 unique haplotypes, of which only 28 occurred in three or more individuals. These 28 common haplotypes were made into a network (Figure 3-4) using the program TCS (Clement et al. 2000). The resulting network revealed a clustering of primarily "southern" and "northern" haplotypes, but genetic distance between these haplotypes was small (1-2 nucleotide differences). One branch of "northern" haplotypes was more deeply divergent than the rest. These divergent haplotypes were found throughout the northern hemisphere, from Canada to Southern México. "Southern" haplotypes were found in northern samples (black slices in white pies) less frequently than "northern" haplotypes in southern samples (white slices in black pies).

From the samples with quantified ML and maturity stage, we found individuals representative of two of the three size-at-maturity forms in both the Northern and Southern groups. In the Northern group, squid from the 2007 Cordell Bank sampling off California were all of the large size-at-maturity form, whereas squid from the Gulf of California in 1999 were all of the medium size-at-maturity form. In the Southern group, squid from the eastern tropical Pacific (ETP) in 2006 were all of the medium size-at-maturity form, and squid from Chile in 2005 were all of the large size-at-maturity form (Table 3-5). There was no significant pairwise difference between Cordell Bank and Gulf of California samples, or between ETP and Chile samples (Table 3-4). We found no representatives of the small size-at-maturity form in our sampling.

3.4.2. Sthenoteuthis oualaniensis

The Eastern Tropical Pacific specimens were largely identified by the presence of a dorsal photophore in adults (Table 3-1); juveniles and paralarvae were identified by molecular techniques only. The single Central Pacific specimen from 2003 was a mature female animal of 9.3 cm ML with no photophore. Those from 2005 included eight with a photophore, and three without; ML for two of those without were 11.4 and 9.7 (both female). All samples from May 2007 were paralarvae.

Four genetic clades were revealed within *Sthenoteuthis oualaniensis* (Figure 3-5). Pairwise genetic distances between these clades, and within each clade, are provided in Table 3-6. The most divergent clade corresponds to the early-maturing, dwarf form that lacks the dorsal photophore, possibly *Sthenoteuthis* sp. nov., as previously suggested (Clarke 1965, Nesis 1993, Yokawa and Jerez 1999). Individuals from this clade were found only in the central Pacific, south of 6.23 °N, and we refer to it as the **Equatorial** clade, consistent with the equatorial presence of this morphotype.

The remaining samples form a strongly supported **Typical** clade, corresponding to the middle-sized, photophore-bearing morphotype of *Sthenoteuthis oualaniensis*. This clade comprises three strongly supported sub-clades. The most divergent of these clades was found only in the eastern Pacific, north of 5.29° N, and we refer to it as **Eastern Typical**. The next clade was found only in the central Pacific, north of 6.23° N; we refer to it as **Central Typical**. The final clade (**Pacific Typical**) was found in the central Pacific from Hawaii to the equator but only south of 5.29° N in the eastern Pacific (Figure 3-2).

Bootstrap analysis with 1000 replicates supports the monophyly of Equatorial (99.3%), Typical (98.9%), Eastern Typical (90.8%), Central plus Pacific Typical (83.8%), Central Typical (97.5%) and Pacific Typical (88.4%) clades (Figure 3-5).

Only one of the four clades, the Pacific Typical, was found in both eastern and central Pacific. AMOVA analysis of this clade gave a non-significant F_{st} (-0.00273), indicating that genetic variation within this clade showed no discernable pattern with geography.

3.5. Discussion

3.5.1. Genetics, Forms, and Morphotypes

Our phylogenetic analysis supports the existence of a morphologically distinct form of *Sthenoteuthis* that is highly genetically divergent (14%) from all other clades (Equatorial clade, Figure 3-4, 99% bootstrap support). This degree of genetic divergence is near that found between cryptic species of the ommastrephid genus *Illex* (16-25% with COI, Carlini et al. 2006). Our Equatorial clade likely represents the dwarf, early-maturing, photophore-less *Sthenoteuthis* sp. nov. that others have suggested (Clarke 1965, see also Nesis 1993, Wormuth 1998, Yokawa and Jerez 1999). In addition to the absence of the photophore, other differential morphological characteristics have been described (Nesis 1977, Wormuth 1998). This form is restricted to equatorial waters of the Indian and Pacific oceans between east Africa to near the Galapagos Islands (Nesis 1977, Nigmatullin et al. 1983a). However, in the eastern Pacific it is extremely rare and its latitudinal range narrows to 1-2°S (Nigmatullin et al., 1983a), so it is not surprising that we found no representatives in our sampling of this region.

Although a full description of *Sthenoteuthis* sp. nov. is beyond the scope of this study, this genus joins a growing pool of ommastrephids harboring cryptic species. Molecular work has uncovered putative genetic groups within the ommastrephids *Illex argentinus* (Thorpe et al. 1986, Carvalho et al. 1992, Carlini et al. 2006) and *Martialia hyadesi* (Brierley et al. 1993), and in each case the authors argued that the groups merited distinction as separate species. Clarifying ommastrephid taxonomy is no mere academic question, as many of these species or species complexes support prominent fisheries.

The discovery of other divergent clades within the typical middle-sized form was an unexpected result. Only one middle-sized form, as determined by gladius structure, has been previously recorded in Hawaiian waters (Young and Hirota, 1998), suggesting that the Central Typical clade may be morphologically indistinguishable from the Pacific Typical. But in the eastern Pacific an early-maturing group of the

middle-sized form has been recorded. These individuals possess the dorsal photophore but mature at dwarf sizes, some as small as 9 cm (Nigmatullin et al. 1983b, Nesis 1993). Could this be the Eastern clade, as illuminated by our molecular work? More thorough morphological data must be collected in conjunction with genetic samples to explore this question.

In the Indian Ocean, distinct gladius structures have been found within the middle-sized group of *Sthenoteuthis oualaniensis* (Nesis 1993). Allozyme electrophoresis, however, suggested that middle-sized forms collected in the extremes of the range (equatorial localities in the Indian and eastern Pacific), together with the giant form from the Indian, are probably all the same species (Yokawa and Jerez 1999). Molecular analysis of *S. oualaniensis* in the form of genetic sequences data from the western part of its range would undoubtedly help to clarify the population structure of this species. Given the results of this study, an equally strong clade structure might be expected in western Pacific populations, particularly those associated with archipelagos. In the Indian Ocean, the giant form known from the Arabian Sea may also suggest a complex population structure (Nesis 1977, Okutani and Tung 1978, Nesis 1993).

As for the three size-at-maturity forms of *Dosidicus gigas*, we found no genetic differentiation between medium and large forms, in agreement with Yokawa's (1995) evidence from isozymes. This result strongly supports phenotypic plasticity, as proposed by Keyl et al. (2008), rather than species *in status nascendi*, as hypothesized by Nigmatullin et al. (2001). Phenotypic plasticity as an explanation for the different size forms would be consistent with the finding that presence and relative abundance of medium and large forms in the Gulf of California may vary according to environmental conditions (Markaida 2006).

Our failure to find any representatives of the small size-at-maturity form in the years of collection is intriguing, especially given that the first *Dosidicus gigas* recorded from the Gulf of California comprised a mature female and male of 21 cm ML taken in 1959 (Wormuth, 1976). Later Sato (1976) found mated females and mature males of <24 cm ML inside the Gulf and off southwestern Baja California in

1971. Despite these records, this form is thought to be limited to a narrow band between 12° N and 5-6° S, and even within this region it is both rare and patchily distributed. Furthermore, over 70% of the small size-at-maturity specimens collected in this region were caught in pelagic trawls using very large nets (Nigmatullin, pers. comm.), a method not employed in our study.

Curiously, both species exhibit their smallest forms in the region of range overlap, although they are capable of reaching large sizes in other parts of their ranges. Food spectra overlap extensively for *D. gigas* and *S. oualaniensis* in this region (Nigmatullin et al. 2001), suggesting that these two species share similar niches and may be competing for resources. Their biogeography may be strongly influenced by such ecological interactions.

3.5.2. North-South genetic break

A concordant biogeographic break for both ommastrephids at 5-6° N (Figures 2.1 and 2.2) was a striking discovery. These findings are consistent with RAPD analysis of *D. gigas* (Sandoval-Castellanos et al. 2007), which separated four sampling locations off North America from four sampling locations off South America. Although Sandoval-Castellanos et al. (2010) did not find robust support for this north-south structure with cytochrome b, this is probably explained by low variation in this marker, with only 20 unique haplotypes. Divergence between the two populations is likely to be relatively recent, although estimates cover an order of magnitude from 10,000 (Sandoval-Castellanos et al. 2007) to 133,000 (maximum estimate from this study) years before present. Given this time frame, it is not surprising to find that both populations have not diverged morphologically, as anatomical analysis of *D. gigas* revealed only a gradual increase from north to south of the right-arm I length-index as well as in the number of suckers per arm (Wormuth 1976, 1998). Existence of different populations from equatorial and Peruvian waters, as suggested by differences in ontogenetic parasitic infection dynamics (Shukhgalter and Nigmatullin 2001) were not supported by our data.

Separation between the two hemispheres could be driven by oceanographic features that are effective in subdividing oceanic populations and promoting genetic isolation (Norris 2000). Although *D. gigas* is found in tropical waters, individual tagged squid of the large form in the Gulf of California spend very little time in water above 25° C (Davis et al. 2007), spending most of their time at cooler depths, particularly the upper region of the oxygen minimum zone (OMZ) at 200-300 m depth (10-15°C; Gilly et al. 2006b). This depth range also corresponds to the daytime location of the deep-acoustic scattering layer, a zone rich in the preferred prey of *D. gigas* (Dunlap 1970, authors' unpubl. data). The OMZ is present throughout the highly productive waters of the eastern Pacific (Fiedler and Talley 2006) and essentially overlaps with the range of *D. gigas* (Figure 1-1). This feature bulges westward at the equator because of equatorial upwelling, but the Equatorial Countercurrent (ECC) brings a finger of warm, oxygenated surface water toward the coast of Central America (Figure 3-1). The resulting increased surface temperature (typical surface temperature in the ECC is 27° C) and depression of the OMZ to greater depth (Fiedler and Talley 2006) might make the equatorial region less attractive to *D. gigas*. Although it is unlikely that this would constitute an insurmountable barrier to migration, it might provide a meaningful impediment to mixing of reproductively competent squid (Clarke and Paliza 2000).

Another mechanism acting to isolate southern and northern populations of *Dosidicus gigas* may arise from seasonality of reproduction. Population differentiation in cetaceans, for example, is frequently driven by opposite reproductive seasonality in Northern and Southern hemispheres (Pastene et al. 2007, Hoelzel 1998). Data on seasonality and location of spawning by *D. gigas* are sparse but tantalizing. *D. gigas* paralarvae and naturally deposited eggs have been identified in the Gulf of California in April, May and June (Gilly et al. 2006a, Staaf et al. 2008, Camarillo-Coop and Salinas Zavala 2008). None were found in February, the cold season (Camarillo-Coop and Salinas Zavala 2008), although reproductively mature females are found throughout the year in the Gulf of California (Markaida and Sosa-Nishizaki 2001).

Paralarvae have been also found off the western Baja California peninsula in February, July-August and October (Ramos-Castillejos et al. 2010).

Studies in the southern hemisphere are even more limited, but a cruise off the coast of Peru collected paralarvae in November and December (Sakai et al. 2008). Mature adults are found throughout the year, with two seasonal peaks (Tafur et al., 2001). These results hint at a potentially opposite seasonality, in which *D. gigas* spawn in the spring and summer of whichever hemisphere they inhabit. This could underlie the observed pattern of genetic divergence as suggested by Clarke and Paliza (2000).

Spawning is clearly possible over a wide range of latitudes, but based on the small degree of genetic divergence within each hemisphere, considerable mixing of reproductive animals must occur. *D. gigas* is capable of horizontal migrations at speeds up to 30 km/day (Gilly et al. 2006b). However, stable isotope analysis has not supported long-distance migrations between regions in the northern hemisphere (Ruiz-Cooley et al. 2010). Thus, the extent to which *D. gigas* takes advantage of its migratory capability is unknown.

The dense sampling of *Dosidicus gigas* in the Baja California area allowed us to consider the possibility of temporal partitioning of genetic variability. None of the pairwise comparisons between Gulf of California samples from March or May 1999, October 2004, June, July, November 2005, May, July, or August 2006 were significant. We found no evidence of temporal genetic variation, even after the strong El Niño of 1999. This extends the results of Sandoval-Castellanos et al. (2007), who found no temporal difference between samples taken in 2001 and 2002 off Mazatlán, México.

Sthenoteuthis oualaniensis shows a similar north-south break to the one discussed above for *Dosidicus gigas*, between Pacific Typical and Eastern Typical in the east and between Central Typical and Equatorial in the west. This suggests that the ECC may also be influential in impeding genetic mixing in *S. oualaniensis*. It is not known whether this species utilizes the oxygen minimum zone in the eastern Pacific, although the giant form in the Arabian Sea is associated with the OMZ.

The overall range of this species is quite different from that of *Dosidicus gigas* (Figure 1-1), but it is possible that only one clade (Pacific Typical) is actually distributed throughout this range, while Eastern Typical and Central Typical clades have more narrow distributions. This may indicate life history differences between clades, in which long-distance migrations as a means of dispersal or gene flow could play a greater or lesser role. The typical form can perform substantial horizontal migrations (Nesis 1993), as Okutani and Tung (1978) proposed along the Kuroshio current. The Eastern Typical and Central Typical may be more local groups, limited to the productive regions of the eastern and central Pacific, respectively. Further behavioral, morphological and genetic data will be needed to elucidate potential stocks within this species, to understand their ecological roles and inform management of the nascent fishery.

3.6. Acknowledgements

Thanks first of all to this study's co-authors: Iliana Ruiz-Cooley, Carl Elliger, Zora Lebaric, Bernardita Campos, Unai Markaida and William Gilly. This work was supported by funds from the Census of Marine Life (Tagging of Pacific Pelagics), National Science Foundation (OCE 0526640), David and Lucile Packard Foundation, National Geographic Society, California Sea Grant/Ocean Protection Council and Hopkins Marine Station Marine Life Observatory. Tissue samples were collected and generously shared by J. Ramos (Centro de Investigaciones Biológicas del Noroeste, México), J. Field (NOAA SWFSC Santa Cruz), J. Hoar, M. Carpenter, H. Fienberg, C. Yamashiro (Instituto del Mar del Perú), J. Cosgrove and K. Sendall (Royal British Columbia Museum, Canada), M. Pedraza (University of Concepción, Chile) and Jerome Delafosse. For ship time and support we are grateful to B. Block (Stanford University), P. Sachs and the crew of the SSV Robert C. Seamans, J. O'Sullivan (Monterey Bay Aquarium) as well as L. Ballance, J. Barlow, R. L. Pitman, A. Henry (NOAA SWFSC La Jolla), and the crew of the David Starr Jordan and the MacArthur II. Maps were made with the assistance of A. Booth (Stanford and Moss Landing Marine Labs). The authors would like to thank S. Palumbi, C. Hanifin, A. Haupt, J.

Ladner, M. Pinsky, and T. Oliver (Stanford) for guidance and advice on molecular data analysis. Discussions with L. Zeidberg (UCLA), C. Reeb (Stanford) and Chingis Nigmatullin (AtlantNIRO) aided our interpretation of results. The criticism of three anonymous reviewers greatly improved the manuscript.

3.7. Tables

Table 3-1. Size at maturity forms for *Dosidicus gigas* and *Sthenoteuthis oualaniensis* (Nesis 1983, Dunning 1998, Nigmatullin et al. 2001). No morphological differences other than size at maturity are known for the forms of *D. gigas*.

Species	*Size at maturity*	*Range*	*Morphology*
D. gigas	13-34 cm ML	Equatorial (tropical)	
	24-60 cm ML	Entire species range	
	40-65 cm ML	Non-equatorial (temperate)	
S. oualaniensis	9-12 cm ML	Equatorial	No photophore (two gladius structures in west)
	12-25 cm ML	Entire species range	Photophore (two gladius structures in west)
	40-50 cm ML	North Indian Ocean	Photophore

Table 3-2. Pooled sample locations and dates of *Dosidicus gigas*, ordered by latitude from North to South. N is the number of individuals from each location. Hap is the number of haplotypes identified from that group. Total of 802 sequences. Abbreviations: RBCM: Royal British Columbia Museum. GC: Gulf of California. ETP: Eastern Tropical Pacific.

Location	*Date*	*Latitude*	*Longitude*	*N*	*Hap*
Alaska & Canada	2004-2005	56.94667	-135.75000	4	3
Canada '08	2008	58.81373	-133.63057	15	11
RBCM, Canada	2004-2005	48.88833	-125.58500	12	11
Oregon, USA	2005 & 2007	45.61058	-123.94430	21	17
Cordell Bank, California, USA	December 2006	37.86683	-123.51267	16	16
Monterey, California, USA	November 2004	36.33000	-122.90000	30	28
Pacific off México 1	August 2005	31.91380	-118.65820	7	6
Ensenada, Pacific, México	September 1999	31.83333	-116.61667	12	14
GC, México '99	1999	27.55879	-112.40106	32	26
GC, México '04-'06	2004-2006	27.55879	-112.40106	318	220
Pacific off México 2	September 2004	26.36583	-114.05833	17	16
Pacific off México 3	September 2005	25.83333	-117.12028	11	11
Topolobampo, GC, México	May 1999	25.60383	-109.04641	15	10
Magdalena Bay, GC, México	June 2005	24.57839	111.99979	30	24
Southern GC, México	June 2005	23.58617	-108.87283	39	27
México	2006	21.79533	-109.304	6	6
Southern México	October 2006	14.40783	-94.922	7	7
Costa Rica Dome	September 2006	7.48083	-85.02194	7	5
ETP	October 2006	-4.71667	-97.55000	90	38
Perú '07	2006-2007	-5.51635	-81.51822	27	14
Perú '06	December 2006	-8.77400	-79.57917	27	13
Chile '05	May 2005	-33.05000	-71.66670	28	16
Chile '06	August 2006	-38.65	-73.91667	31	18

Table 3-3. Sample locations and dates for *Sthenoteuthis oualaniensis*. N is the number of individuals sampled at each location. Hap is the number of haplotypes identified from that group. Total of 107 sequences. Latitude and longitude not included as a large area was covered in each location—see Figure 3-2 for marked sampling sites.

Location	*Date*	*N*	*Hap*
Eastern Tropical Pacific	October 2006	53	12
Central Tropical Pacific	2003	1	1
Central Tropical Pacific	May 2005	14	13
Central Tropical Pacific	May 2007	33	27

Table 3-4.

Pairwise F_{st} between 23 pooled populations of *Dosidicus gigas*, calculated with Kimura 2P. Values in bold are significant at $p<0.05$.

	AKCA	CA	RBCM	OR	COR	MBARI	PAC1	ENSE	GC99	GC04	PAC2	PAC3	TOP	MAG	SOU	MEX	SMEX	CR	ETP	Per07	Per06	Chi05	Chi07
Alaska&Canada	0.000																						
Canada	0.131	0.000																					
RBCM	0.058	-0.006	0.000																				
Oregon	0.056	0.001	-0.018	0.000																			
Cordell	0.029	-0.026	-0.012	-0.010	0.000																		
MBARI	0.047	0.007	-0.005	-0.022	-0.004	0.000																	
Pacific 1	**0.207**	-0.052	-0.035	0.008	-0.022	0.017	0.000																
Ensenada	-0.060	0.002	-0.030	-0.047	-0.043	-0.048	0.034	0.000															
GC 1999	0.071	-0.026	-0.046	-0.025	-0.056	-0.007	-0.029	-0.029	0.000														
GC 2004-2006	0.041	-0.015	-0.019	-0.035	-0.017	-0.015	-0.013	-0.036	-0.038	0.000													
Pacific 2	0.071	0.014	-0.034	-0.034	0.003	-0.019	0.006	-0.034	-0.015	-0.030	0.000												
Pacific 3	0.024	0.023	-0.015	-0.031	-0.006	-0.029	0.022	-0.063	-0.008	-0.023	-0.036	0.000											
Topolobampo	0.037	0.001	-0.001	-0.025	-0.012	-0.020	0.011	-0.043	-0.024	-0.028	-0.020	-0.024	0.000										
Magdalena Bay	0.019	-0.028	-0.072	-0.039	-0.049	-0.016	-0.022	-0.064	-0.079	-0.056	-0.048	-0.049	-0.035	0.000									
Southern Gulf	0.093	-0.024	-0.006	-0.009	-0.015	0.009	-0.019	-0.003	-0.027	-0.036	0.001	0.012	-0.009	-0.033	0.000								
Mexico	0.013	-0.004	0.011	0.014	-0.019	0.015	0.004	-0.027	-0.049	0.002	0.030	0.028	0.007	-0.035	0.008	0.000							
Southern Mex	0.040	-0.013	-0.003	-0.008	-0.014	0.003	-0.017	-0.022	-0.043	-0.019	0.000	0.004	-0.006	-0.045	-0.012	0.001	0.000						
Costa Rica	0.030	-0.012	0.000	0.002	-0.011	0.017	-0.020	-0.013	-0.057	-0.020	0.010	0.012	0.002	-0.055	-0.019	-0.004	-0.004	0.000					
ETP	**0.426**	**0.254**	**0.160**	**0.193**	**0.231**	**0.204**	**0.239**	**0.293**	**0.222**	**0.218**	**0.161**	**0.235**	**0.202**	**0.191**	**0.246**	**0.220**	**0.114**	**0.202**	0.000				
Peru 07	**0.425**	**0.223**	**0.118**	**0.136**	**0.190**	**0.153**	**0.238**	**0.243**	**0.220**	**0.165**	**0.112**	**0.165**	**0.144**	**0.155**	**0.207**	**0.181**	**0.097**	**0.145**	**0.023**	0.000			
Peru 06	**0.318**	**0.174**	**0.083**	**0.120**	**0.138**	**0.121**	**0.175**	**0.181**	**0.154**	**0.131**	**0.093**	**0.145**	**0.124**	**0.122**	**0.167**	**0.132**	**0.084**	**0.124**	0.006	**0.066**	0.000		
Chile 05	**0.305**	**0.176**	**0.092**	**0.112**	**0.141**	**0.123**	**0.180**	**0.170**	**0.151**	**0.131**	**0.090**	**0.127**	**0.122**	**0.103**	**0.164**	**0.144**	**0.086**	**0.126**	-0.003	0.018	0.003	0.000	
Chile 06	**0.262**	**0.152**	**0.075**	**0.101**	**0.119**	**0.108**	**0.143**	**0.149**	**0.110**	**0.112**	**0.081**	**0.117**	**0.110**	**0.084**	**0.143**	**0.124**	**0.077**	**0.110**	0.006	**0.041**	-0.010	-0.009	0.000

Table 3-5. Mantle lengths (mean ± standard deviation) of mature individuals (Stages 4 and 5) from samples representative of two size-at-maturity forms from the Northern and Southern groups of *Dosidicus gigas*.

Location	*Year*	*N*	*ML*	*Size-at-maturity form*
Mexico	1999	25	31.5 ± 4.1	Medium
Cordell Bank	2007	16	67.6 ± 4.6	Large
ETP	2006	79	32.8 ± 3.6	Medium
Chile ‘05	2005	30	72.1 ± 7.4	Large

Table 3-6. Pairwise genetic distances between and within *Sthenoteuthis oualaniensis* clades, calculated with Kimura 2P. Genetic distance as percentage=number of (corrected average) pairwise differences divided by total number of loci (1027), multiplied by 100. Bold values are significant at $p<0.05$.

	Pacific Typical	*Central Typical*	*Eastern Typical*	*Equatorial*
Pacific Typical	0.310			
Central Typical	**1.993**	0.259		
Eastern Typical	**4.202**	**4.716**	0.676	
Equatorial	**13.544**	**14.117**	**14.211**	0.195

Table 3-S1. Sample locations and dates of *Dosidicus gigas* (802 sequences total). Sites that appear in a single outlined box were pooled together for some analysis (see main text, Table 1). N is the number of individuals sampled at each location. Abbreviations: RBCM: Royal British Columbia Museum. GC: Gulf of California. ETP: Eastern Tropical Pacific.

Location	*Date*	*Latitude*	*Longitude*	*N*
Alaska, USA	October 2004	56.94667	-135.75000	2
Canada ‘05	August 2005	58.81373	-133.63057	2
Canada ‘08	2008	58.81373	-133.63057	15
RBCM, Canada ‘04	2004	48.88833	-125.58500	6
RBCM, Canada ‘05	2005	50.40611	-128.03667	6
Oregon, USA	September 2005	45.61058	-123.94430	2
Oregon, USA	August 2007	44.653	-125.118	19
Cordell Bank, California, USA	December 2006	37.86683	-123.51267	16
Monterey, California, USA	November 2004	36.33000	-122.90000	30
Pacific off México 1	August 2005	31.91380	-118.65820	7
Ensenada, Pacific, México	September 1999	31.83333	-116.61667	12
Punta Prieta, GC, México	March 1999	27.55879	-112.40106	7
San Bruno, GC, México	May 1999	26.22014	-111.41073	4
Santa Rosalía, GC, México	May 1999	27.34076	-112.27075	6
Volcán Marías, GC, México	May 1999	27.55879	-112.40106	15
Punta Prieta, GC, México	May 2006	27.55879	-112.40106	22
San Pedro Martír 5, GC, México	July 2006	28.52958	-112.78088	22
San Pedro Martír 6, GC, México	July 2006	28.32083	-112.16683	27
San Pedro Martír 7, GC, México	July 2006	28.20000	-112.33000	19
Santa Rosalía ‘04 1, GC, México	May 2004	27.34076	-112.27075	17
Santa Rosalía, ‘04 2 GC, México	October 2004	27.34076	-112.27075	49
Santa Rosalía ‘05 1, GC, México	June 2005	27.34076	-112.27075	30
Santa Rosalía ‘05 2, GC, México	July 2005	27.34076	-112.27075	29
Santa Rosalía, ‘05 3,GC, México	November 2005	27.34076	-112.27075	15
Santa Rosalía ‘06 1, GC, México	July 2006	27.34076	-112.27075	22
Santa Rosalía ‘06 2, GC, México	July 2006	27.34076	-112.27075	31
GC, México	August 2006	26.91733	-111.16133	1
Punta Marcial, GC, México	May 2006	25.72783	-111.25819	34
Pacific off México 2	September 2004	26.36583	-114.05833	17
Pacific off México 3	September 2005	25.83333	-117.12028	11
Topolobampo, GC, México	May 1999	25.60383	-109.04641	15
Magdalena Bay, GC, México	June 2005	24.57839	111.99979	30
Southern GC, México	June 2005	23.58617	-108.87283	39
México 1	August 2006	21.79533	-109.304	1
México 2	August 2006	19.86867	-108.623	3
México 3	August 2006	19.67083	-111.80167	1

México 4	November 2006	16.08667	-106.67833	1
Southern México 1	October 2006	14.40783	-94.922	6
Southern México 2	October 2006	9.60000	-96.46667	1
Costa Rica Dome 1	September 2006	7.48083	-85.02194	2
Costa Rica Dome 2	September 2006	8.75	-84.28333	3
Costa Rica Dome 3	September 2006	8.38083	-89.4765	2
ETP1	October 2006	-4.71667	-97.55000	14
ETP2	October 2006	-2.18333	-96.28333	72
ETP3	October 2006	0.48333	-95.33333	4
Perú ‘07	March 2007	-5.51635	-81.51822	25
ETP4	October 2006	-1.28333	-81.46667	1
ETP5	October 2006	-5.58167	-85.13833	1
Perú ‘06 3	December 2006	-8.77400	-79.57917	27
Chile ‘05	May 2005	-33.05000	-71.66670	28
Chile ‘06	August 2006	-38.65	-73.91667	31

Table 3-S2. *Dosidicus gigas* mitochondrial forward primers.

Name	Sequence	Location in Genome
SqIF	GAATGAACGGATTATATTGATG	972-993
DND3F	CCACGAATGAAATCAAGGATC	1339-1359
LCO 1490	GGTCAACAAATCATAAAGATATTGG	1438-1462 & 8461-8485
DCOF	CTGACCGAAATTTTAATACAAC	2047-2068 & 9070-9091
DCOF2	TGTCAACGTAACTTTCTTTCC	2675-2695 & 9698-9718
DgCO2F	AGCCCTTCCTTCATTACG	3186-3203 & 10209-10226
DgA6F	AAATGATAACATGATAGTAGAC	3862-3883 & 10891-10912
DgA6F2	AAATTGGTATTGGTATTATTC	4491-4511 & 11520-11540
Sq12SF	GTATAACCGCAGATGCTG	5384-5401
SqQF	TCCAAAAATTTACGTGCC	5804-5821
DNC3’F	GATCACCTGATAATTCTATACACAC	6309-6333 & 20220-20244
SqSF	GCTGCTAACTTTATTTTGAGC	7393-7413
DgN5F	CTCACATTAGTGTAAACATC	12075-12094
DgN5F2	GAAGCCAACTTCTAAAAGG	12706-12724
DgNF	GAAAAAACAATACATAACATAAG	14903-14925
DgCBF	AACGCAAAATGGCATAAGC	15463-15481
DgCBF2	TTAGCATGTACATAACGTAAC	16056-16076
SqLF	CTTAAATTCTATGCACTGATC	17864-17884
Dg16SF	AGATTAACCTTCGTCAAACC	18443-18466
SqGF	TTGTTTGGAAAACAAACRTACT	19640-19661
DgEF	GAAATTGAAAATCTCATGTGC	19718-19738

Table 3-S3. *Dosidicus gigas* mitochondrial reverse primers.

Name	Sequence	Location in Genome
SqCO3R	AGGTCAAGGACTATATTCTAC	25-45 & 6430-6450
DgCO3R2	GTCAGAAATAGAGAATGAGG	545-564 & 6950-6969
RSqI	CATCAATATAATCCGTTCATTC	972-993
DCOR2	ATTAGTCTTAGAGAAGTTCC	1503-1522 & 8526-8545
HCO2198	TAAACTTCAGGGTGACCAAAAAATCA	2121-2146 & 9144-9169
DgA6R	GTTCATGTTATAAAATGAGCTG	3924-3945 & 10953-10974
DgA6R2	GACTATTAATCTAAAACCACC	4076-4096 & 11105-11125
Dg12SR2	ATAACAGTTTGTGTATTGCTG	5014-5034
Dg12SR	TCGTTTTGTTTGTGTACATTG	5546-5566
DNC5'R	GTCTTCGAGATATGGCTAATAGAC	5912-5935 & 19829-19852
RSqS	GCTCAAAATAAAGTTAGCAGC	7393-7413
DND2R	AAAATAAATAAGAAGTTGGAAGG	7454-7476
SqND2R	AAGAGGGGCTAGYTTTTGYC	7839-7858
DgND5R	GATTCGTAAATGTATGTAGAG	13468-13488
DgN4R2	TTTGAACGAAATACTGTTTAG	13992-14012
DgND4R	TATTAGCTAGAAATTATTCTG	14512-14532
SqTR	CTAATTTTGGTTTACAAGACC	15069-15089
DgN1R2	CATTGGAAGTTAGAAATTGAG	16842-16862
DgN1R	TTTTCTAATTCTAAATATGCG	17436-17456
Dg16SR	TGCTTCTTTTAGTACGAGAG	18001-18020
16SAR	CGCCTGTTTATCAAAAACAT	18592-18611
Dg16SR2	GTTTACTAAATTGTGTTGAGG	19249-19269

Table 3-S4. PCR primers used for amplification of *D. gigas* mitochondrial DNA.

Primer Pair[1]	Fragment Range in MT Genome
DGEF / SqCO3R	19718-00045
DNC3'F / DCOR2	20220-1522
SqIF / HCO2198	972-2146
DCOF / DNC5'R	2047-5935
Sq12SF / SqCO3R	5384-6450
DNC3'F / SqND2R	6309-7858
SqSF / DGA6R2	7393-11125
DgA6F / SqTR	10891-15089
DgNF / Dg16SR	14903-18020
SqLF / DNC5'R	17864-19852

Table 3-S5. *Sthenoteuthis oualaniensis* forward primers.

Name	Sequence	Location in Genome
SoCO3F	CACCATTTTGGTTTTGAAG	685-703 & 7088-7106
SoAF	AGAAGATATGATTTGCAATC	831-850
SqIF	GAATGAACGGATTATATTGATG	972-993
DND3F	CCACGAATGAAATCAAGGATC	1340-1360
LCO 1490	GGTCAACAAATCATAAAGATATTGG	1436-1460 & 8458-8482
DCOF	CTGACCGAAATTTTAATACAAC	2045-2066 & 9067-9088
SoCOF	GTATTTGCTTTGTTTGCTGG	2569-2588 &9591-9610
SoCO2F	TGAACAGTTCCATCATTAGG	3443-3462 & 10465-10484
DgA6F	AAATGATAACATGATAGTAGAC	3860-3881 & 10882-10903
DgA6F2	AAATTGGTATTGGTATTATTC	4489-4509 & 11511-11531
SoA6F	TATCTTTGAAATTGGTATTGG	4481-4501 & 11503-11523
Sq12SF	GTATAACCGCAGATGCTG	5380-5398
SoCF	TGTTTCCTAAAGTTTGCAAC	5727-5746
SqQF	TCCAAAAATTTACGTGCC	5810-5827
SqSF	GCTGCTAACTTTATTTTGAGC	7389-7409
SoN5F	CCTCAAATAATGTAGAAAGA	12099-12118
SoN5F2	AGTAGGTGCTGCTATAGC	12674-12691
SDHF	TTTATCTGYAAGCCCACAAC	13325-13344
DgCBF	AACGCAAAATGGCATAAGC	15456-15474
SoCBF	AAAGAAGCACCATTAGCATG	16036-16055
SoND6F2	AAATTATAAARAAATATATAAATAC	16547-16571
SqLF	CTTAAATTCTATGCACTGATC	17857-17877
Dg16SF	AGATTAACCTTCGTCAAACC	18439-18458
DgEF	GAAATTGAAAATCTCATGTGC	19708-19728

Table 3-S6. *Sthenoteuthis oualaniensis* reverse primers.

Name	Sequence	Location in Genome
SqCO3R	AGGTCAAGGACTATATTCTAC	25-45 & 6428-6448
SoCO3R	TAGTTAGTGTTATAGATTGAG	473-493 & 6876-6896
RSqI	CATCAATATAATCCGTTCATTC	972-993
SCOR	GTTCGGTACGGATTATTAATC	1514-1534 & 8536-8566
HCO2198	TAAACTTCAGGGTGACCAAAAAATCA	2119-2144 & 9141-9166
SoCO2R	TAATGATGGAACTGTTCACG	3441-3460 & 10463-10482
DgA6R	GTTCATGTTATAAAATGAGCTG	3822-3943 & 10944-10965
SoA6R	TGGCTGCTAGTCGAATAG	4348-4365 & 11370-11387
Dg12SR2	ATAACAGTTTGTGTATTGCTG	5015-5035
So12SR	GAGAGTTTGATATAGTTAGTG	5425-5445
DNC5'R	GTCTTCGAGATATGGCTAATAGAC	5913-5936 & 19818-19841
RSqS	GCTCAAAATAAAGTTAGCAGC	7389-7409
SqND2R	AAGAGGGGCTAGYTTTTGYC	7836-7855
SoHR	TGGGCTTACAGATAAAAATTTC	13319-13372
SoND4R2	TTTCTAAATGAGATGTTGATC	13885-14005
SoND4R	GTTGATGCTGCTGGCTAG	14514-14531
SqTR	CTAATTTTGGTTTACAAGACC	15062-15082
SoCBR	GAAATTAGTATATTRTTCCC	15563-15582
SoCBR2	GGGATTGTGTTTAGTCGTTC	16173-16192
SoND1R2	GTACTTATCTTTTGATATGAG	16810-16830
SoND1R	TCTAAYTCTAAATATGCATT	17427-17446
Dg16SR	TGCTTCTTTTAGTACGAGAG	17993-18012
16SAR	CGCCTGTTTATCAAAAACAT	18584-18603
So16SR	ACAATACTGAATAAGGGTC	19316-19334

Table 3-S7. Additional *Sthenoteuthis oualaniensis* primers specific to the Pacific Typical clade.

Name	Sequence	Location in Genome
DS2ND4F	CTCACATGAACTTGCTTAAG	13832-13851
DS2N4LF	CTCTAATATAAATAAAACTGCC	14977-14998
DS2ND1F	CAAACCACATAATTATCATG	17252-17271
DS2N4R	ATTGGCGAGTAATTATTCGG	14501-14520
DS2CBR	ATTGAAATTAGTATATTATTTCC	15561-15583

Table 3-S8. Additional *Sthenoteuthis oualaniensis* primers specific to the Equatorial clade.

Name	Sequence	Location in Genome
WGNCF	CCTTATTCTTTATTTATAAC	6234-6253 & 20135-20154
WGN4LF	TTATCAAACTATTATCACTCC	14863-14883
WGCBF	AACCACACCAATATTTCAAG	15964-15983
WGCO2R	TATATTGACAATTTCTAGTG	3596-3615 & 10623-10642
WGN5R	CTGTTTTGGTGGTTCTAGG	12826-12844
WGN4R3	TGTGTGTAGAGAACATCTAC	13466-13485
WGN4R2	TTTGATAGGAGTATTCTTTC	14018-14037
WGN4R	GGAATATTAGTAGTATTGAGG	14562-14582
WGCBR2	CTAGTAATGTCTATTTGTGTC	15418-15438
WGCBR	ATAGTTATAAAGATTTATTTGG	15626-15647
WGND1R	TTGTTCCTCTGTGTTTCTAG	17499-17518

Table 3-S9. PCR Primers used for amplification of Eastern Typical clade of *Sthenoteuthis oualaniensis* mitochondrial DNA.

Primer Pair[1]	Region Amplified in MT Genome
DgEF / SCOR	19708-1534
DNC3'F / DgA6R	1340-3943
DCOF / DG12SR2	2045-5035
DgA6F / DNC5'R	3860-5936
Sq12SF / SqND2R	5380-7855
SqSF / DgA6R	7389-10965
DgA6F / SqTR	10882-15082
SoN5F / SoCBR	12099-15582
DGCBF / Dg16SR	15456-18012
SqLF / DNC5'R	17857-19841

Table 3-S10. PCR Primers used for amplification of the Pacific Typical clade of *Sthenoteuthis oualaniensis* mitochondrial DNA.

Primer Pair[1]	Region Amplified in MT Genome
DgEF / SCOR	19703-1532
DNC3'F / DgA6R	1338-3941
DCOF / DG12SR2	2043-5033
DgA6F / DNC5'R	3858-5931
SoCF / SqND2R	5722-7853
SqSF / DgA6R	7387-10963
DgA6F / DgND5R	10880-13478
SDHF / SoCBR2	13323-16190
DGCBF / Dg16SR	15454-18010
SqLF / DNC5'R	17855-19836

Table 3-S11. PCR Primers used for amplification of the Equatorial clade of *Sthenoteuthis oualaniensis* mitochondrial DNA.

Primer Pair[1]	Region Amplified in MT Genome
DgEF / RSqI	19719-00994
SoAF / SCOR	834-1545
SqIF / HCO2198	994-2155
DCOF / DG12SR2	2056-5049
DgA6F / DNC5'R	3870-5952
SoCF / RSqS	5742-7425
SoCO3F / SqND2R	7104-7871
SqSF / DgA6R	7405-10981
SoA6F / WGN4R3	11519-13485
SDHF / WGCBR	13340-15647
DGCBF / Dg16SR	15471-18027
SqLF / DNC5'R	17872-19852

The superscript 1 is used to remind the reader that specific primers may occur within either copy 1 or 2 of the duplicated regions of the mitochondrial genome, but the second primer defines the region amplified.

3.8. Figures

Figure 3-1. *Dosidicus gigas.* Locations of pooled samples. The Northern genetic group is indicated by black triangles, the Southern by white. The Equatorial Countercurrent is indicated flowing from west to east.

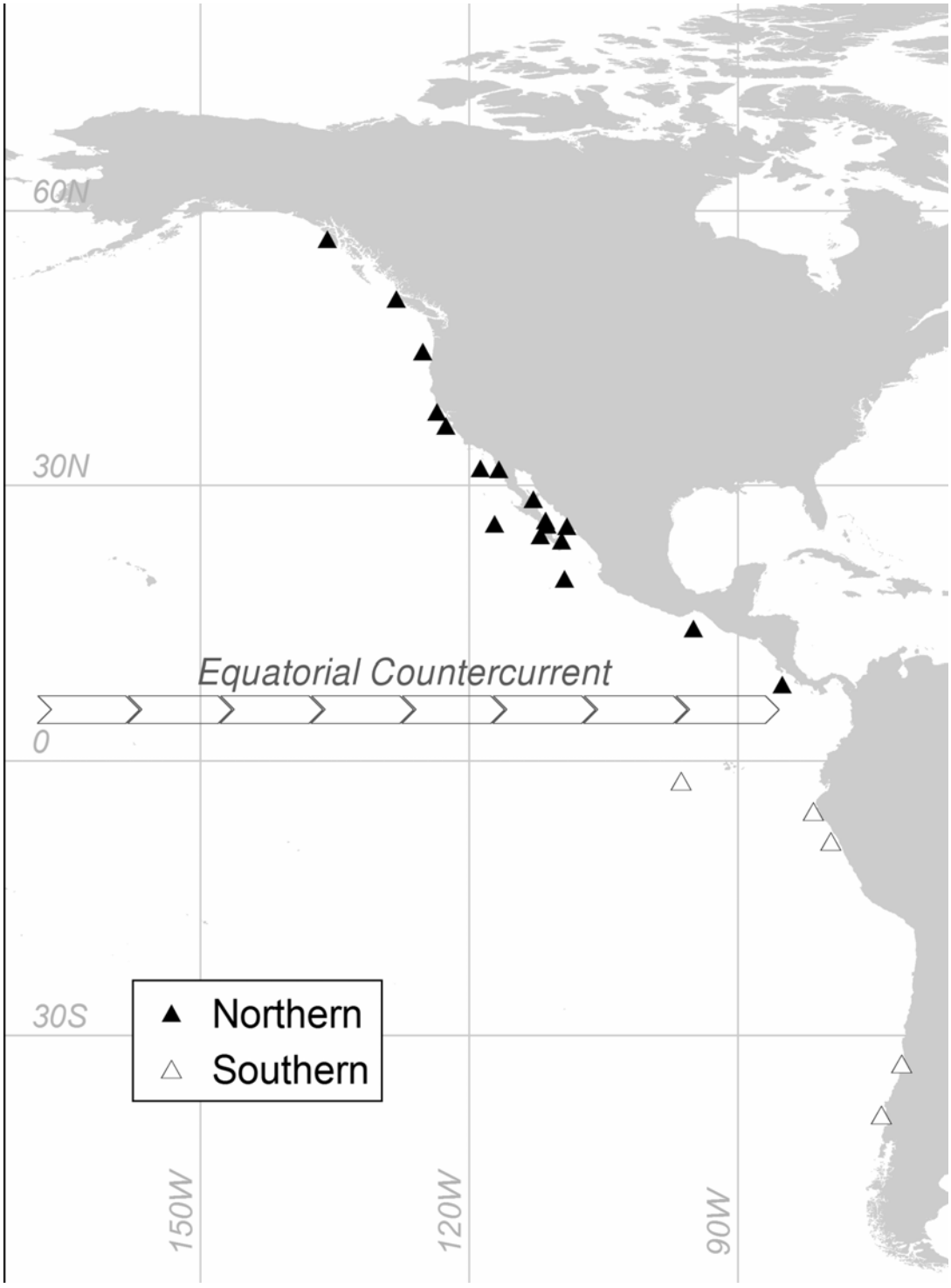

Figure 3-2. *Sthenoteuthis oualaniensis*. Geographic distributions of the four clades. Equatorial is indicated by white stars, Eastern Typical by light gray squares, Central Typical by dark gray triangles, and Pacific Typical by black circles. The Equatorial Countercurrent is indicated flowing from west to east.

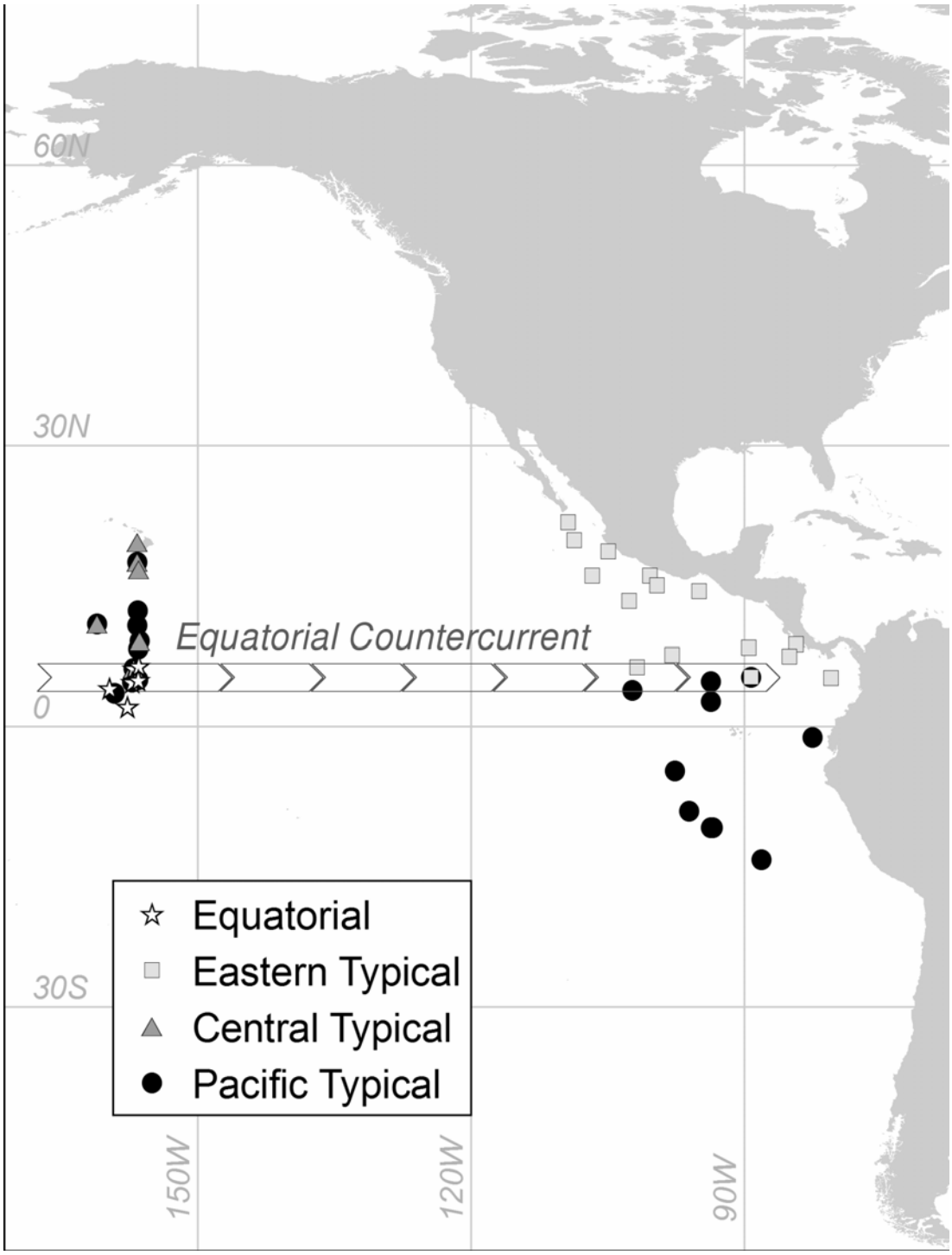

Figure 3-3. *Dosidicus gigas.* Isolation by distance of *Dosidicus gigas*. Slatkin's linearized pairwise F_{st} plotted against linear geographic distance between sites.

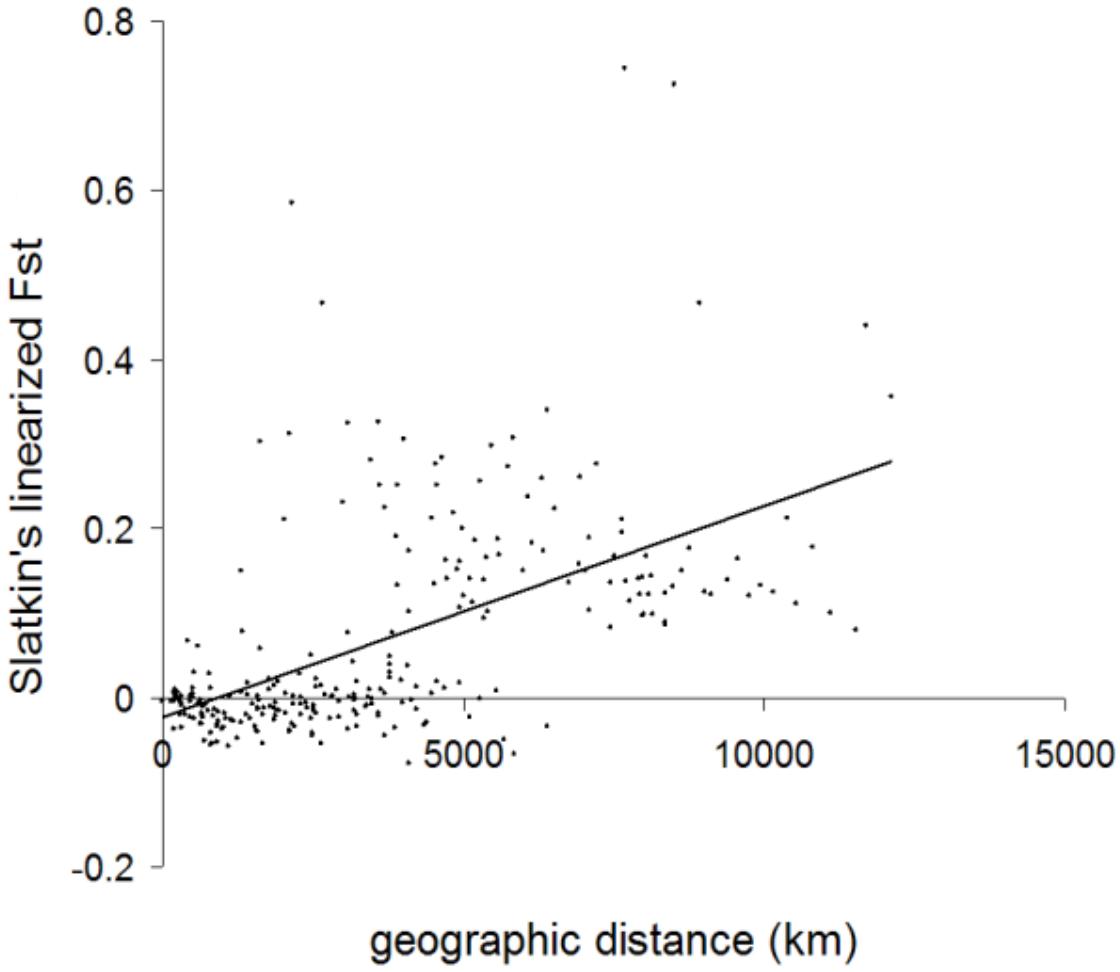

Figure 3-4. *Dosidicus gigas.* Network of the most common haplotypes of *Dosidicus gigas*. Each haplotype is represented by a pie chart. The size of the pie chart indicates how many total individuals were found with that particular haplotype. Black indicates individuals from Northern sampling sites, and white corresponds to Southern sites. Each line between haplotypes represents one nucleotide change, and small dots indicate "absent" haplotypes. Thus, two haplotypes separated by three small dots between them, and therefore four line segments, are separated by four nucleotide changes.

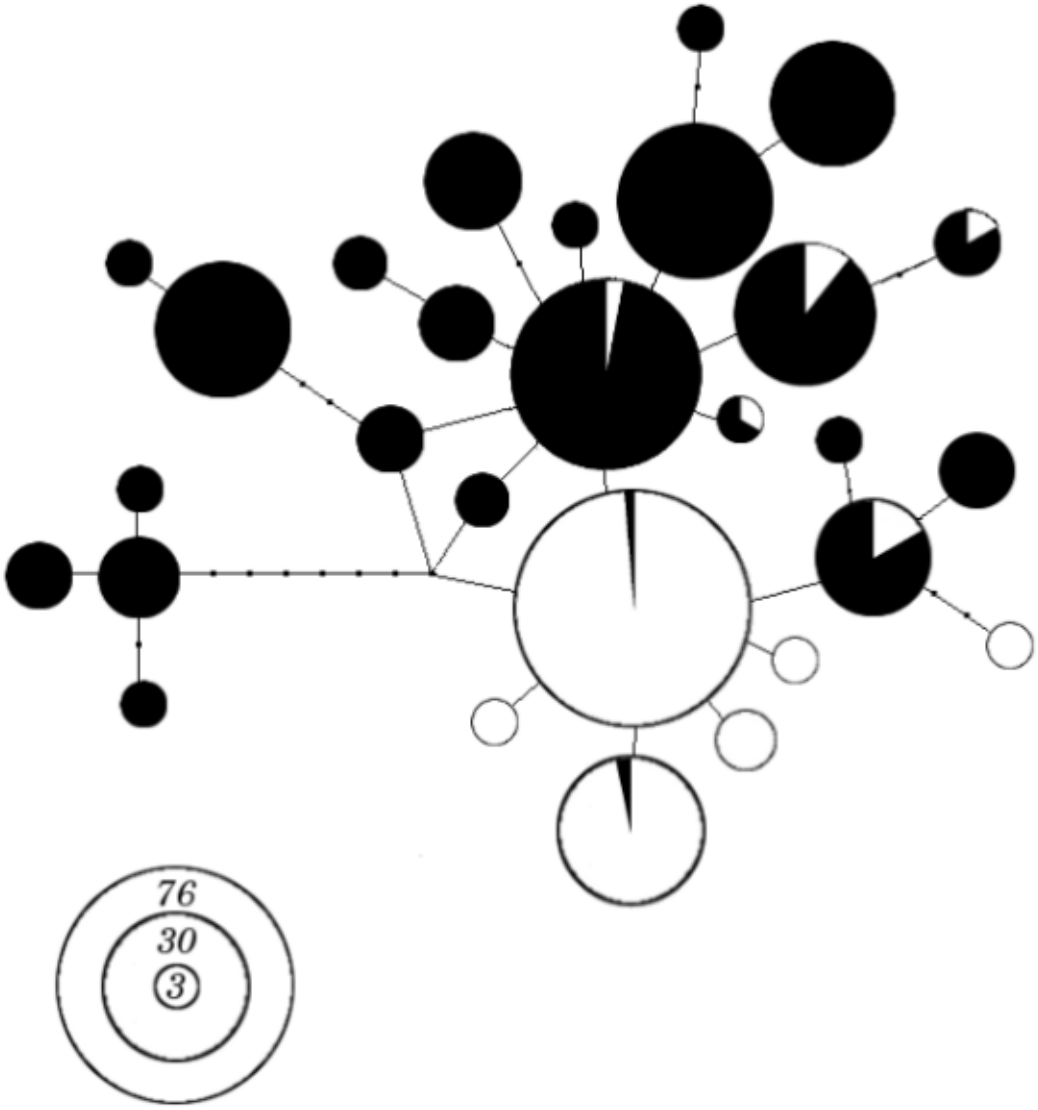

Figure 3-5. *Sthenoteuthis oualaniensis*. Maximum likelihood phylogeny of *Sthenoteuthis oualaniensis*, with *Dosidicus gigas* as an outgroup, using the GTR + I model of nucleotide substitution. Bootstrap values obtained from 1000 replicates are indicated for each clade. Specimen ID numbers were given according to the collector; the sampling locations of each clade can be seen in Figure 3-2.

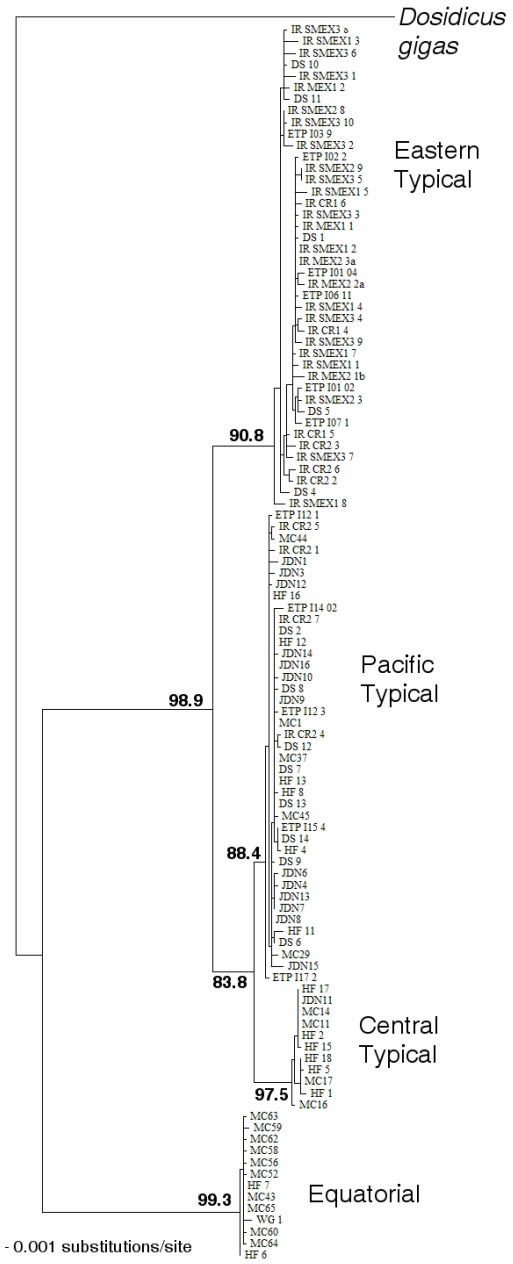

Chapter 4
Squid kids in hot water:
Ommastrephid paralarvae in the eastern tropical Pacific

4.1. Abstract

Dosidicus gigas and *Sthenoteuthis oualaniensis* (Teuthida: Ommastrephidae) are thought to spawn in the eastern tropical Pacific (ETP), an area of complex, variable oceanography. By studying plankton net tow and oceanographic data collected over 10 years in this region, we piece together the reproductive habits of these two ecologically and commercially important squid. Occurrence of ommastrephid paralarvae in both surface and subsurface plankton tows is influenced primarily by sea surface temperature, with paralarvae increasingly likely to occur at higher temperatures.

4.2. Introduction

Dosidicus gigas paralarvae have been reported from each of the major oceanographic regions in this species' range: the California Current, the Peru Current, and the eastern tropical Pacific. In some samples, they are conflated with paralarvae of *Sthenoteuthis oualaniensis*, and in the California Current, a number of additional ommastrephid species have been found.

Every year a small number of ommastrephid paralarvae, or rhynchoteuthions, are found in CalCOFI samples off the coast of California. All have been identified by the presence of unequal proboscis suckers as the genus *Ommastrephes* (W. Watson pers. comm.). Incidence of ommatrephid paralarvae increases to the south; Okutani and McGowan (1969) found only 1 of 17 unidentified rhynchoteuthions in Californian waters and the other 16 off the Pacific coast of the Baja California peninsula. Paralarvae definitely identified as *D. gigas* or *S. oulaniensis* have never been reported from California; the furthest north they have been found is Punta Eugenia, Baja California (Camarillo-Coop et al. 2006, Hernandez-Rivas et al. 2007, J. Ramos pers. comm.).

Five ommastrephid species have been identified off the Pacific coast of the Baja peninsula, based on juveniles that are large enough to identify morphologically: *D. gigas*, *S. oualaniensis*, *Eucleoteuthis luminosa*, *Hyaloteuthis pelagica,* and *Ommastrephes bartramii*. *D. gigas* has generally been the most abundant of these. Smaller paralarvae that cannot be distinguished to species are assigned to either the "SD complex" (*S. oualaniensis* and *D. gigas*,) or the "EHO complex" (the other three species). These two complexes cluster not only by morphology, but also by environmental conditions (Hernandez-Rivas et al. 2007), as *D. gigas* and the SD complex are associated with warmer subtropical waters on the Pacific coast of the Baja peninsula (Camarillo-Coop et al. 2006).

Curiously enough, on the other side of the Baja peninsula, the Gulf of California appears to be the exclusive spawning ground of *D. gigas*. No other ommastrephids, including *S. oualaniensis*, have been described from this region. Three areas within the Gulf have been identified as spawning grounds for *D. gigas*. In the San Pedro Martír Basin, putative mating behavior was observed in adults, and paralarvae and juveniles were captured and molecularly identified as *D. gigas* (Gilly et al. 2006a). In the Guaymas Basin, an egg mass was found and molecularly identified as *D. gigas* (Staaf et al. 2008), and in both Guaymas and Carmen basins, juveniles have been caught with dip nets and paralarvae with subsurface oblique tows (Camarillo-Coop et al. in press). Thus, inside the Gulf, any rhynchoteuthion of the SD complex is assumed to be *D. gigas,* even when molecular ID is not carried out.

Unlike the case of the California Current, the Peru Current in the southern hemisphere has yielded only samples of *D. gigas* paralarvae, captured with subsurface oblique-tows and identified with molecular techniques (Sakai et al. 2008). The situation thus resembles that in the Gulf of California.

However, in the eastern tropical Pacific (ETP), the large area between the Peru Current and the Gulf of California (Figure 4-1), both species are present. Unlike other regions, where the majority of sampling has been conducted with subsurface oblique-tows, the ETP has been sampled extensively with surface tows, and this method reveals higher densities of paralarvae. Vecchione (1999) reported extraordinary

abundances (>10,000 in a single tow) of very small paralarvae of the SD complex (either *Sthenoteuthis* or *Dosidicus*) from surface tows in the Costa Rica Dome area during the 1987-88 El Niño. Ueynagi and Nonaka (1993) also report high abundances of ommastrephid paralarvae in the ETP from a combination of both surface and subsurface tows. By contrast, Okutani's 1974 report of EASTROPAC data based on only subsurface tows had fairly low catches of ommastrephid paralarvae.

Method-dependent differences in paralarval abundance could reflect ontogenetic changes in vertical position in the water column. For example, one might expect a higher incidence of recently spawned, small paralarvae in shallower tows, and simply due to natural mortality, greater abundance as well. As paralarvae grew (with decreasing numbers due to mortality) and moved into greater depths, larger individuals might become more apparent in sub-surface tows. In the case of the ommastrephid *Todarodes pacificus*, the size of paralarvae increased significantly with depth at which sampling was carried out, and abundance decreased slightly, but not significantly (Yamamoto et al. 2002, 2007).

Diel vertical migrations could also underlie different abundances in surface and subsurface tows, as has been reported for loliginids (Zeidberg and Hamner 2002). Results are less certain for ommastrephids. Piatkowski et al. (1993) reported that *S. oualaniensis* paralarvae in the Arabian Sea were deeper during the day and shallower at night, but after considering vertical migration as a possible cause, they concluded that simple patchiness was the most compelling explanation. Young and Hirota (1990) had conflicting results for day vs. night abundance of ommastrephid paralarvae in Hawaii. From surface tows, both *O. bartramii* and *S. oualaniensis* were more abundant during the day than at night, whereas MOCNESS tows found more *O. bartramii* at the surface at night than during the day. However, sample sizes were low and results were statistically inconclusive. Earlier work in Hawaii (Harman and Young 1985) and Japan (Saito and Kubodera 1993) also found no difference in the abundance of *S. oualaniensis* between day and night.

The studies outlined above have provided tantalizing glimpses into the reproduction and early life of ommastrephid squid in the Eastern Pacific. However, to

date they have been highly localized in space and time, making generalizations difficult. On the other hand, NOAA ETP cruises have been regularly collecting and archiving oceanographic data and plankton samples over a large geographic area for many years.

The eastern tropical Pacific contains the entire region of range overlap between *Dosidicus gigas* and *Sthenoteuthis oualaniensis* (Figure 1-1). The oceanography of the region is complex, beginning with the entry of two eastern boundary currents: the California Current from the north, and the Peru Current from the south. Both currents divert westward as they approach the equator and tropical water. Thus, the equatorial region is dominated by east-west flowing currents, rather than north-south flowing currents (Figure 4-1).

Thermocline ridges occur along the boundaries between currents, where the thermocline is brought closer to the surface. The countercurrent thermocline ridge runs along 10° N and shoals ever shallower towards the continent, with a local minimum occurring at ~89° W. This area is known as the Costa Rica Dome, but its characteristics and exact geographic location vary seasonally and interannually (Fiedler and Talley 2006).

Water mass characteristics vary across the ETP. Warm, high-salinity Tropical Surface Water comprises both the North Equatorial Countercurrent and the Eastern Pacific Warm Pool off the coast of southern Mexico. Equatorial Surface water is colder throughout the year, reaching a temperature minimum in September-October (Fiedler and Talley 2006).

The thermocline in the ETP is strong and shallow and serves as a strong nutricline (Fiedler and Talley 2006). Whenever it approaches the surface, primary productivity increases. Relevant mechanisms include 1) wind mixing, as in the Costa Rica Dome and the gulfs of Central America, 2) coastal upwelling off the Baja peninsula and off Peru, or 3) equatorial upwelling along the cold tongue (Pennington et al. 2006). Zooplankton biomass tends to follow primary productivity in these regions, although variable ecologies split zooplankton taxa into biogeographic regions (Fernandez-Alamo and Farber-Lorda 2006). A goal of this study is to discover the

biogeographic region of *D. gigas* and *S. oualaniensis* paralarvae and infer ecological and reproductive characteristics of these species.

Here I present the first analysis of teuthoplankton (planktonic squid) from the NOAA dataset, focusing on the ommastrephids *Dosidicus gigas* and *Sthenoteuthis oualaniensis*. My aims are to uncover relationships between paralarval abundance and oceanography and to compare surface and subsurface tows to address questions of vertical migration. In addition, I use molecular techniques on a subset of samples to determine whether the two species have distinct spawning areas or habitat preferences within their range overlap.

4.3. Methods

4.3.1. Data collection

Plankton were sampled with net tows during cruises conducted by the Southwest Fisheries Science Center (NOAA Fisheries) from July to December of 1998, 1999, 2000, 2003, and 2006. The UNOLS research vessel *Endeavor* (1998), and the NOAA research vessels *David Starr Jordan* (all years), *McArthur* (1998, 1999, 2000), and *McArthur II* (2003, 2006) were used as platforms; tracklines for all ships for all years are shown in Figure 4-2. Net tows were conducted approximately 2 h after sunset on each day of the cruise, for a total of 979 manta (surface) tows and 762 bongo (oblique) tows over the eight-year period.

Manta nets (Brown and Cheng 1981) constructed of 0.505-mm nylon mesh were towed in the dark for 15 minutes at a ship speed of 1-2 knots. Bongo nets (McGowan and Brown 1966, Smith and Richardson 1977) consisted of a pair of circular net frames, 0.505-mm or 0.333-mm net mesh, and 0.333-mm cod-end mesh, and were towed in the dark for a 15-minute double oblique haul to ~200 m depth at a ship speed of 1.5-2 knots.

Volume of water filtered during manta and bongo tows was estimated with a flowmeter suspended across the center of the net. Contents of the cod ends were preserved in 5% formalin buffered with sodium borate. In the years 2003 and 2006, one cod end of each bongo tow was frozen in seawater at -20° C, while the other was

preserved in 5% formalin. Also in 2006, one cod end of every fourth bongo tow (38 samples total) was preserved in 70% ethanol instead of formalin.

Bongo (1998, 2000, 2003, 2006) and manta (1998, 1999, 2003, 2006) samples were sorted at the Southwest Fisheries Science Center in La Jolla, CA, by manual removal of all cephalopods, resulting in a total of 654 bongo and 784 manta tows sorted. Bongo samples with >25 ml of plankton were fractioned to ~50% of the original sample volume before sorting. Counts from both bongo and manta tows were adjusted for volume of water filtered, as computed from flowmeter readings, to give abundance per cubic meter.

The distinct rhynchoteuthion paralarvae of ommastrephids were easy to recognize by the presence of the proboscis (Figure 1-2). For individuals with a split or missing proboscis, ID was based on the characteristic inverted-T funnel-locking cartilage of this family. When proboscis suckers were visible, these were checked to separate *Ommastrephes* from *Dosidicus* and *Sthenoteuthis*. Given that *Ommastrephes* is relatively rare in the ETP (none of the molecularly identified ommastrephids in this study belonged to this genus, see also Yatsu 1999), any specimens damaged such that the terminal suckers could not be seen were assigned to the SD complex.

Morphological techniques for reliable differentiation between the rhychoteuthions of *Dosidicus gigas* and *Sthenoteuthis oualaniensis* are not available (Ramos-Castillejos et al. 2010). These authors found morphological indices that are statistically different between the two species, but do not permit identification of individual specimens. Wormuth et al. (1992) and Yatsu (1999) used proboscis length and photophores, but the muscular proboscis can extend and retract (Staaf et al. 2008), and there may be variability in ontogenetic timing of eye and intestinal photophores (Gilly et al. 2006a). Thus, we attempted no species-level identification of formalin-preserved SD complex specimens.

SD complex ommastrephids from ethanol-preserved samples were returned to Hopkins Marine Station in Monterey, CA, for molecular identification, which followed protocols outlined elsewhere (Gilly et al. 2006a). Two of the frozen bongo-net samples were also sent to Hopkins Marine Station for sorting and molecular

identification. The frozen samples were selected based on a high abundance of ommastrephid paralarvae in the matching cod end, and were sorted primarily to test whether it is possible to reliably identify paralarvae from a frozen plankton sample.

Mantle lengths of ommastrephid paralarvae from 1998 manta and bongo tows were measured with an ocular micrometer. For tows with 10 or fewer ommastrephids, all were measured; for tows with more than 10 ommastrephids, 10 were arbitrarily selected for measurement.

Oceanographic data were collected with conductivity-temperature-depth profilers (CTDs) before sunrise and after sunset and with expendable bathythermographs (XBTs) daily at 0900, 1200, and 1500 hrs (local ship time). Surface chlorophyll was measured at 1-3 m depth both from CTD bottles and surface bucket samples taken concurrently with XBT casts. Sea surface temperature (SST) and salinity (SSS) were measured continuously with a thermosalinograph while the ship was under way.

On the *McArthur II* in 2006, during one leg of the cruise, nightly jigging for adult squid was undertaken. Specimens captured in this way were identified to species based on the presence of a fused funnel-locking cartilage in *S. oualaniensis* and the absence of the fused structure in *D. gigas*.

4.3.2. Data analysis and modeling

I constructed a dataset of corrected ommastrephid paralarval abundance and five in situ oceanographic variables: SST, SSS, mixed layer depth, temperature at thermocline, and surface-concentration of chlorophyll a. Time of collection, latitude and longitude were all checked to ensure temporal and spatial matching of net tow and oceanographic data. Any data points with differences in collection location greater than 10 nautical miles, or differences in collection time greater than 12 h, were discarded. A total of 148 bongo and 176 manta samples were discarded by these criteria, leaving 506 bongo and 608 manta samples to analyze. A large portion of the discards (69 bongo and 71 manta) were lost from the McArthur in 2003, when the thermosalinograph did not operate correctly.

Relationships between ommastrephid abundance and oceanographic variables were explored with generalized linear models (GLMs) in the R statistics package (R Development Core Team, 2005). We chose to use GLMs based on their utility in modeling relationships between cetaceans and oceanographic habitat in the ETP (Redfern et al. 2006) and between cephalopod paralarvae and oceanographic habitat in western Iberia (Moreno et al. 2009).

As one might expect for biological counts, our paralarval abundance data are highly overdispersed, meaning that the dataset contains a large number of zeroes and a few very large samples. Following Moreno et al. (2009), we performed our analysis in two steps, using a binomial presence/absence dataset and a nonzero dataset of abundance at positive stations. Analysis of the binomial data allowed us to assess which oceanographic variables influence the probability of paralarval *occurrence*, while the nonzero dataset was used to assess which variables influence paralarval *abundance*.

To analyze the presence/absence dataset, we used a binomial distribution with a logit link, and for the nonzero dataset we used a gamma distribution with a log link. The volume of water filtered in each tow was used as an offset (i.e., to normalize) to the raw counts. We used an automated forward/backward stepwise approach based on Akaike's information criterion (AIC) to select the variables for inclusion in the model.

4.4. Results

4.4.1. Abundance

Ommastrephid paralarvae of the SD complex were found in 781 of the 1438 plankton tows with formalin-preserved samples. Broken down by net, 355 of 656 bongo tows (54.28%) and 426 of 784 manta tows (54.34%) were positive for paralarvae. The greatest abundance in a single manta tow was 1588 paralarvae, versus 64 paralarvae in a single bongo tow.

Abundance corrected for tow volume for all years is plotted in Figure 4-3 to show geographical distribution. Paralarvae of the SD complex taken in bongo tows

were distributed over a broader geographical area than those captured in manta tows (Figure 4-3), but density of paralarvae was substantially greater in manta tows.

4.4.2. Size

Average mantle length in manta tows was 1.94 ± 1.29 (n = 779) versus 1.86 ± 1.0 (n = 148) in bongo tows. The size range was 0.7-15 mm ML in manta samples and 0.6-7 mm ML in bongo samples. The greatest abundance in both types of nets was between 1 and 1.5 mm ML (Figure 4-4). No significant difference was found between these distributions (1-way ANOVA, p = 0 .44).

4.4.3. Relationship of abundance to environmental variables and modeling

Paralarval abundance is plotted against environmental predictors (SST, SSS, chlorophyll a, mixed layer depth, temperature at mixed layer depth, and year) for manta and bongo tows in Figs. 4.5 and 4.6, respectively. In general, paralarvae were found over a wide range for each variable, but the highest densities with both methods were found over comparably narrower ranges.

AIC values for various models of paralarval presence are shown in Table 4-1. The notably larger decreases in AIC achieved by SST compared to any other variables reveals SST as the strongest predictor of ommastrephid paralarval presence in both bongo and manta tows.

Analysis of non-zeros revealed no strong predictors of paralarval abundance in bongo tows. The step function selected both chlorophyll and SST as predictor variables in the final model (AIC = 1601), but each one only decreased AIC by 1. In manta tows, the step function diverged too much to solve.

The results of the binomial GLM were used to predict the probability of encountering ommastrephid paralarvae in manta or bongo tows as a function of SST (Figure 4-7). Raw binomial data are indicated as tick marks on this figure. For the purposes of this one-dimensional prediction, the other variables were set to their median values.

4.4.4. Species identification

A total of 95 ommastrephid paralarvae of the SD complex were found in twelve of the 37 ethanol-preserved tows. Of these, 79 were identified genetically as *Sthenoteuthis oualaniensis* and 16 as *Dosidicus gigas*. The area over which *S. oualaniensis* paralarvae were found was much greater that that for *D. gigas* (Figure 4-8A).

123 adult squid were jigged, consisting of 118 *D. gigas* and 5 *S. oualaniensis*. Adult *D. gigas* were found primarily in the southernmost sampling sites off Peru, whereas the few adult *S. oualaniensis* were more broadly distributed (Figure 4-8B).

From the two frozen samples, a total of 8 ommastrephid paralarvae were removed and identified molecularly as *S. oualaniensis*. It is clearly possible to extract and identify paralarvae from a frozen plankton sample.

4.5. Discussion

4.5.1. Vertical Distribution

Manta tows sampled only the top 15 cm of the water column. Bongo tows were double-oblique hauls, integrating across the entire water column from the surface to 200 m. Although it is not possible to know the exact depth at which a bongo paralarva was caught, the bongo net spends virtually no time shallower than 15 cm, and so the two nets are considered to sample different sections of the water column. We found no difference in the size of paralarvae between manta and bongo tows (Figure 4-4), in agreement with Yatsu (1999). This fails to support a hypothesis of ontogenetic vertical migration such as Yamamoto et al. (2002, 2007) proposed for *Todarodes pacificus*. Ontogenetic migration to depth may be a species-specific trait not common to all ommastrephids.

Diel, rather than ontogenetic, vertical migrations have been proposed for the paralarvae of various ommastrephids, including *S. oualaniensis*, but empirical results have been inconclusive at best (Harman and Young 1985, Young and Hirota 1990, Piatkowski et al. 1993, Saito and Kubodera 1993). Plankton tows for this study were all taken at night, shortly after sunset, and the frequency of positive samples was

strikingly similar between the two types of net: 54%. This is consistent with an early life history that does not include appreciable diel migration, but it does not rule out such migration. All of the bongo-caught specimens could have come from near-surface waters, and no daytime tows were done.

Although the *incidence* of capture in surface and subsurface tows was nearly identical, the *abundance* of paralarvae was much greater in surface tows. This seems surprising, when one considers that ommastrephid egg masses are neutral or slightly negatively buoyant (O'Dor and Balch 1985), and are never found at the surface. The only wild egg mass of *D. gigas* ever reported was found at 16 m depth (Staaf et al. 2008).

Nonetheless, finding paralarvae at the surface is common. Ueynagi and Nonaka (1993) found ommastrephid paralarvae in greatest abundance in surface tows in the ETP, compared to subsurface tows. Vecchione's (1999) tremendous abundances of SD complex paralarvae (12,354 individuals) came from surface tows, and Palomares-García et al. (2007) found 819 rhynchoteuthions using a surface net for 30 min off Jalisco, Mexico.

Paralarvae are themselves quite negatively buoyant (see Chapter 2), so finding them in great abundance at the surface suggests active swimming behavior to maintain that position. Paralarvae in the laboratory that swim to the surface of the water sink as soon as they stop swimming (Chapter 2), indicating that surface tension is insufficient for passive retention. Saito and Kubodera (1993) suggest that *S. oualaniensis* will remain near the surface except when avoiding unfavorable conditions. These authors found paralarvae in Japanese waters sinking below 30m depth to avoid surface salinity below 34 ppt. However, in the ETP we found many paralarvae in surface waters with even lower salinity; indeed, our highest abundance was in salinity of 33 ppt. We found little predictive value of salinity on abundance or incidence (Table 4-1, Figure 4-5). Perhaps some other condition of nearshore surface Japanese waters is unfavorable for *S. oualaniensis*, or perhaps it is a different population with different environmental preferences.

If paralarvae actively swim to the surface, what would drive such energy expenditure? Yamamoto et al. (2007) suggest nutrition as a motivation. The exact diet of ommastrephid paralarvae remains frustratingly elusive, but copepods and other zooplankton have been found in the guts of *Illex argentinus* from Brazil (Vidal and Haimovici 1998). The case has also been made for their use of dissolved and particulate organic material (O'Dor et al. 1985, Vidal and Haimovici 1998). Surface waters of the ocean can have high concentrations of these foods, although the depth of the chlorophyll maximum in the ETP ranges from surface waters in the coastal boundary regions to 60-90 m depth in the open-ocean regions (Pennington et al. 2006).

4.5.2. Oceanography

Our discovery that the probability of finding paralarvae in both bongo and manta nets increases with SST (Table 4-1, Figure 4-7) is consistent with the literature. The preference of *S. oualaniensis* for warm temperatures (28-31° C) has been documented by Saito and Kubodera (1993) in Japanese waters, and Vecchione's (1999) discovery of large numbers of SD complex paralarvae in 1987 was coincident with the 29° C SST isotherm, the warmest water then available. Similarly, in the Gulf of California, *D. gigas* paralarvae were preferentially found during the warm season, with mean monthly SST of 27.7 - 29.4° C (Camarillo-Coop et al. in press), and the only natural egg mass was found at 26° C at a depth of 16 m (Staaf et al. 2008). However, paralarvae have also been collected at lower temperatures in an upwelling region within the Gulf of California (17.8 – 22.7° C SST, Gilly et al. 2006a). Despite the lower probability of occurrence (Figure 4-7) at lower temperatures, it is important to note that the lowest SST measured in this study at which paralarvae were found was 17.1° C.

We found no decrease in paralarvae at extremely high temperatures--the highest SST at which paralarvae were found was 31.0° C, and the model generated a monotonic increasing relationship with temperature. This is interesting, given that *in vitro* developmental studies have shown a window for optimal temperature for development of *D. gigas* from 17-25° C, with 30° C apparently being too warm (see

Chapter 5). One possibility is that paralarvae can withstand warmer temperatures than eggs, in which case egg masses would be restricted to slightly cooler depths, and paralarvae could swim to the warmer surface waters after hatching. It is also possible that environmental differences between laboratory and field can make 30° C favorable or unfavorable for development. Relevant differences include the presence of natural egg jelly in the wild, a feature that may retard microbial growth and associated damage to the embryos.

Vecchione (1999) suggested that warm El Niño waters, when surface temperatures averaged 3.5 degrees warmer than during the same period of the following year, were probably the reason for the high abundance of 1987. Our strong positive relationship between paralarval occurrence and temperature is consistent with that hypothesis. We have no El Niño samples, as the 1997-1998 El Niño ended before the study period began, but our dataset includes 1998 La Niña conditions. Our peak abundances throughout the study remained an order of magnitude lower than the extraordinary abundance of 1987.

In general, zooplankton biomass in the ETP is highest in the four major upwelling regions: the Gulf of Tehuantepec, the Costa Rica Dome, the Equatorial Cold Tongue, and the coast of Peru (Fernandez-Alamo and Farber-Lorda 2006). Ommastrephid paralarvae were present more frequently in the Gulf of Tehuantepec and Costa Rica Dome than in the Equatorial Cold Tongue or off Peru (Figure 4-3), probably because the former are warm and the latter, cold. We found no relationship between SD complex paralarvae and primary productivity, as measured by chlorophyll or mixed layer depth (where the thermocline is shallow, primary productivity tends to be higher (Pennington et al. 2006)).

Although paralarvae are found in some areas of high productivity, it is possible that this association is not due to productivity, but rather to an aggregating mechanism of physical oceanography. Vecchione (1999) suggested anticyclonic eddies in the Costa Rica Dome region as just such a mechanism. Chlorophyll in this region was reduced by 50% during the El Niño of 1987, in comparison with previous years,

indicating that productivity was not a driver of the extraordinary abundance of paralarvae.

4.5.3. Species-specific spawning speculations

The SD complex of paralarvae treated in this study comprises two related species: *Sthenoteuthis oualaniensis* and *Dosidicus gigas*. *D. gigas* grows much larger and reaches into temperate and even subpolar waters, whereas *S. oualaniensis* ranges across the entire Pacific and into the Indian Ocean. Both are pelagic, but *S. oualaniensis* is more truly oceanic (Harman and Young 1985) and is not found in nearshore waters. *D. gigas* is much more associated with the continental margin (Figure 1-1).

Paralarvae can only be definitely identified to species by molecular methods, or if they are captured in an area where the other species is certain not to occur[1]. *S. oualaniensis*, for example, spawns in the western Pacific (Saito and Kubodera 1993), where no *D. gigas* has ever been reported, and the inverse is true for the Gulf of California (Gilly et al. 2006a, Staaf et al. 2008, Camarillo-Coop et al. in press).

Molecularly identified *D. gigas* paralarvae have been reported from inside the Gulf (Gilly et al. 2006a), off Peru (Wakayabashi 2008), and now in the ETP. However, we found that most molecularly identified paralarvae in the ETP were *Sthenoteuthis oualaniensis*. *Dosidicus gigas* only occurred in two samples, samples which also had *S. oualaniensis* in appreciable numbers, despite the greater abundance of adult *D. gigas* within the ETP (Figure 4-8). Neither the geographic locations nor the oceanographic features of these two sampling locations were distinct from locations where only *S. oualaniensis* was found, so we can say nothing about differences between the two species, except that *S. oualaniensis* paralarvae appear to be more abundant.

Yatsu (1999) attempted to distinguish between these two species in the ETP with a combination of proboscis length, photophore presence, and chromatophore

1 As it is commonly printed (e.g. Roper et al. 1984), the range of *S. oualaniensis* is in error, as it fails to include parts of Central and South America where *S. oualaniensis* adults have been found (see Chapter 3).

patterns for specimens larger than 3.5 mm ML. (Smaller specimens, 1.5-3.5 mm ML, were not identified to species.) As discussed above, these parameters are of questionable reliability. But if we accept his ID, we learn than *D. gigas* was found only in oblique tows, whereas *S. oualaniensis* occurred primarily in surface tows (70%). In the oblique tows, *D. gigas* was in slightly cooler temperatures compared to *S. oualaniensis*.

We found abundant *S. oualaniensis* and some *D. gigas* in subsurface tows, but we have no molecular ID from surface tows. It would be interesting to test the hypothesis that *D. gigas* paralarvae are found only in subsurface waters in the ETP. As surface waters are warmer than subsurface, it would also be necessary to test the related hypothesis that *S. oualaniensis* paralarvae prefer warmer water than *D. gigas* does.

Fishery catches of both species in the ETP indicate that cold water favors adult *D. gigas* over *S. oualaniensis* (Ichii et al. 2002). Further south, off Peru, the water is cold (18-20° C) and only paralarvae of *D. gigas* have been found (Sakai et al. 2008). However, *D. gigas* paralarvae in the Gulf of California can survive very warm water (29° C). And temperatures this high would seem ideal for *S. oualaniensis* as well, so why is this species absent from the Gulf?

Paralarval abundances of *S. oualaniensis* in Hawaii are greater offshore than inshore (Young and Hirota 1990), so a possible hypothesis is that *S. oualaniensis* only spawns in a truly open-ocean environment. *D. gigas*, meanwhile, may be a more nearshore animal. Off the Pacific coast of the Baja peninsula, *D. gigas* and the SD complex (which was probably dominated by *D. gigas*) were primarily found within 50 km of the coast (Hernandez-Rivas et al. 2007). Alternatively, or in addition, *D. gigas* are known to prey on ommastrephids (Markaida et al. 2007), and the large size of *D. gigas* in the Gulf of California (Nigmatullin et al. 2001) may make it such an effective predator on *S. oualaniensis* that the latter species cannot establish a population.

Whatever the cause, *S. oualaniensis* does not spawn within the Gulf. These squid can spawn off the western coast of Baja peninsula, but their paralarvae become more abundant as one moves south into warmer waters. The ETP Warm Pool may be

their primary spawning area, used to a lesser extent by the northern population of *D. gigas*, to supplement its primary spawning grounds off both sides of the Baja peninsula.

The southern hemisphere hosts an abundant and genetically distinguishable (see Chapter 2) population of *D. gigas*. It seems unlikely that these animals swim all the way to the Gulf of California to spawn, and Anderson and Rodhouse (2001) suggest that this southern stock spawns near the edge of the Peruvian shelf. Eggs and paralarvae may be carried north in the current, to mature in the circulating eddies where the Peru Current goes west into the South Equatorial Current, before returning to the shelf to spawn in their turn.

The contrasting findings of high unidentified ommastrephid paralarval abundance in the Costa Rica Dome (Vecchione 1999) and low adult catches of adult *D. gigas* off Peru after the El Niño of 1997-1998 (Waluda and Rodhouse 2006) are consistent with the hypothesis that the paralarvae found in the CR Dome were mostly *S. oualaniensis*. If any were *D. gigas*, they were likely spawned by adults of the northern population rather than the southern population, and probably migrated north as they matured.

4.6. Acknowledgements

A small army of dedicated people is necessary to collect the data for a long-term study such as this. I am deeply indebted to them all. To the coordinators who organized the cruises, the oceanographers who dropped nets in the water night after night, the students and contractors who sorted the tows, my boundless gratitude. The massive task of making sense of the oceanography data was also done largely by other dedicated souls. Bill Watson, Jessica Redfern, George Watters, and Mark Ohman were of immeasurable assistance. Annie Townsend went out of her way to help me with the ethanol-preserved samples, and Louisa Lorenzo lent a hand with sorting.

4.7. Table

Table 4-1.

Generalized Linear Models of presence/absence of ommastrephid paralarvae in manta and bongo tows based on four in situ oceanographic variables: sea surface temperature (SST), sea surface salinity (SSS), mixed layer depth (MLD), temperature at thermocline (TT) and surface-concentration of chlorophyll a. A stepwise approach selected SST, MLD, and TT for the final manta model, and SST, MLD, and SSS for the final bongo model. The resulting Akaike Informaiton Criteria (AIC) of these models were primarily driven by SST, with MLD, SSS, and TT contributing minimally.

Manta		*Bongo*	
model	**AIC**	**predictor**	**AIC**
SST x MLD x TT	750.3	SST x MLD x SSS	597.4
SST x MLD	759.3	SST x MLD	599.5
SST x TT	751.5	SST x SSS	605.5
MLD x TT	791.1	MLD x SSS	684.3

4.8. Figures

Figure 4-1. Oceanography of the eastern tropical Pacific (after Fiedler and Talley 2006).

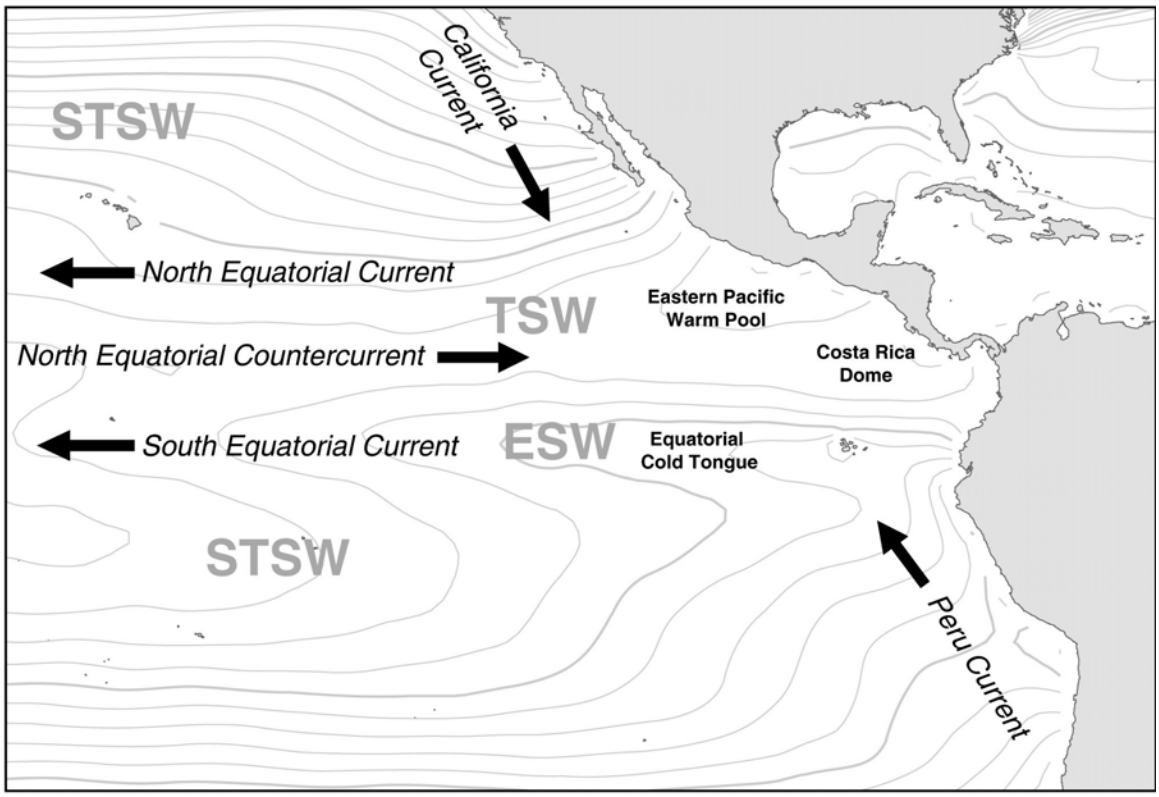

Figure 4-2. Tracklines of NOAA oceanographic surveys from 1998 to 2006. Plankton tows with manta and bongo nets were conducted at each station along the tracklines.

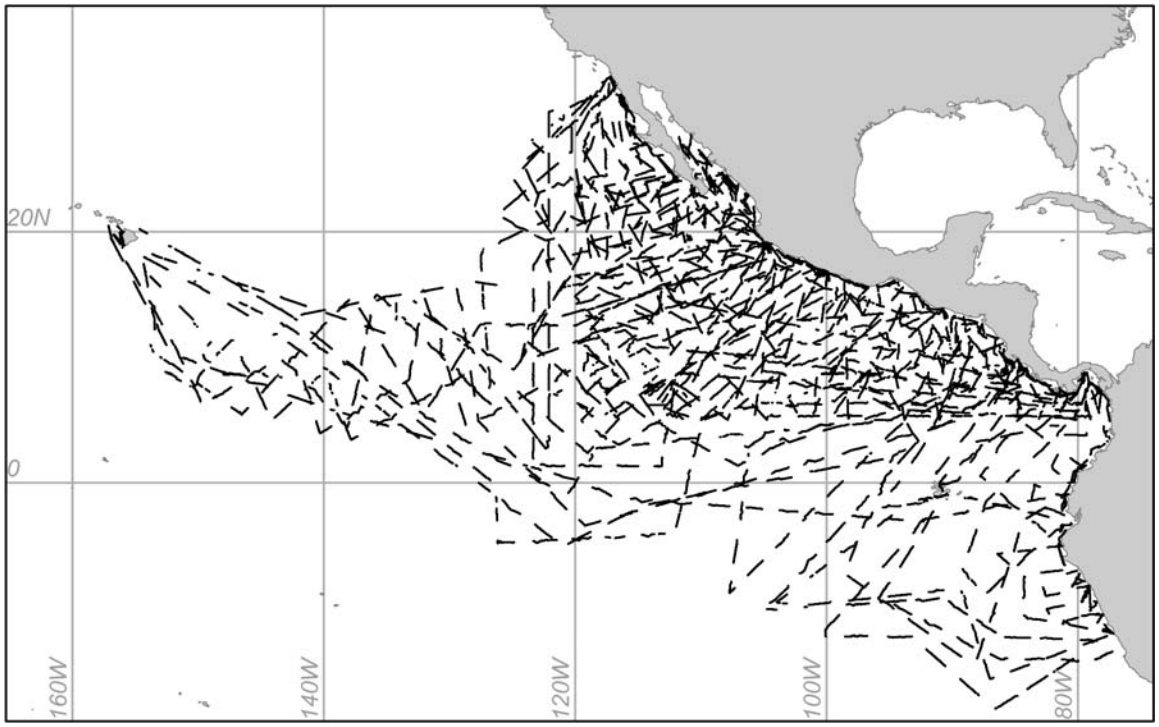

Figure 4-3. Abundance data from all years for A) manta and B) bongo tows. Interpolated with inverse distance weighting with a cell size of 1 and a fixed search radius of 5 map units.

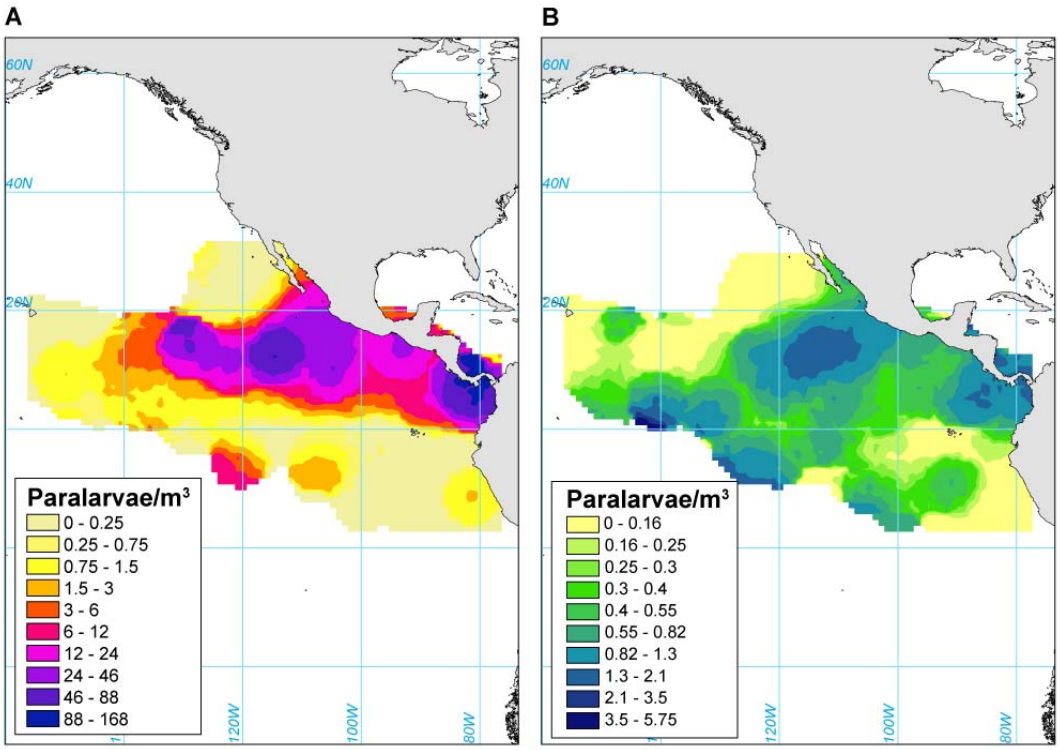

Figure 4-4. Distribution of mantle lengths in A) manta and B) bongo tows from 1998.

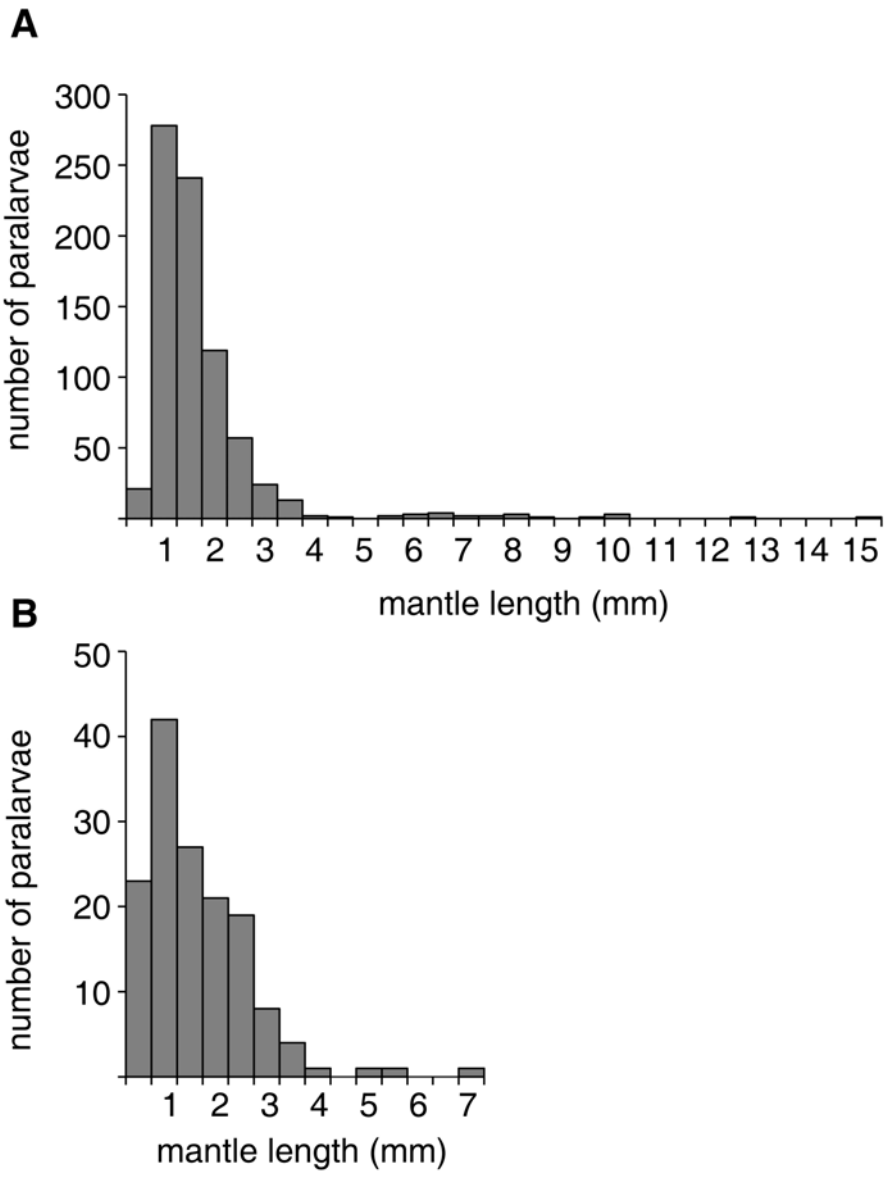

Figure 4-5. Ommastrephid paralarvae counts, including zeroes, in manta tows plotted against in situ oceanographic variables.

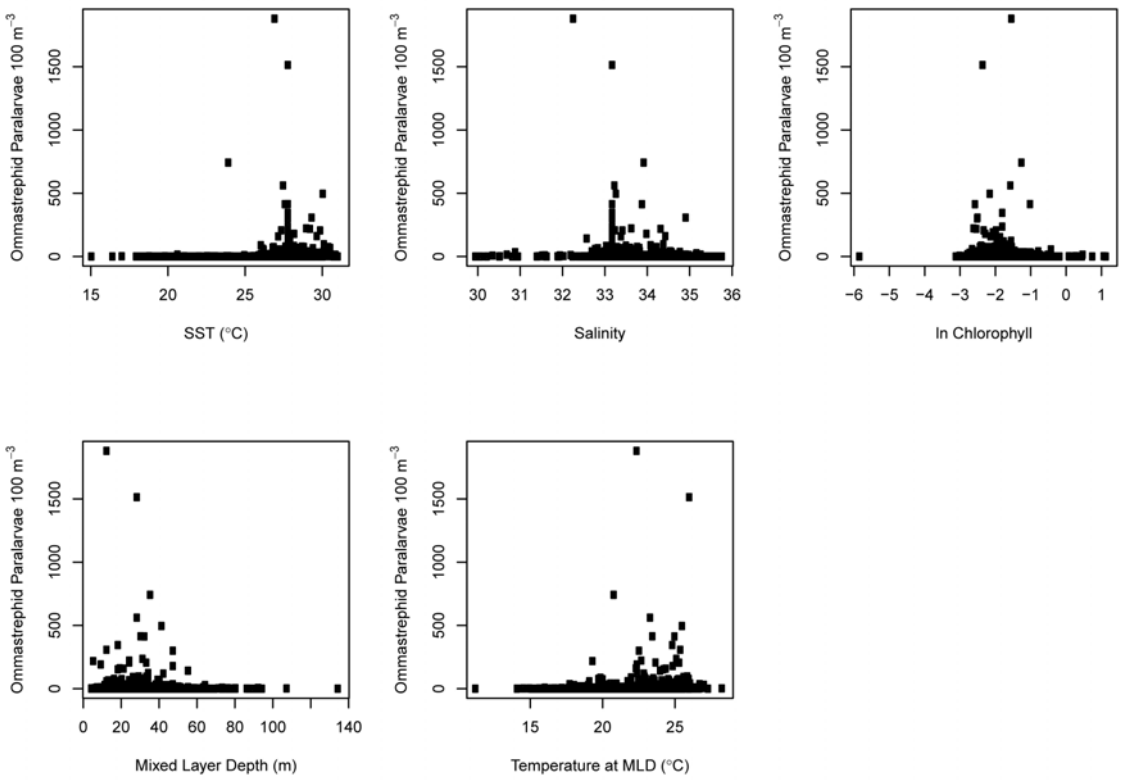

Figure 4-6. Ommastrephid paralarvae counts, including zeroes, in bongo tows plotted against *in situ* oceanographic variables.

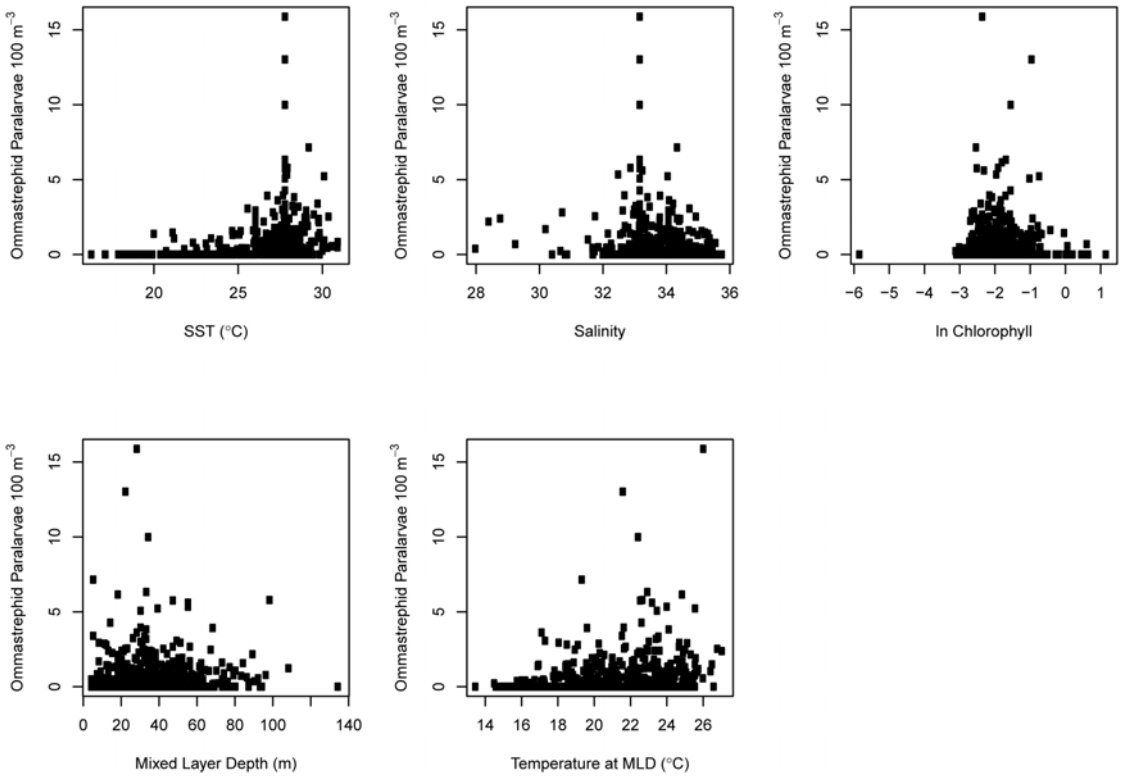

Figure 4-7. Probability of finding paralarvae as a function of sea surface temperature in manta and bongo tows. All other variables set to their median values. Dashed lines indicate standard error (SEM) intervals.

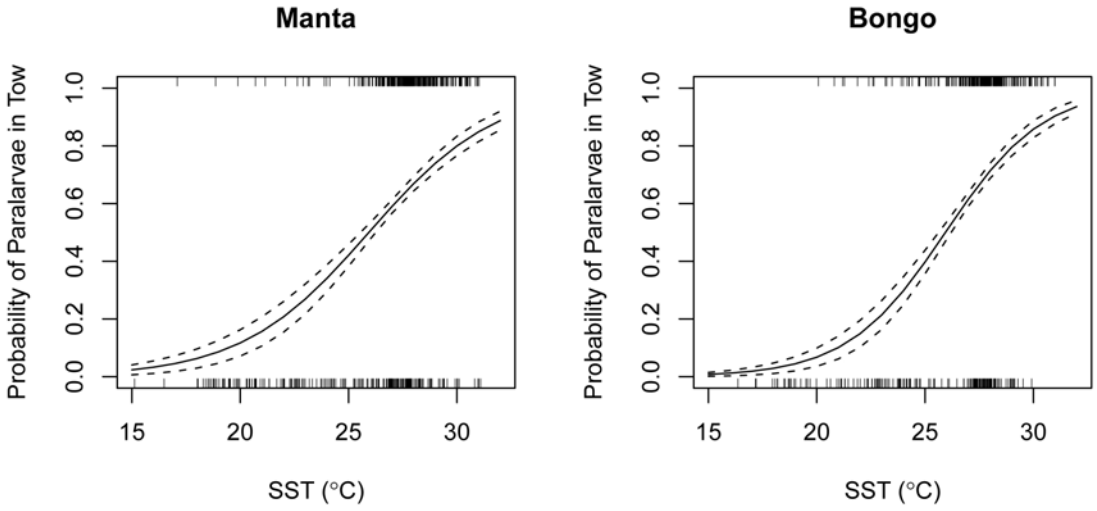

Figure 4-8. Geographic distribution and abundance of A) paralarvae and B) adults caught in 2006 and identified as either *Sthenoteuthis oualaniensis* (white) or *Dosidicus gigas* (black).

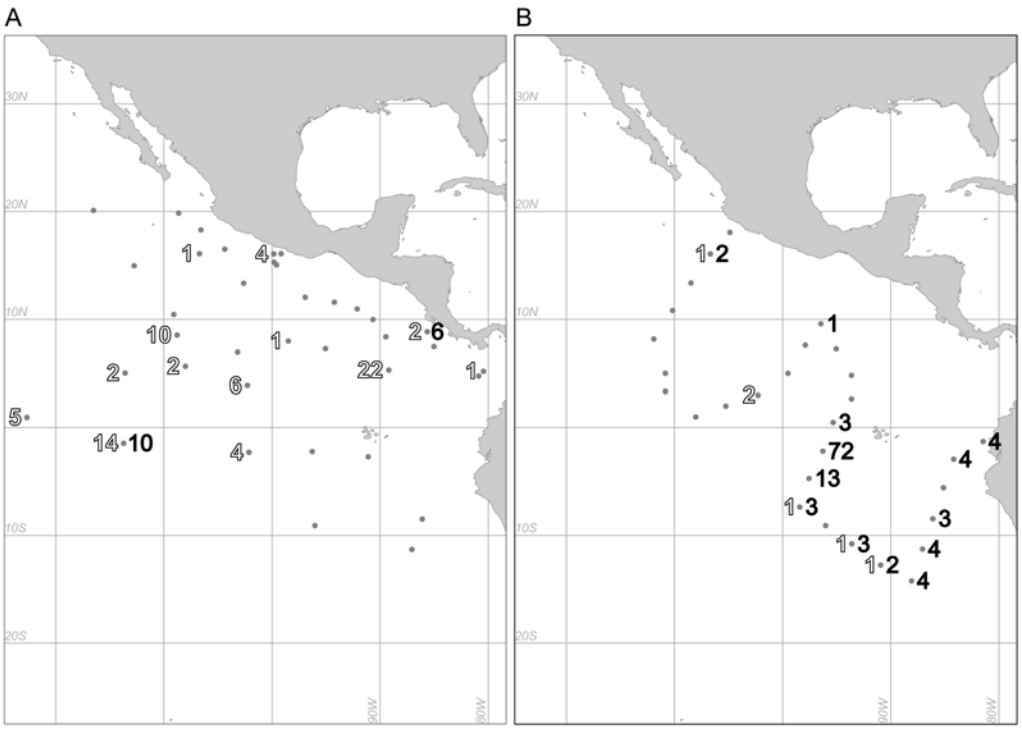

Chapter 5
Making squid babies:
Temperature effects on embryonic development

5.1. Abstract

Artificially fertilized eggs of the Humboldt squid *Dosidicus gigas* were exposed to temperatures found throughout the species' range (5-30 °C). Techniques to improve the notoriously low success rate of artificial fertilization of oceanic squid eggs were also explored. I discovered that unfertilized *D. gigas* eggs will undergo limited parthenogenesis, developing through blastodisc formation, which has not previously been described in cephalopods. Hatching was observed at 15 °C, and maximal hatching success occurred between 18 and 25 °C. Development of successfully fertilized eggs did not proceed to hatching at temperatures less than 15 °C. Development at 30 °C was also unsuccessful, although this may be an artifact of the *in vitro* technique. Rate of development increased with increasing temperature. These findings are used to discuss the geographic region over which *D. gigas* might naturally spawn and considered in the context of this species' recent range expansion.

5.2. Introduction

Embryonic development of cephalopods has received its best study in nearshore species that lay eggs on shallow substrates or in the laboratory. Naef (1928) used *Loligo vulgaris* to generate the first set of developmental stages for cephalopod embryos, and Arnold (1965) expanded these stages with *Loligo pealii*. The extremely large eggs of the cuttlefish *Sepia* have been of particular service to the field as a "showcase for cephalopod embryology" (Boletzky et al. 2006).

Although nearshore species have provided invaluable insight into cephalopod development, these findings can hardly be generalized to all cephalopods, given the remarkable diversity of this molluscan class. Cephalopods can be found from the deep sea to the intertidal zone, from hydrothermal vents to estuaries. Their lifestyles range from passive drifters to aggressive predators and their sizes cover over 3 orders of

magnitude. For many cephalopods, especially those of the open ocean and deep sea, reproduction has received essentially no study and naturally deposited eggs have never, or only rarely, been found in the wild. Adults are often difficult to impossible to keep alive in the laboratory, let alone coax into normal spawning behavior.

Thus, artificial fertilization of gametes collected from mature adults has stepped in to advance cephalopod embryology for a greater diversity of species. Artificial fertilization of squid eggs has been conducted for over a century to yield ample material for study of early cleavage stages (Watase 1891). But for almost a century, artificially fertilized eggs arrested before organogenesis, due to constriction of the chorionic membrane, which failed to expand to contain the developing embryo as it would in the wild (Arnold et al. 1974).

Since the primary missing ingredient from artificially fertilized eggs is the jelly produced by the female when she deposits eggs naturally, Klein and Jaffe (1984) cultured artificially fertilized eggs on a layer of agarose jelly, and obtained the first hatching from artificial fertilization. Arnold and O'Dor (1990) went a step further, and instead of agarose jelly, used a gelatinous material created from the freeze-dried accessory nidamental glands of *Loligo*. Fortunately, this worked to expand the chorions of four pelagic (non-loliginid) squid species. One of these, *Sthenoteuthis oualaniensis,* became the first ommastrephid to be successfully hatched from artificially fertilized eggs.

Ommastrephids do not have accessory nidamental glands as do loliginids; instead they have oviducal glands. Of the ommastrephid female reproductive organs, only material from the oviducal glands has been found effective in supporting chorion expansion (Sakurai and Ikeda 1994, Ikeda 1995). Sakurai and Ikeda (1994) successfully hatched *Todarodes pacificus*, and Sakurai et al. (1995) returned to *Sthenoteuthis oualaniensis* and added *Ommastrephes bartramii* to the list of species used successfully in this procedure.

Artificial fertilization of *Dosidicus gigas* was first accomplished by Yatsu et al. (1999), but with that achievement, the ommastrephid artificial fertilization boom of the 1990's seemed to end. Publications on the topic were not subsequently seen for

almost another decade, and even then it was only a brief mention (Staaf et al. 2008), in which the authors used oviducal gland from *D. gigas* itself, rather than from *O. bartramii*, which had been the standard material for all previous studies on ommastrephid artificial fertilization, regardless of the species that was being fertilized.

Development of *D. gigas* is of particular interest in the context of the recent range expansion of this species into the California current. Although adults are now abundant in this region, it remains unknown whether they are spawning in cold water or migrating south (or west) to warmer waters to spawn. Even if *D. gigas* did spawn in California waters, where sea surface temperatures are colder than the known spawning grounds of this species (Huyer 1983, Camarillo-Coop et al. in press), would the embryos develop? The range of temperatures for which development will proceed (window of successful development) varies tremendously among species. Preliminary temperature experiments on the development of ommastrephid squid (Arnold and O'Dor 1990) have covered only a narrow range of temperatures (22-26 °C) and have treated only *Sthenoteuthis oualaniensis*.

Here, I expand considerably on the work presented in Staaf et al. 2008 (Appendix A), including observations on unfertilized eggs, alterations of the artificial fertilization technique and, most importantly, temperature dependence over a full range of ecologically relevant temperatures.

5.3. Methods

Samples were collected in the Gulf of California, Mexico, on the R/V *New Horizon* from 8-22 June 2006 (NH06) and from 29 May to 12 June 2007 (NH07), on the R/V *Pacific Storm* from 16-24 March 2007 (PS07), and on the *Don Jose* from 10-16 May 2008 (DJ08). Samples were collected in waters off California on the David Starr Jordan from Cordell Bank from 13-15 November 07 (CB07), on a small NOAA boat from Soquel Canyon on 31 December 08 (SC08), on the *Hulicat* from Half Moon Bay on 11 January 2009 (HMB09), and on the *New Seaforth* from San Diego on 1 February 2010 (SD10). Samples were collected in the equatorial eastern Pacific on the R/V *MacArthur II* on 10 October 2006 (ETP06). Sampling locations are indicated in

Figure 5-1 and relevant details are summarized in Table 5-1. Specimens of *Dosidicus gigas* were captured with jigs on hand lines or rod and reel, immediately sacrificed by decapitation, and their mantles opened with a ventral cut.

5.3.1. Preparing oviducal gland powder

Oviducal glands were extracted from mature female *D. gigas* and frozen at -20 °C for up to one year. For lyophilization, frozen glands were cut with a razor blade, and small (approx. 1 cm^3) pieces were inserted into round-bottomed cryovials (Nunc, Roskilde, Denmark). A stainless steel ball was added to each vial. Each open vial was covered with a folded Kimwipe, affixed with a rubber band around the neck of the vial. The vials were all packed into a lyophilizer (Labconco, Kansas City, Mis.), and freeze-dried for 24 hours until completely dry.

After lyophilization, the vials were re-capped and shaken individually with a Wig-L-Bug (*Crescent Dental* Manufacturing Co., Lyons, Ill.) shaker. The presence of the ball bearings within the vials caused the dried gland to be ground into a fine powder. These vials of oviducal gland power, still containing balls, were kept frozen at -20 °C until use.

5.3.2. Gamete collection

Reproductive maturity of *D. gigas* is identified by six stages: I, immature; II and III, maturing; IV and V, mature; VI, spent (Lipiński and Underhill, 1995). Ripe eggs are characteristic of both stage IV and V females, but stage IV oviducts have fewer eggs, while stage V oviducts are packed full. Eggs from both stage IV and V females were used for artificial fertilization (Table 5-1). Stage VI females were never seen. Oviducts and the attached oviducal glands were manually removed without cutting, and the ripe eggs were obtained by either cutting the oviduct open with a clean razor blade or letting the eggs drip out through the oviducal gland. No qualitative difference in developmental success was noted between these two techniques for egg extraction.

Female *D. gigas*, in typical cephalopod fashion, can store sperm for some time after copulation. Stored sperm in the form of both spermatangia (discharged spermatophores attached to the skin) and spermathecae (seminal receptacles) was found in the buccal area of virtually all mature females examined. Spermatangia were pulled free with blunt-tipped tweezers. Sperm was extracted from spermathecae by squeezing the base with sharp-tipped tweezers. The sperm was then wiped off the tweezers into a small glass dish.

Spermatophores were also collected from mature males, which were identified by the abundance of spermatophores, either within the spermatophoric sac or loose in the penis and mantle cavity after extrusion from the penis. Mature spermatophores were collected from these regions.

Whenever possible, gametes were used for artificial fertilization within 1-2 hours, but when a greater delay was unavoidable, gametes were kept on ice. (See Table 5-1 for gamete storage times.) During the first artificial fertilization trials, I tested the effect of cold storage on viability by refrigerating gametes at 10 °C for 12 hours (NH06) and freezing at -20 °C for 12 hours (NH07) before attempting fertilization.

5.3.3. Artificial fertilization

Sterile tissue-culture plastic-ware was used whenever possible, and seawater was filtered through a 0.2 μm filter before use in all steps of artificial fertilization. In general, our techniques follow those of Yatsu et al. (1999), which in turn follow those of Sakurai and Ikeda (1994) and Sakurai et al. (1996).

For some experiments, antibiotics were added to the filtered seawater before use. Antibiotics consisted of 25 mg/L each ampicillin/penicillin and streptomycin (HyClone, Logan, Utah), the treatment used by Rosa and Seibel (2010) in respirometry experiments. This combination was briefly unavailable for one experiment, and 20 mg/ L trimethoprin was substituted (CB07). For DJ08 experiments, 50 mg/L ampicillin and streptomycin were added to a subset of dishes to test the effect of increasing antibiotic quantity.

Lyophilized oviducal gland powder was stirred into seawater (approximately 0.1 g/ 100 mL) to make 0.1% "jelly water." NH06 experiments used two sources of lyophilized oviducal gland. "LZ" had been frozen, lyophilized, and ground by L. Zeidberg, according to the technique outlined above. "CS" was lyophilized directly from fresh gland by C. Salinas and was not ground, so it consisted of larger flakes and pieces, rather than being a true powder. All subsequent experiments used a newer batch of powder, lyophilized according to the LZ protocol. DJ08 experiments included an oviducal gland powder treatment, a 0.5% bovine serum albumin (BSA) (0.5 g / 100 mL, following Crawford 2002) treatment, and a control with neither oviducal gland nor BSA. These three treatments were replicated in regular dishes, and in dishes prepared with a thin layer of 0.2% agarose, in an attempt to simulate the naturally gelatinous environment of the embryos (following Klein and Jaffe 1984).

Spermatophores or spermatangia were placed in a small, dry dish and a razor blade was used to chop them into several pieces each. Water was then added to the dish. Sperm extracted from spermathecae was simply diluted with the addition of water. Sperm motility was observed under a microscope before "sperm water" was used for fertilization. Sperm from spermatophores, spermatangia, and spermathecae all resulted in successful fertilization (NH06, DJ08), although post-fertilization developmental success was not quantified in these cases.

In NH06 experiments, I tested the effect of order of procedural steps when performing artificial fertilization. Sakurai et al. (1995) found that eggs must be immersed in seawater before they can be successfully fertilized, but that pre-treatment of eggs with the oviducal jelly-water was better accomplished with eggs that were simply removed from the oviduct and placed directly into a dry dish. Their protocol settled on adding sperm and jelly water to these eggs, prior to adding seawater.

I modified this protocol for "water last" treatments. Eggs were extracted from a female as described above and placed in a dry dish. Spermatophores were chopped as previously described, but water was not added to them. Rather, the chopped pieces were spread over the eggs with tweezers. Jelly water was added and, then, after 15 minutes, the dish was filled with seawater. For "water first" treatments, eggs were

extracted from the oviduct and placed directly into seawater. These eggs were transferred with a plastic pipette into a Petri dish filled with seawater. First sperm water, then jelly water was added to the eggs.

After finding no difference between these treatments on developmental success (Table 5-2, Pearson's Chi-squared = 1.96, df = 1, p = 0.16), I standardized the fertilization procedure. Eggs were placed in a dish, sperm water was added, then jelly water, then sufficient additional filtered water to fill the dish. Dishes were kept covered.

Starting with DJ08 experiments, I rinsed the eggs before and after fertilization by stirring them gently with a pipette in filtered seawater, then pipetting them into another clean dish with seawater and rinsing again (following Arnold and O'Dor 1990).

For PS07 and DJ08 experiments, tools and work surfaces were cleaned with 70% ethanol to enhance sterility. No positive effect was observed on hatching success (see Results), and the use of ethanol was abandoned for future experiments, although I strove to maintain a careful, clean technique.

Having made some puzzling observations of development in unfertilized eggs, I decided in SC08 and HMB09 to perform explicit unfertilized controls. These consisted of going through the technique outlined above without the addition of sperm.

5.3.4. Embryo care

Water was changed once daily (twice in NH06) by pipetting out water until the embryos were only just covered, then pouring in clean water, or by gently pipetting the eggs into a clean dish with clean water. The former technique was used when clean dishes were limited and the latter when they were not. The new water was always filtered and contained antibiotics according to treatment. In some cases, additional jelly water or BSA was also added with water changes (ETP06, DJ08, respectively).

During NH06, I attempted to keep eggs in small snap-cap vials, which could be easily floated in water baths for temperature control. However, development in vials

was unsuccessful, probably because of crowding and lack of oxygen (Strathmann and Strathmann 1995). All other experiments used 50 mm Petri dishes with lids.

Approximately 100 eggs were fertilized in each dish, with the exception of SD10, when I fertilized thousands of eggs in a large glass dish. In this case, successfully developing (cleaving) embryos were identified by observation with a stereomicroscope and gently removed 12-24 hours after fertilization with a glass pipette. Ten embryos were placed into each Petri dish.

Temperature control was accomplished with a combination of incubators, ambient room temperatures, and a temperature-control apparatus using Peltier plates that could maintain four individual dishes at different temperatures. During DJ08 experiments, some spikes in temperature occurred due to the apparatus overheating (see Results).

Temperatures were recorded every 1-2 hours at the beginning of experiments, and if they were stable, once per day thereafter. In most cases embryos were photographed at the time of water changes. Developmental stages of embryos were later assessed from these photographs as described below. For the SD10 experiments, developmental stage of each of the ten embryos was assessed and noted directly under the microscope, so no photographs were taken.

Dead embryos were removed as soon as they were observed.

5.3.5. Data analysis

For NH06, DJ08, SC09, and SD10, embryos were staged according to Watanabe's (1996) stages throughout the time course of development. The stages were grouped into five developmental categories, slightly modified from those of Watanabe (see Results, Tables 3.3 and 3.4). For NH07, CB07, PS08, and HMB09, only hatching success (or lack thereof) was noted.

Temperatures were taken to be the mean of measured temperatures throughout the experiment. Standard deviations were usually less than 1 °C. Ambient temperature treatments were more variable, with standard deviations of 1-3 °C, and one 5 °C

treatment had a SD of 1.18 °C. One 29 °C treatment had an SD of 3.01 °C, due to mechanical problems with the temperature-control apparatus.

5.4. Results

5.4.1. Maturity and size of adults

In Mexico, the majority of captured adult squid of both sexes were mature (Stages IV and V). In California, about half of the males were mature, whereas only a small fraction of females were mature. In the eastern tropical Pacific (ETP), nearly all males but few females were mature (Figure 5-2). Dorsal mantle lengths of the specimens (mean ± SD) were 51.4 ± 14.2 cm in Mexico, 58.1 ± 8.9 cm in California, and 32.4 ± 4.4 cm in the ETP. Significance of maturity differences within and between regions are shown in Table 5-5.

5.4.2. Development of unfertilized eggs

In experiments that omitted the addition of sperm, I observed the presence of a micropyle in unfertilized eggs, and found that expansion of the perivitelline space could be stimulated simply by addition of powdered oviducal gland. Furthermore, unfertilized eggs placed in seawater developed reliably to the formation of a blastodisc (Figure 5-3).

5.4.3. Development of fertilized eggs

I found it quite straightforward to stage *D. gigas* embryos according to the *Todarodes pacificus* atlas (Watanabe et al. 1996), so I will follow Yatsu et al. (1999) in presenting my results according to Watanabe's stages.

However, I will differ slightly in broad developmental categories. Watanabe et al. divided their 34 stages into 5 categories, 4 of which are true embryogenesis (pre-hatching) (Table 5-3). Having found that the three stages of Phase I, "Fertilization and Meiosis," do not actually require fertilization, I have re-named this phase "Meiosis and Blastodisc Formation."

I further divided “Organogenesis” in two categories: “Organogenesis” and “Pigmentation” (Table 5-4). The appearance of pigment marks the appearance of eyes and chromatophores, a developmental milestone that can be easily identified.

As for hatching stage, I have found it to be quite variable, occurring anywhere between stages 20 and 26.

5.4.4. Artificial fertilization methodology

NH06 gametes kept at 10 °C for 12 hours produced viable development. Gametes kept on ice for 48 hours (DJ08, CB07, SD10) also fertilized and developed successfully, but after 72 hours (CB07) development was not successful. Fertilization with frozen eggs and sperm (NH07) was not successful.

I found that using jelly water from oviducal gland material prepared by both LZ and CS methods resulted in fertilization and development (NH06), but chorion expansion was significantly greater with LZ powder (Table 5-2, one-way ANOVA, $p < .001$). Neither the order of events nor addition of antibiotic had any significant effect on chorion expansion (one-way ANOVAs, $p = 0.38$ and $p = 0.84$, respectively). Survival to 45 h was significantly greater with LZ powder (Table 5-2, Pearson’s Chi-squared = 85.49, df = 1, $p < 0.001$) and, within LZ-powder treatments, in those replicates in which antibiotic was added 22h after fertilization (Table 5-2, Pearson’s Chi-squared = 50.74, df = 1, $p < 0.001$). However, all embryos died before hatching.

In CB07 experiments, the use of antibiotics at fertilization increased hatching success from 0% in dishes without antibiotic to approximately 3% in those with antibiotic. However, the opposite trend was seen in PS07 experiments, with 0% hatching from antibiotic-treated dishes and up to approximately 10% hatching in dishes without. There was no obvious difference between the use of 25 mg/L and 50 mg/L antibiotic (DJ08).

I noted considerable variability among the developmental rates of eggs from individual females in NH06 experiments, when the time to develop to the same stage could vary by more than a day (Figure 5-4A). The maturity stage of the female (IV or V) seemed to affect hatching success. In PS07 experiments, fertilized eggs from a

stage IV female had 0% hatching, while those from stage V females reached up to approximately 10% hatching.

In DJ08 experiments, 0% hatching was observed in treatments with BSA and in the control without BSA or oviducal gland powder. All treatments in agarose-lined dishes failed to produce hatching. Only the treatment with oviducal gland powder and without agarose produced viable hatching (approximately 10% success).

5.4.5. Temperature effects

Developmental rate was clearly temperature-dependent, with colder embryos consistently developing more slowly than warmer embryos. The fastest development was observed at 18-25 °C (Figures 5.4, 5.5).

Developmental success was never high, but it was lowest at the high and low temperature extremes (Figure 5-6). Even in the middle of the temperature range, typically fewer than half of the fertilized eggs exhibited cleavage and less than a third reached blastoderm formation. Only about 10% entered organogenesis, and half or fewer of these hatched successfully. This can also be seen in Figure 5-5, in which each temperature treatment included only ten embryos that had been identified as successfully cleaving.

Hatching was only observed within the 15-25 °C temperature range (Figure 5-7). Embryos from one 10 °C treatment (SC08) reached stage 22 by 300 hours post-fertilization, a stage at which embryos at other temperatures had been seen to hatch (Figure 5-7), but these never hatched. In the literature, ommastrephid hatching has generally been reported no earlier than Stage 26, although artificially fertilized eggs always seem to hatch before naturally deposited ones (*Todarodes pacificus*, Watanabe et al. 1996, *D. gigas*, Staaf et al. 2008). It is tempting to classify stage 20 hatchlings (Figure 5-8) as premature, but I would suggest that we do not yet know enough about this group of squid to allow this conclusion.

Survival and growth of the hatchlings have already been reported and discussed elsewhere (Staaf et al. 2008, reprinted in Appendix A). Studies on their swimming behavior and kinematics are presented in Chapter 2.

5.5. Discussion

5.5.1. Artificial fertilization technique

Eggs can be kept at approximately 5-10 °C for up to 48 hours and remain viable. Huffard et al. (2007) found that sperm from spermatangia stored in filtered seawater at 12 °C remain viable for up to 5 days. This limits the application of the technique to seasons when mature squid are available, and the distance one can travel with gametes in 48 hours. One advantage of the 48-hour travel time is that fertilization need not be done on ship-board, as all prior ommastrephid fertilization studies have been; rather, gametes can be brought to a (possibly better equipped) terrestrial laboratory. Our results support those of Ikeda et al. (1993b) that sperm taken directly from mature males and stored sperm from females can both be used to fertilize eggs, so only one mature, mated female must be sacrificed to perform artificial fertilization.

I found considerable variability between females, possibly due to maturity state, with the eggs of more mature females developing more successfully. Kagan's (1935) observations of embryology in the killifish *Fundulus* may be equally applicable to *Dosidicus*: "*Eggs of different individuals vary so considerably that it was early found that experiments in which more than one female was used were valueless except that they convinced one of the variability factor.*"

Successful development of squid embryos requires chorion expansion, which in turn requires some kind of jelly, normally produced by the female's oviducal glands. Artificial fertilization has used agarose (Klein and Jaffe 1984), BSA (Crawford 2002), and lyophilized oviducal gland (Arnold and O'Dor 1990, Sakurai et al. 1995, Yatsu et al. 1999). In my experiments, I was able to obtain chorion expansion only with lyophilized oviducal gland. This may be broadly indicative of ommastrephid and perhaps oegopsid squid, as the success with agarose and BSA were found only in loliginids. Obviously, further experiments are needed to test the hypothesis that oegopsid embryos are "pickier" than myopsids.

As previously reported (Staaf et al. 2008), oviducal gland powder from *D. gigas* appears to work as well as that from *O. bartramii* (Yatsu et al. 1999) for

fertilizing *D. gigas* eggs, but not better, which would suggest that there is no species-specific component of the jelly.

Variable success was seen between the two techniques for lyophilization of oviducal gland. I suspect that the advantage of the LZ lyophilization technique is a minimization of microbial contaminants, perhaps through freezing. Arnold and O'Dor (1990) claimed that the lyophilization procedure sterilized *Loligo* nidamental gland, and if this is true, it should presumably have also sterilized the steel balls used in our preparation. However, sterilization of all materials by filtering, ethanol or UV treatment would probably be more reliable, and we suggest that in the future one of these techniques be used, to ensure that oviducal gland powder is truly sterile. In addition, any lubricant on the balls, which we did not attempt to remove, could have affected development. Degreasing with a suitable solvent, followed by washing, is recommended for future work.

Despite the use of sterile plastic-ware and antibiotics, microbial contamination remained a prominent concern in our experiments. It is interesting to note that the intact gelatinous matrix of a natural ommastrephid egg mass, generated by oviducal and nidamental glands, appears to protect the eggs within from microbial infection (Durward et al. 1980, Bower and Sakurai 1996, Staaf et al. 2008). Understanding this natural protective mechanism may be a critical step toward reducing laboratory mortality.

5.5.2. Partial parthenogenesis

Watanabe (1996) indicated that fertilization is followed by the appearance of the micropyle, but I observed the micropyle in unfertilized eggs of *D. gigas* (Figure 5-3). This observation has also been noted for unfertilized loliginid eggs (Arnold and Williams-Arnold, 1976). Furthermore, both Watanabe and Ikeda (1993) also associate expansion of the perivitelline space with post-fertilization development. In contrast, I found that expansion of the perivitelline space of unfertilized eggs could be simply stimulated by addition of reconstituted oviducal gland. Both of my observations

suggest that Watanabe's definition of broad developmental periods may merit reconsideration.

Finally, there is the formation of the blastodisc, which I found reliably in unfertilized eggs placed in seawater. Similar development of unfertilized eggs to the blastodisc stage, but not into cleavage, has been shown in teleost fishes (Kagan 1935, Okada 1961). Probably this has never been reported for squid before because the primary research interest is in fertilized eggs. However, in the case of *Fundulus* (Kagan 1935), once unfertilized eggs have developed blastodiscs, they cannot be fertilized, and thus the "fertilizable life" of *Fundulus* eggs is only 15-20 minutes. It would be important to figure out whether early parthenogenesis has also been inhibiting artificial fertilization for *D. gigas*.

5.5.3. Temperature Effects on Development and Relation to Range Expansion

This study represents the most thorough study to date of temperature effects on the development of *D. gigas* and extends previous limited work (Yatsu et al. 1999) that examined only two temperatures. My results indicate that optimal development *in vitro* occurs in the window of 18-25 °C (Figures 5.6 and 5.7). Development is slow and less successful, but hatching is possible, at 15 °C. Temperatures below 15 °C and above 25 °C do not appear to be permissive of complete development, although one experiment at 10 °C came tantalizingly close to producing hatchlings.

This upper thermal limit is close to that reported by Arnold and O'Dor (1990), who found that temperatures over 26 °C resulted in 100% embryo mortality of the ommastrephid squid *Sthenoteuthis oualaniensis,* a relative of *D. gigas* that shares its range in the eastern tropical Pacific. It is likely significant that the only wild egg mass of *D. gigas* thus far reported (Staaf et al. 2008) was found at 26 °C at a depth of 17 m below the surface in the Gulf of California (in more than 1000 m of water). Sea-surface temperatures in the Gulf of California, the best-studied spawning ground of *D. gigas*, often exceed 30 °C. Thus, in their natural environment, surrounded by a gelatinous egg mass in the open ocean, embryos may be more tolerant of high

temperature, but if 30 °C is indeed too hot for development, as laboratory results suggest, viable egg masses will be found only in the cooler depths.

The lower bound of the optimal window for development is intriguing in the context of the range expansion of this species. At temperatures between 5-15 °C, embryos don't hatch (this study) and hatchlings die (Staaf et al. 2008), but adults function effectively in the cool depths of the ocean (Gilly et al. 2006b).

Figure 5-8 illustrates seasonal average temperatures at 20 m depth (near the presumptive depth of natural egg masses) in the eastern Pacific, in 1 °C isotherms. The area corresponding to the 15-25 °C temperature range, at which I obtained successful hatching in the laboratory, is stippled. It is clear that the temperatures in the Gulf of California and off the Pacific coast of Baja California should be amenable to successful development of *D. gigas* during most of the year. Although temperatures immediately off the California coast appear to be too cool, a large body of suitable water is present offshore the US west coast in the summer (July-Sept in Figure 5-8). Adults captured in the far north of their range, therefore, are probably not spawning in nearshore environments where they were captured in this study, and are instead likely to migrate south (or west in some cases) to spawn. This proposed migration would be consistent with the higher proportion of mature squid of both sexes in Mexico relative to coastal California (where it is too cold for optimal development) and the eastern tropical Pacific (where it may be too warm for optimal development) (Figure 5-2).

The long-distance migratory capabilities of *Dosidicus gigas* remain a subject of some speculation, but maintained speeds of up to 30 km/day have been reported in the Gulf of California (Markaida et al. 2005, Gilly et al. 2006b). Longer migrations clearly occur in the Pacific Ocean, and one tagged squid traveled from Monterey, California to Ensenada, Mexico in 17 days, representing a maintained minimal speed of 35 km/day (J. Stewart, unpublished data). Such speeds would allow a migration between Canada and the Pacific coast of Baja California, a distance of some 2400 km, in less than 70 days. A squid born off the Pacific coast of Baja California could thus theoretically make a feeding migration to Canada and return to Baja California to

spawn in just several months. The estimated lifespan of *D. gigas* is 1-2 years (Markaida et al. 2004), consistent with this hypothesis.

However, it must be noted that in the summer, suitable spawning habitat (i.e., 15-20 °C at 20 m depth) is present only a little distance offshore from Oregon, Washington, and British Columbia (Figure 5-8). *D. gigas* may thus spawn in these offshore waters, which have not been extensively studied or sampled for planktonic squid paralarvae. If so, this immense, seasonal body of potential habitat could be a critical environmental feature related to the recent range northward expansion of this species and their long-term ecological success in this new environment. Studies like this one on *in vitro* development illuminate the *possible*, but they can only point to the necessity of *in situ* sampling to determine the *actual*.

5.6. Acknowledgements

Chad Widmer kindly shared his husbandry experience and incubators. Lou Zeidberg assisted with rearing embryos and trained me to make powdered oviducal gland. Cesar Salinas, Raul Ramirez-Rojo, Susana Camarillo-Coop, and Al Nyack were all part of the Gulf of California artificial fertilization crew, and Unai Markaida was our champion dip-netter. John Lee built the amazing "Peltier bomb" for temperature control, using control boxes donated by Stuart Thompson. John Field and Julie Stewart collected gametes even when it was not convenient to do so. The crews of the *New Horizon*, *Pacific Storm*, *Don Jose*, *Hulicat*, and *New Seaforth* were all incredibly generous, and this work could never have been done without them.

5.7. Tables

Table 5-1. Each set of artificial fertilization experiments is given a unique identity (ID), based on location and year. The table indicates for each experiment the number of females from which eggs were extracted, their stages of maturity, the source of sperm, the time and temperature of gamete storage before fertilization, and the experimental variables that were manipulated. Ab, antibiotic, OG, oviducal gland, BSA, bovine serum albumen.

ID	***Location***	***How many females***	***Female Stage***	***Sperm source***	***Gamete storage***	***Variables***
NH06	Gulf of California	3 for Ab 3 for temp 1 in refridge	V	male and female	used immediately some at 10 °C for 12 hr	10, 18-22 °C antibiotic Y/N order of events cold gametes female variability
ETP06	Eastern Tropical Pacific	1	IV	male	used immediately	14hr add OG again
NH07	Gulf of California	2 1 frozen	V	male	used immediately some at -20 °C for 12 hr	frozen gametes female variability
PS07	Gulf of California	2	IV, V	female	used immediately	antibiotic Y/N sterile tech female variability
CB07	Cordell Bank	3	V	male	~ 8 hr	15, 17, 20, 25 °C antibiotic Y/N gamete storage
DJ08	Gulf of California		V			14, 18, 20, 22, 25, 26, 29 °C antibiotic quantity BSA agarose sterile tech
SC08	Soquel Canyon	1	V	male	6 hr 30 hr	5, 10, 15, 18.5, 20, 25, 30 °C gamete storage
HMB09	Half Moon Bay	1	IV	female	8 hr	5, 10, 15, 18.5, 20, 25, 30 °C
SD10	San Diego	3	V	male	48 hr	4, 7.5, 10, 12.5, 15, 18 °C female variability

Table 5-2. Chorion expansion and survival for two different sources of oviducal gland powder and two different orders of events. Antibiotic was added 22 hours after fertilization, or not at all. Survival was measured 45 hours after fertilization. The chorion:embryo ratio is the longest dimension of the chorion divided by the longest dimension of the embryo, as measured from photographs.

		CS Gland		*LZ gland*	
		% survival	*chorion:embryo*	*% survival*	*chorion:embryo*
water first	*no antibiotic*	2	1.10 ± 0.06	15	1.18 ± 0.10
	Antibiotic	6	1.12 ± 0.04	74	1.17 ± 0.06
water last	*no antibiotic*	0	1.08 ± 0.06	8	1.20 ± 0.07
	Antibiotic	2	1.09 ± 0.06	67	1.17 ± 0.07

Table 5-3. Pre-hatching embryogenesis according to Watanabe et al. (1996) for *Todarodes pacificus*.

Category	***Stages***
Fertilization and Meiosis	1-3
Cleavage	4-10
Germ Layers and Growth of Blastoderm	11-15
Organogenesis	16-26

Table 5-4. Pre-hatching embryogenesis proposed for *Dosidicus gigas*.

Category	***Stages***
Meiosis and Blastodisc Formation	1-3
Cleavage	4-10
Germ Layers and Growth of Blastoderm	11-15
Organogenesis	16-19
Pigmentation	20-26

Table 5-5. Differences in maturity of male and female *Dosidicus gigas* within and between sampling regions, measured with Chi-squared test, df = 1. χ^2 values for comparisons of male maturity between regions are below the diagonal; comparisons of female maturity between regions are above the diagonal; comparisons between male and female maturity within a region are shown on the diagonal. ETP, Eastern Tropical Pacific. ** indicates $p < 0.01$; * indicates $p < .05$; $^{+}$ indicates $p < 0.1$.

	California	Mexico	ETP
California	39.36^{**}	68.01^{**}	5.36^{*}
Mexico	3.26^{+}	0.1345	28.86^{**}
ETP	15.97	4.36^{*}	43.90^{**}

5.8. Figures

Figure 5-1. Biogeographic distribution of *Dosidicus gigas*, including recent range expansion. Historical range is colored red, 2002 range is orange, and 2010 range is yellow. Yellow circles mark locations where adult *D. gigas* were sampled to collect gametes for artificial fertilization.

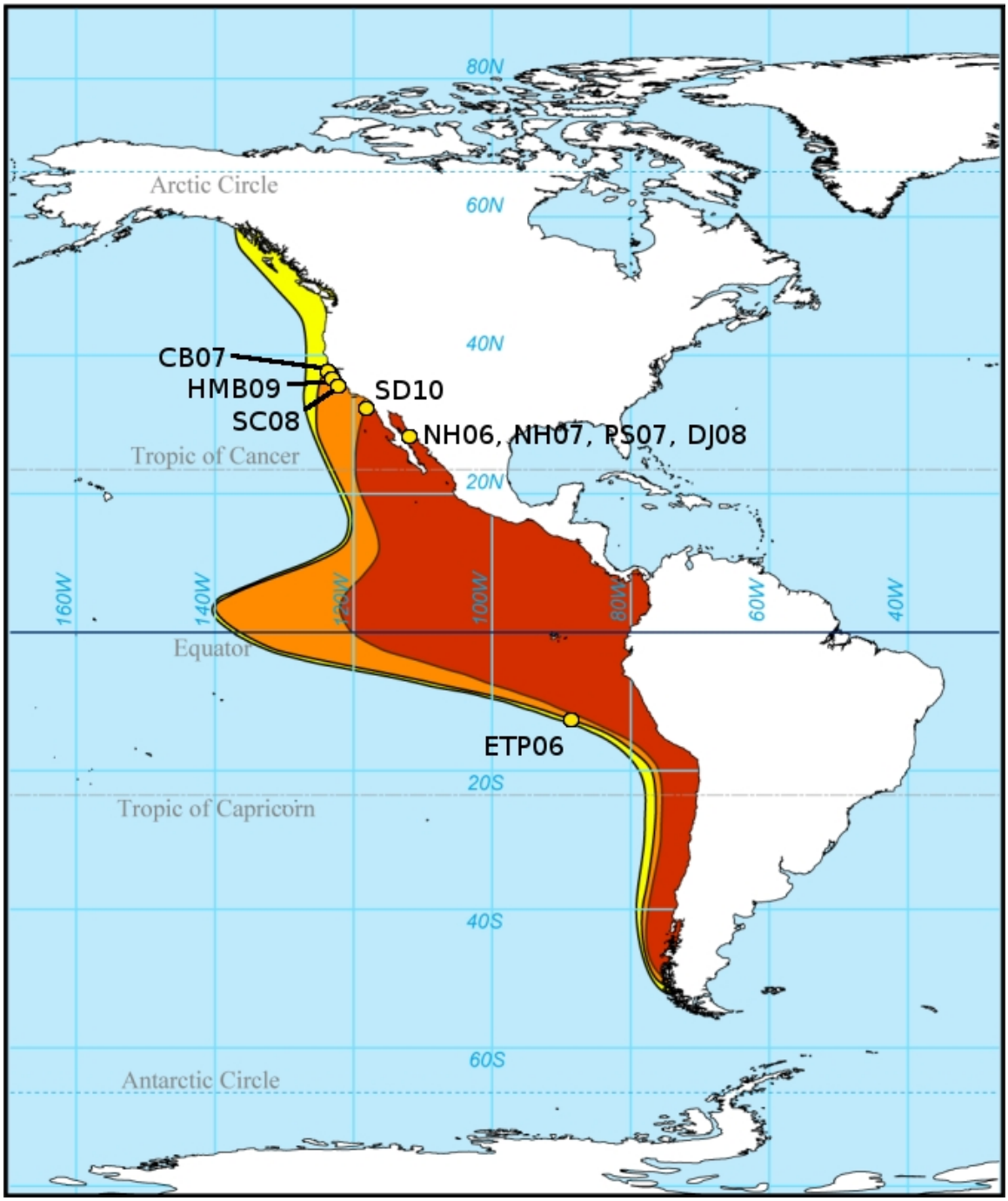

Figure 5-2. Percent maturity of adult *Dosidicus gigas* captured in California, Mexico, and the eastern tropical Pacific (ETP).

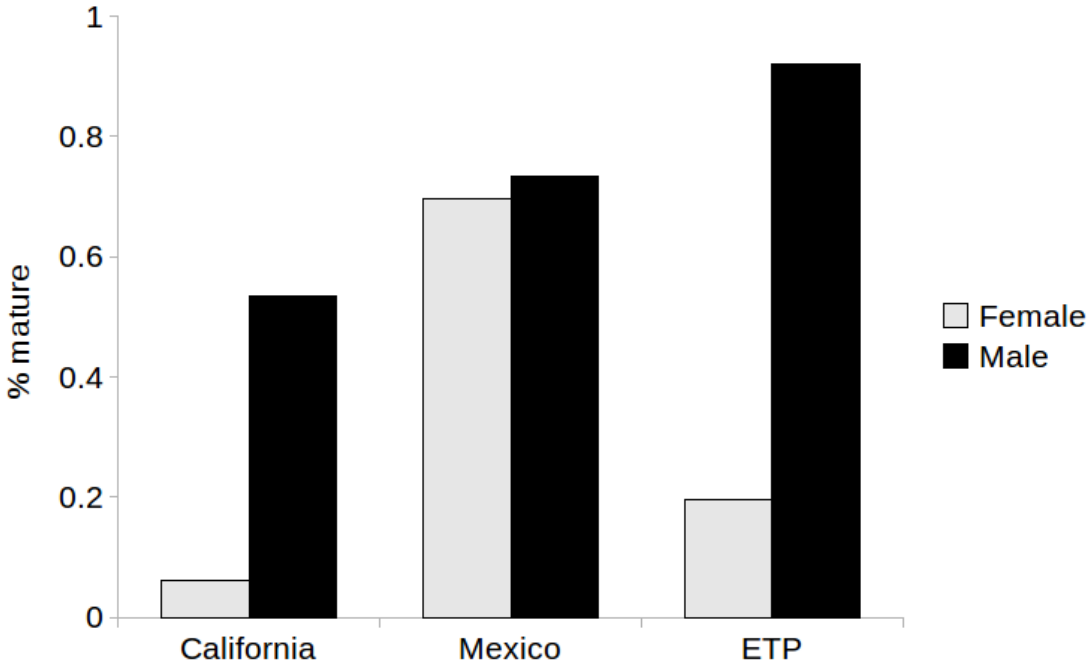

Figure 5-3. Partial parthenogenesis in an unfertilized egg of *Dosidicus gigas.* Labels indicate the micropyle (mp), blastodisc (bd), and expanded perivitelline space (ps), features previously associated with fertilization.

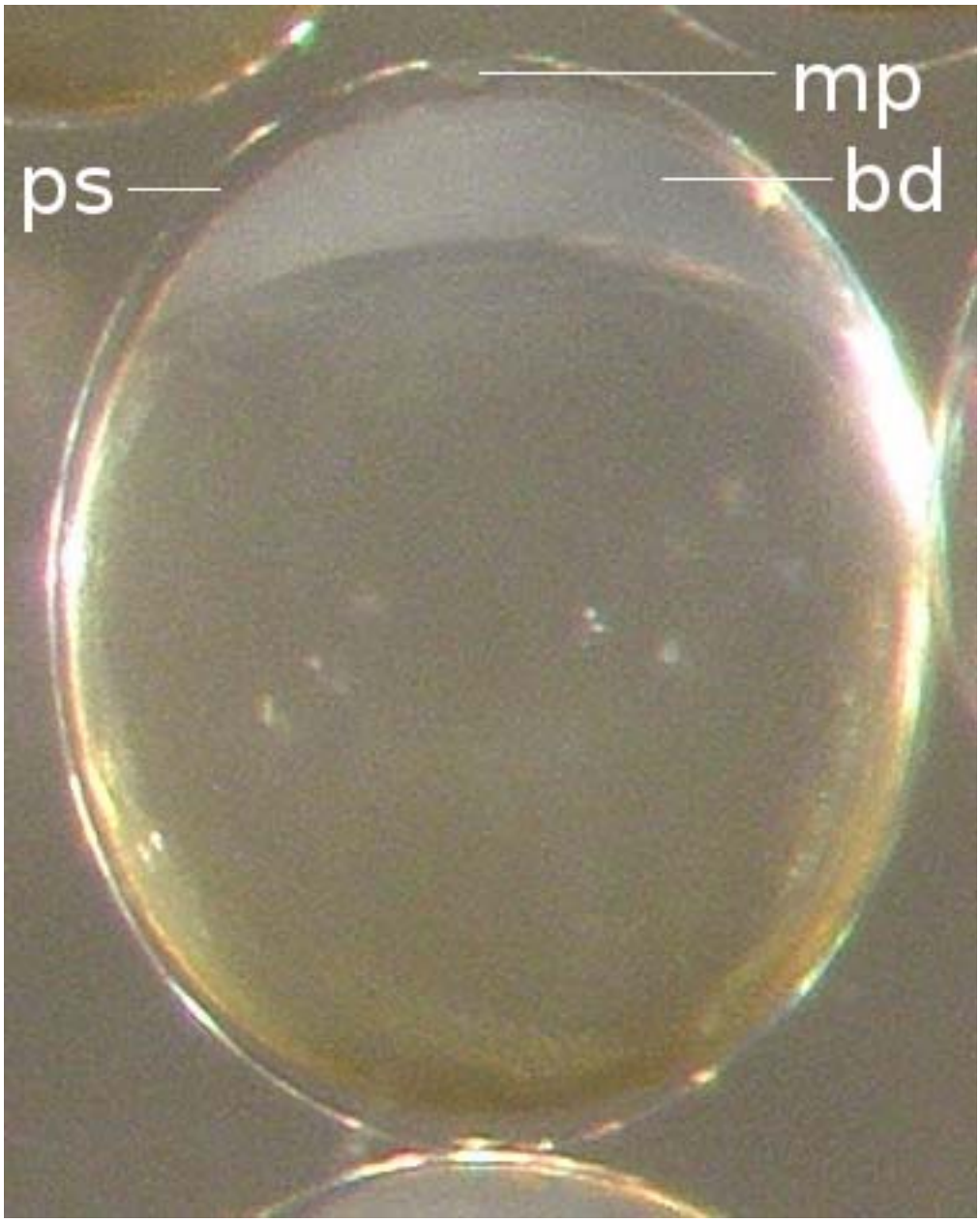

Figure 5-4. Variability and effect of temperature on developmental rate of *Dosidicus gigas* by stage. Furthest stage in development at a given temperature is plotted against time after fertilization in hours. A, Gametes and fertilization in Gulf of California (NH06). B, Gametes from Soquel Canyon, fertilization in Monterey (SC08). C, Gametes from San Diego, fertilization in Monterey (SD10). Each curve is a single dish; in panels B and C, eggs from different females are indicated by different markers (triangles, squares, and diamonds). Pluses (+) in the legend indicate temperatures within one degree above the value. Thus, 10+ includes values from 10 to 10.9 °C.

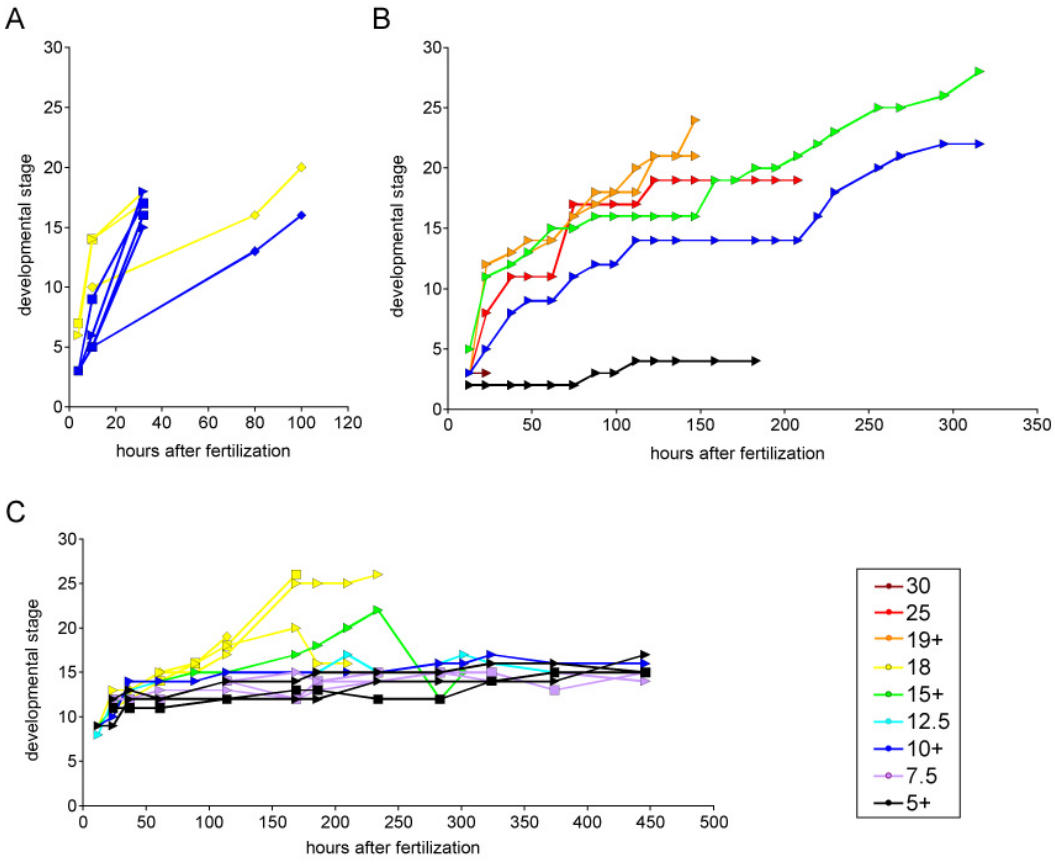

Figure 5-5. Effect of temperature on developmental rate of *Dosidicus gigas* by category. The category of each of ten cleaving embryos (from San Diego games, SD10) is plotted against time after fertilization, starting 12 hours after fertilization. White indicates blastoderm formation, light gray is organogenesis, dark gray is pigmentation, and black is hatching.

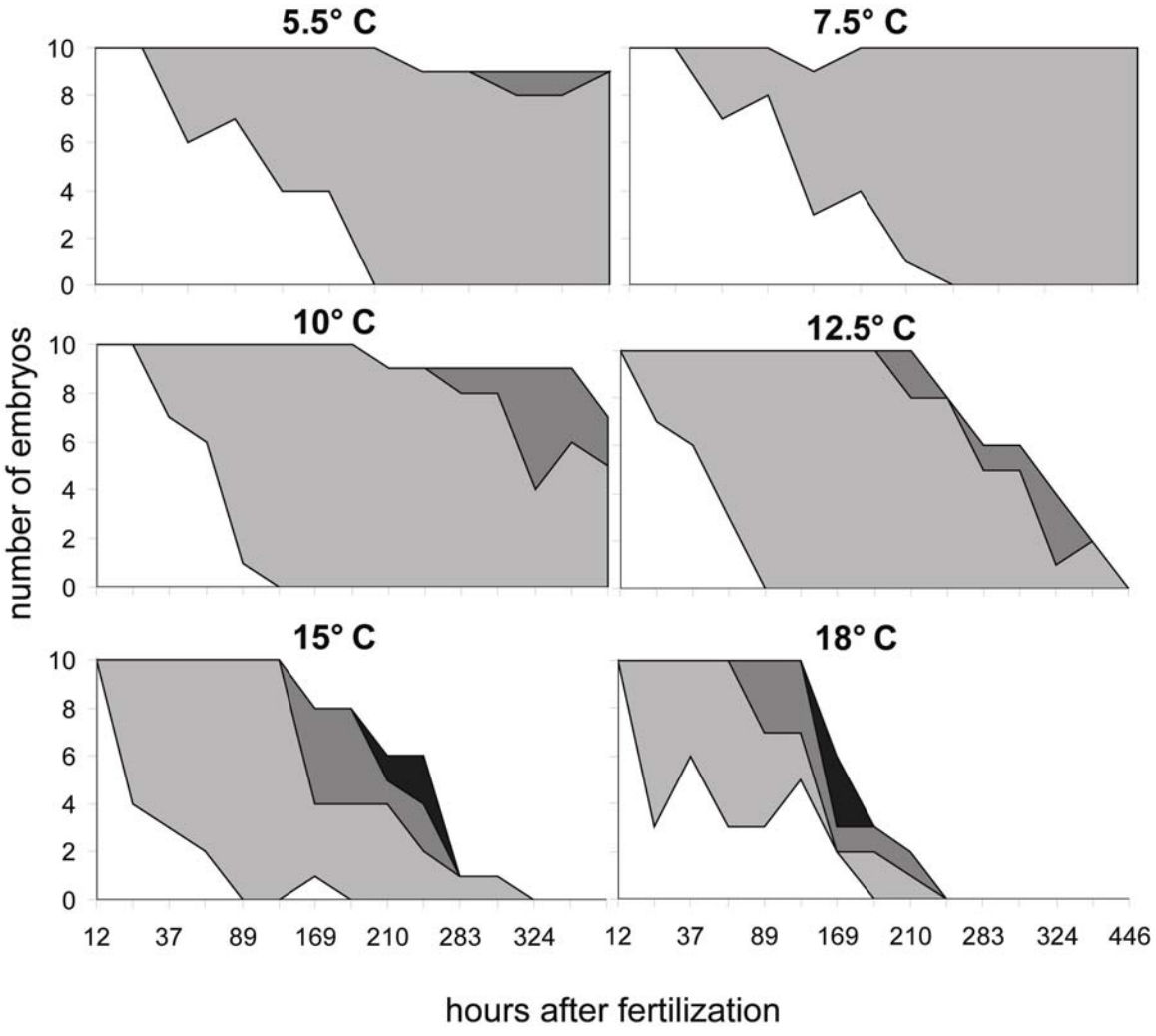

Figure 5-6. Effect of temperature on developmental success of *Dosidicus gigas*. Percent successful development of gametes from Soquel Canyon (SC09) to each category: cleavage, blastoderm, organogenesis, pigmentation, and hatching. Each point represents a single dish of eggs. The number of embryos observed in each category was divided by the total number of eggs in the dish.

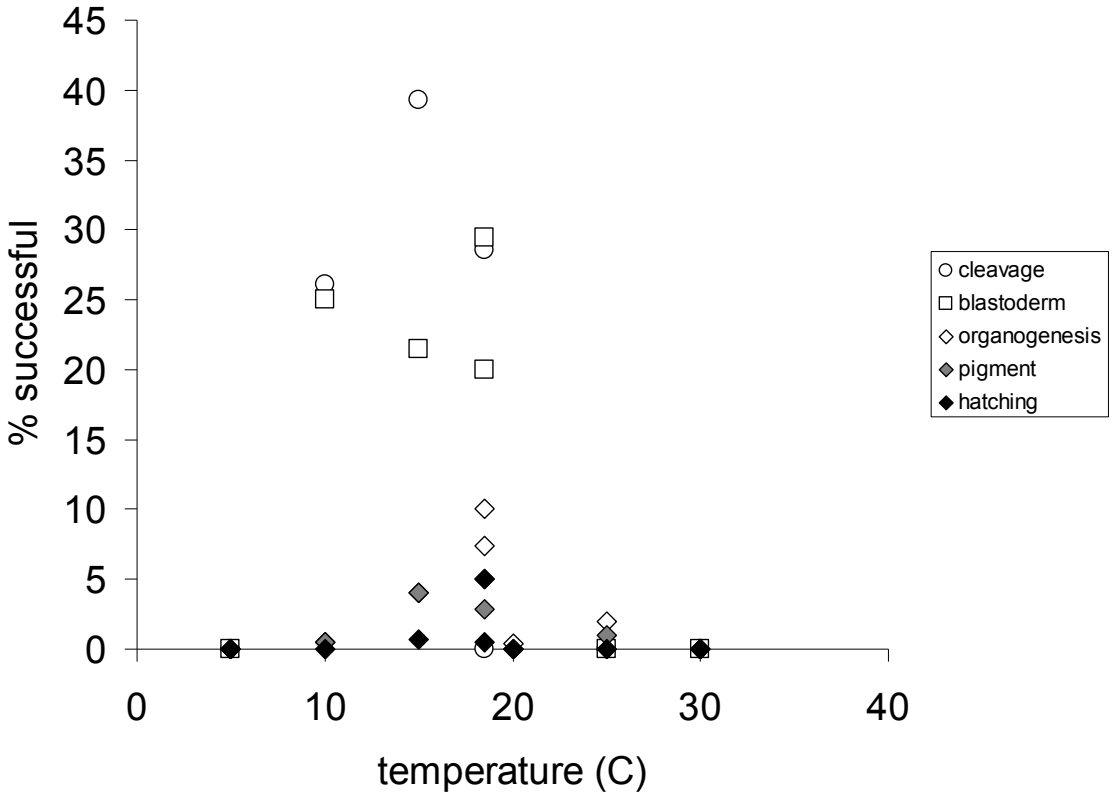

Figure 5-7. Effect of temperature on developmental success of *Dosidicus gigas*. Furthest stage reached plotted against temperature, for gametes from the Gulf of California (DJ08), Soquel Canyon (SC09), and San Diego (SD10). Each point represents the most advanced embryo observed in a single dish of eggs. Black dots indicate that hatching occurred. Gray dots indicate that no hatching was observed.

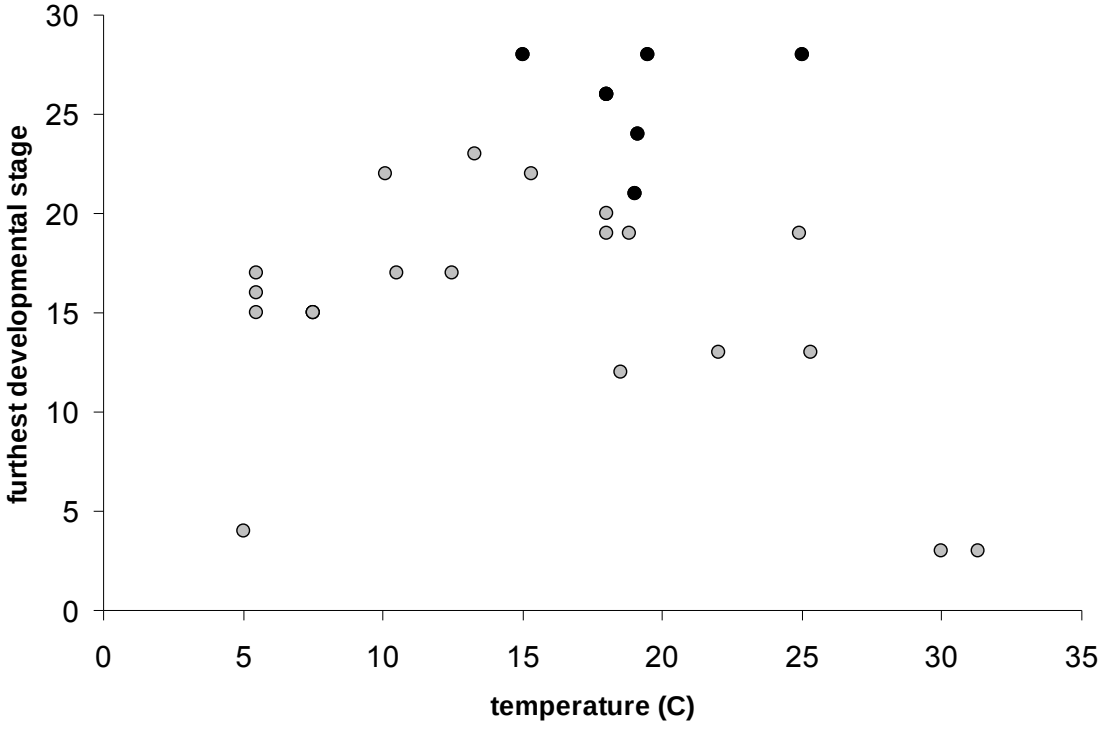

Figure 5-8. Average seasonal sea surface temperature isolines for the eastern Pacific, from the World Ocean Atlas 2005. The range of successful hatching as predicted from the temperature-dependence observed with artificially fertilized eggs is indicated with patterned fill.

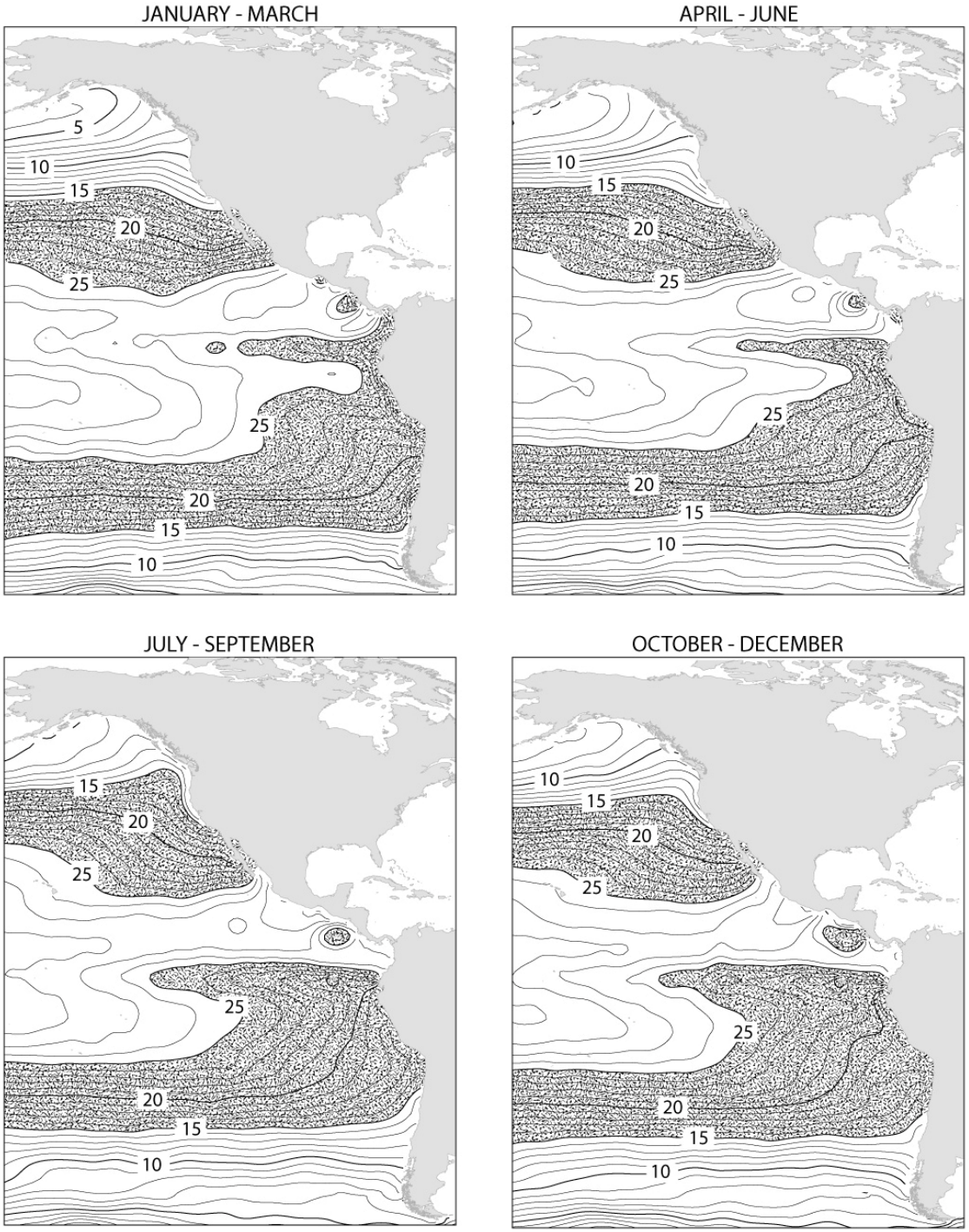

Appendix
Natural egg mass deposition by Humboldt squid in the Gulf of California

A.1. Abstract

The jumbo or Humboldt squid, *Dosidicus gigas*, is an important fisheries resource and a significant participant in regional ecologies as both predator and prey. It is the largest species in the oceanic squid family Ommastrephidae and has the largest known potential fecundity of any cephalopod, yet little is understood about its reproductive biology. We report the first discovery of a naturally deposited egg mass of *Dosidicus gigas*, as well as the first spawning of eggs in captivity. The egg mass was found in warm water (25-27^{o}C) at a depth of 16 m and was far larger than the egg masses of any squid species previously reported. Eggs were embedded in a watery, gelatinous matrix and were individually surrounded by a unique envelope external to the chorion. This envelope was present in both wild and captive-spawned egg masses, but it was not present in artificially fertilized eggs. The wild egg mass appeared to be resistant to microbial infection, unlike the incomplete and damaged egg masses spawned in captivity, suggesting that the intact egg mass protects the eggs within. Chorion expansion was also more extensive in the wild egg mass. Hatchling behaviors included proboscis extension, chromatophore activity, and a range of swimming speeds that may allow them to exercise some control over their distribution in the wild.

A.2. Introduction

Squids are broadly divided into the primarily nearshore Myopsida and mostly oceanic Oegopsida. Myopsids are more tractable study organisms and consequently provide most of our knowledge of squid biology, including reproduction and development (Gilbert et al. 1990). Much less is known about the oegopsids. “Our almost complete ignorance of the eggs and early larval stages of oegopsid squids is the most extraordinary omission in our knowledge of cephalopod biology.” This assertion was made over 40 years ago (Clarke 1966), and information concerning the spawning

and egg masses of these oceanic cephalopods remains sparse (see reviews: Young et al. 1985a, Boletzky 2003). The few oegopsid egg masses that have been observed are larger than those of myopsids and show greater diversity of form. Some are gelatinous, free-floating, and contain many small (1.2-1.8 mm) eggs, such as those of *Thysanoteuthis rhombus* Troschel, 1857 (Sabirov et al. 1987) and *Brachioteuthis* sp. Verrill, 1881 (Young et al. 1985b). In other cases, as in *Gonatus onyx* Young, 1972, a few larger (2-3 mm) eggs are brooded by the female (Seibel et al. 2000). This diversity is not surprising, given that oegopsids inhabit all open ocean environments throughout the world, from the surface to great depths.

Of the 23 oegopsid families, the family Ommastrephidae is unique in passing through a post-hatching paralarval stage called the rhynchoteuthion. During this stage, the two tentacles are fused into a proboscis, the use and development of which is not well understood (Shea 2005). Rhynchoteuthion paralarvae have been produced by artificial fertilization (Arnold and O'Dor 1990, Sakurai et al. 1995), captured in plankton tows (e.g. Brunetti 1990), and collected from spawned egg masses. Spawning in captivity has been documented only for *Todarodes pacificus* Steenstrup, 1880 (Bower and Sakurai 1996) and *Illex illecebrosus* Lesueur, 1821 (O'Dor and Balch 1985). Wild egg masses have been discovered only for *Sthenoteuthis pteropus* Steenstrup, 1855 (Laptikhovsky and Murzov 1990) and *Nototodarus gouldi* McCoy, 1888 (O'Shea et al. 2004).

Though our knowledge of ommastrephid reproduction and development is limited, ommastrephids are considered monocyclic, with adults reaching sexual maturity and reproducing during a single continuous spawning season. This reproductively active time may be a single session in which all of a female's eggs ripen and are spawned during a brief period (simultaneous terminal spawning, Rocha et al. 2001), as occurs with *Doryteuthis (=Loligo) opalescens* Berry, 1911. Or there may be a more prolonged spawning season, during which eggs ripen and are spawned in sequential batches. In some species that pursue this strategy, mature adults stop eating and divert all their energy into reproduction (intermittent terminal spawning,

Rocha et al. 2001), while individuals of other species continue to feed and grow during their reproductively active time (multiple spawning, Rocha et al. 2001).

Nigmatullin and Laptikhovsky (1994) divided the ommastrephid family into two groups in which reproductive and ecological strategies align. The "offshore" ommastrephids, like *Todarodes pacificus* (Ikeda et al. 1993a) and *Illex* spp. (Laptikhovsky and Nigmatullin 1993), are intermittent terminal spawners, while the "oceanic" ommastrephids, like *Sthenoteuthis oualaniensis* Lesson, 1830 (Harman et al. 1989) and *Dosidicus gigas* d'Orbigny, 1835 (Nigmatullin et al. 2001), are multiple spawners.

Dosidicus gigas attains the greatest size of any ommastrephid and supports the largest invertebrate fishery in the world, which is also the 14th largest of all fisheries, with record landings of 768,848 t in 2005 (ftp://ftp.fao.org/fi/stat/summary/a1e.pdf). This species also plays a significant and variable role in regional ecologies. In the Gulf of California, adult jumbo squid consume an enormous quantity of small mesopelagic fishes, crustaceans, and squids (Markaida and Sosa-Nishizaki 2003), while serving as a prominent prey item for larger fishes and marine mammals (Klimley et al. 1993, Abitía-Cárdenas et al. 2002, Rosas-Aloya et al. 2002, Ruiz-Cooley et al. 2004). In the California Current of central California, on the other hand, they feed at a higher trophic level, preying heavily on a variety of larger neritic fishes (Field et al. 2007).

The historical range of *D. gigas* is in the tropical and subtropical Eastern Pacific from 30°N to 25°S, with episodic appearances as far as 40°N and 47°S (Nigmatullin et al. 2001). This area remains the center of the species' range, which has recently expanded northward. *D. gigas* has been resident in the Monterey Bay (37°N) since the 1997-98 El Niño (Zeidberg and Robison 2007) and individuals have been reported from as far north as southeast Alaska (59°N) (Cosgrove 2005, Wing 2006, unpublished data). Within its range *D. gigas* shows considerable phenotypic plasticity in size at first maturity, with DML ranging from 14-100 cm (Nigmatullin et al. 1999). Jumbo squid that mature at the larger end of this size range have the largest potential fecundity of any cephalopod, ranging from 5 to 32 million oocytes in a single female (Nigmatullin et al. 1999, Nigmatullin and Markaida 2002).

Laboratory studies have employed artificial fertilization of *D. gigas* eggs to reveal embryonic development *in vitro* (Yatsu et al. 1999), but natural spawning and early development are poorly understood. Based on an abundance of rhynchoteuthion paralarvae, the Costa Rica Dome is thought to be a major spawning area for either *D. gigas* and/or *Sthenoteuthis oualaniensis* (Vecchione 1999). Spawning of *D. gigas* has also been identified in the central Gulf of California, based on the presence of newly hatched paralarvae (genetically identified) and putative mating by adults (Gilly et al. 2006a). In no case have naturally deposited eggs been observed.

To our knowledge, this paper constitutes the first report of naturally deposited eggs of *D. gigas* and of the first spawning in captivity by this species. We present observations of the embryos and hatchlings from these egg masses, and compare them with embryos and hatchlings produced by artificial fertilization.

A.3. Methods

Field observations presented in this paper were made on the R/V New Horizon in the Gulf of California, from 8-22 June 2006, and from 29 May to 12 June 2007.

A.3.1. Blue water diving

Blue-water dives were carried out daily, as conditions permitted, according to procedures in Haddock and Heine (2005). Thirty dives were conducted during the two research cruises. On 21 June 2006, a dive was conducted at 27°7.1'N 111°16.0'W, where the sea floor was at a depth of approximately 1800 m (Fig. 1). At a depth of 16 m, the divers encountered an egg mass and took video *in situ*. Divers sampled the mass by filling inverted jars with exhaled air and extending them well into the mass. When a jar was turned upright to allow the air to escape, it became filled with a sample that presumably reflected ambient egg concentration in the mass. In this manner, one 1 l collecting vessel (Jar 1) and two 500 ml jars (Jars 2 and 3) were filled with egg mass and returned to the ship. Forty ml of egg mass from each jar were poured into individual 50 ml clear plastic vials, and the eggs in each sample were then counted to assess egg density.

Two vertical water column profiles were measured in close proximity to the site of the egg mass discovery, one on 19 June 2006 at 27°6.06'N 111°14.37'W, and another on 20 June 2007 at 27°5.63'N 111°11.24'W (Figure A-1). The instrument used to measure these profiles was a Sea-Bird 911*plus* CTD with sensors for pressure (401K-105), temperature (SBE3*plus*), conductivity (SBE4C), and dissolved oxygen (SBE43).

A.3.2. Capture and maintenance of adult squid

Squid were caught nightly with weighted jigs, usually between 2000 h and 2200 h. Individual live squid were held on the ship in either a 514 l acrylic tank or a 280 l fiberglass tank. The fiberglass tank was oxygenated with constantly running surface seawater (28°C). In 2006, water in this tank was also partially circulated through a chiller to maintain temperature at 23°C. The cooler temperature seemed to have no effect on the squid, so the chiller was not used in 2007. The acrylic tank was filled with surface seawater and aerated with a bubbler. An oxygen probe was used to ensure that oxygen saturation was comparable to ambient levels. Over the course of 5-10 h, this tank was chilled to either 10 or 20°C for other research purposes.

Both tanks were kept dark and covered, with minimal disturbance by observers. Individual squid were maintained on board the ship for 24 h or less. If squid inked, the tank was flushed as quickly as possible with surface seawater until the water was clear. Spawned egg masses were removed from the tanks upon discovery, which was always in the early to mid-morning. Moribund post-spawning females were removed from tanks and euthanized by rapid decapitation (Boyle 1991, Moltschaniwskyj et al. 2007). They were then weighed, measured, and dissected for examination of the reproductive organs. Maturity stage was assigned following Lipiński and Underhill (1995).

A.3.3. Artificial fertilization

Arnold and O'Dor (1990) obtained the first success from artificial fertilization to hatching of an ommastrephid with *Sthenoteuthis oualaniensis*. The technique was

refined and modified by Sakurai and Ikeda (1994) for *Todarodes pacificus*, and later applied to *Sthenoteuthis oualaniensis* and *Ommastrephes bartramii* by Sakurai et al. (1995) with some further modifications. Yatsu et al. (1999) successfully applied the technique to *Dosidicus gigas*.

The protocol used in the current study was based on techniques in Sakurai et al. (1995) and Yatsu et al. (1999) with two modifications. First, lyophilized oviducal gland material was isolated from *Dosidicus gigas* rather than *Ommastrephes bartramii*. Second, antibiotics were used. After filtering seawater with a 0.2 μm filter, 25 mg/l each of ampicillin and streptomycin was added, resulting in noticeable improvement in the survival of embryos cultured in this treated water.

A.3.4. Maintenance of eggs and paralarvae

Developing eggs from artificial fertilization, captive-spawned egg masses, and the wild egg mass were all kept in filtered, antibiotic-treated seawater at room temperature (18-20°C). This temperature range was between the previously reported culture temperature of 18°C (Yatsu et al. 1999) and the temperature at which the natural egg mass was found (25-27°C, see Fig. 2). Water was changed daily and the developing embryos were photographed periodically. Artificially fertilized eggs and portions of the captive-spawned masses were kept in sterile petri dishes, while the wild embryos were kept in the jars in which they had been collected.

Approximately 24 h after collection, eight hatchlings from the wild egg mass were moved from Jar 1 into a 650 ml flask. All of the remaining hatchlings in Jar 1 were preserved in ethanol for DNA analysis. Both living and preserved samples were transported back to CIBNOR, Guaymas, and ultimately to Hopkins Marine Station, where the live paralarvae were maintained in a rectangular 1 l aquarium at room temperature (~20°C). Attempts were made to feed these hatchlings with rotifers, brine shrimp nauplii, and various algae that were cultured at the Monterey Bay Aquarium, as well as wild zooplankton from surface net tows in Monterey Bay. Standard measurements (dorsal mantle length, mantle width, head width and proboscis length) were made from video clips (see next section) of paralarvae on 3 and 6 days post-

hatching. Jar 2 was taken to the CIBNOR laboratory in Guaymas, and the hatchlings were all counted and preserved in 80% ethanol approximately 2 days after hatching.

Individual embryos and paralarvae fixed in ethanol and formalin for analyses reported in this paper were provided by C. Salinas, CIBNOR, Guaymas, to be archived at Hopkins Marine Station.

A.3.5. Video observations

Videos were taken of the hatchlings from the wild egg mass, both in the 1 l aquarium and in a smaller, thin acrylic chamber (72x47x7mm), with a Sony DCR-TRV70 mini-DV camcorder. Selected sequences that covered a range of swimming movements were captured with Adobe Premier Elements and exported as frames into ImageJ to analyze the dynamics of mantle contraction and speed of swimming. Rate of mantle contraction was calculated as the number of mantle contractions per second. Magnitude of mantle contraction was calculated as a fraction, by dividing the ratio of mantle width (MW) to dorsal mantle length (DML) (MW:DML) in each frame by the maximum MW:DML measured in that clip. Sequences that contained proboscis extensions were also captured and exported as frames. Proboscis extension was measured as the ratio of proboscis length to mantle length (PL:DML) in a given frame divided by the resting PL:DML in that sequence. Swimming speed was measured as the absolute distance traveled per second based on a scale included in the video field and a 29.97 Hz frame rate.

Chromatophore activity also occurred frequently. A representative 10 min video segment was selected for analysis of the duration and degree of chromatophore expansion and of responsiveness to stimuli.

A.4. Results

A.4.1. Wild egg mass

CTD casts near the site of the egg mass discovery show that temperature, oxygen, and salinity all changed rapidly at or near the 16 m depth at which the egg mass was discovered (Figure A-2). Temperature and salinity began to drop, while

oxygen began to rise to a subsurface peak at 20-30 m before dropping off again. Temperature at 16 m was 25 °C in the 19 June cast and 27 °C in the 20 June cast.

The egg mass resembled a semi-transparent gray cloud (Figure A-3). Its shape was an ellipsoid, with the broad axis parallel to the sea surface. Divers' estimates of the dimensions ranged from 2-3 m for the minor equatorial diameter, from 3-4 m for the major equatorial diameter and from 2-3 m for the polar diameter. The consistency of the mass was loosely gelatinous, but not firm enough to offer tangible resistance to an ungloved hand. Embedded within this gelatinous matrix were individual eggs, each containing a single developing embryo, distributed diffusely enough that divers were clearly visible through the entire thickness of the mass. The distribution of eggs appeared homogeneous.

The only variability in the homogenous nature of the mass was in a small area near the periphery, where the gelatinous matrix formed slightly denser, whitish strands (bottom of Figure A-3). The divers observed two dead fish attached to this area and tentatively identified them as myctophids (lanternfish). One of these fish was relatively intact, while the other appeared to be partially decayed.

Egg densities in the 40 ml samples were 0.427 (Jar 1), 0.600 (Jar 2), and 0.650 (Jar 3) eggs/ml. In addition to these sample counts, the total number of eggs in Jar 2 yielded a density of 0.192 eggs/ml. Assuming an ellipsoid shape for the egg mass and using the most conservative estimate of its dimensions, its volume was calculated to be 3.13 m^3, or 3,130 l. With an egg density of 192 to 650 eggs/l, the potential number of eggs in the entire mass ranges from 0.6 to 2 million.

Over 99% of the collected eggs were fertilized, and all of these were classified as developmental stage 25 (Watanabe et al. 1996) based on the presence of distinct chromatophores, lens primordia, and a gutter (apical groove) in the inner yolk sac. In *Todarodes pacificus*, hatching from artificially fertilized eggs occurs at stage 26, but may be induced in stage 25 by external stimulation (Watanabe et al. 1996).

Each egg was surrounded by a discrete spherical envelope, slightly larger than the chorion (Figure A-4A). The chorion was expanded to more than twice the length of the embryo within (Table A-1). The embryos were always observed in a vertical

position, with the head and arms hanging down, as reported for *Todarodes pacificus* (Bower and Sakurai, 1996), and they remained stationary in this position when the eggs were suspended in a jar. However, when eggs were placed with a small amount of jelly in a culture dish for photography, the embryos swam in circles in the horizontal plane around the inside of their eggs.

No developmental abnormalities were visible. Paralarvae began hatching in the evening of the day the egg mass was discovered and continued hatching throughout the night. Analysis of cytochrome *c* oxidase I sequences from embryos taken back to Hopkins Marine Station confirmed their identity as *Dosidicus gigas* (Gilly et al. 2006a, GenBank Accession No. DQ191367).

A.4.2. Egg masses spawned in captivity

Four squid spawned egg masses on the 2007 cruise, all within 12 h of capture. The first two egg masses were discovered on the morning of 30 May 2007—one in the chilled acrylic tank at 0500 h (DML: 43 cm, mass: 3.1 kg) and one in the fiberglass tank at 0730 h (not measured). Both of these masses contained fertilized eggs. The third and fourth egg masses were discovered at 0930 h on 31 May 2007 (DML: 42 cm, mass: 2.6 kg), and at 0500 h on 3 June 2007 (DML: 35.5 cm, mass: 1.76 kg), both in the chilled acrylic tank. Eggs in these two masses were not fertilized. One squid (DML: 57 cm, mass: 5.1 kg) spawned an egg mass containing fertilized eggs on the 2006 cruise. It was discovered around 0100 h on 15 June 2006. All squid survived for some hours after spawning events, but to our knowledge none spawned more than once in captivity.

Four of the five moribund females were sacrificed and dissected after they deposited eggs. The oviducts were extended and flaccid, but empty of eggs, and the ovary appeared granular with yellowish oocytes. The nidamental and oviducal glands were large, white, and well developed. Had these squid not been known to spawn in captivity, they would have been classified as stage IV in the scheme of Lipiński and Underhill (1995). Stage IV is defined as a maturing female that does not yet have ripe

eggs in the oviducts, whereas stage V females are fully mature, with ripe eggs in the oviducts.

The spawned egg masses were transparent and gelatinous, with no apparent internal structure. Their consistency was similar to that of the wild egg mass but denser and less watery. They were fragmented, and while some parts of each mass contained eggs, other substantial areas were devoid of eggs. In addition, many more eggs were generally found loose on the bottom of the tank, perhaps having been separated from the mass by aeration, or perhaps never incorporated into it. This indicates that the eggs themselves, when independent of the gelatinous mass, are negatively buoyant. Although the fragmented nature of the masses prevented them from being completely extracted from the tanks, the volume that could be successfully retrieved was in the range of 1-2 l for each mass.

Chorion expansion in the captive-spawned eggs was slightly greater than that of artificially fertilized eggs but considerably less that of the wild eggs when measured at a comparable stage of development (Table A-1). Some, but not all, of the captive-spawned eggs appeared to be surrounded by a spherical outer envelope similar to that described above for wild-spawned eggs. This envelope was often present even around unfertilized eggs (Figure A-4B). Many of the developing embryos suffered mortality, apparently due to bacterial infection, and many showed developmental abnormalities. Viable hatchlings began to emerge from portions of the successfully fertilized egg masses 3 days after spawning while being maintained at room temperature. None of the loose eggs hatched successfully.

A.4.3. Artificial fertilization

Artificially fertilized eggs suffered a great deal of microbial contamination which was only somewhat ameliorated by treatment with antibiotics. Chorion expansion occurred to a lesser extent in these eggs than in either the captive-spawned or the wild eggs, and changed relatively little over the course of development (Table A-1). No outer envelope like that in the egg masses was ever seen. Some successful hatchlings were obtained from these eggs.

A.4.4. Growth and development

Hatchlings from artificially fertilized eggs, captive-spawned masses, and the wild egg mass were all morphologically similar to *D. gigas* hatchlings previously described by Yatsu et al. (1999), which were in turn quite similar to other ommastrephid hatchlings (e.g. Sakurai et al. 1995).

During the first 3 days post-hatching, the wild paralarvae increased markedly in mantle length, mantle width, and head width, and the proboscis appeared and grew considerably in length (Table A-2). However, after 3 days, the paralarvae remained constant in most dimensions, shrinking somewhat in mantle length. The initial growth was fueled by yolk consumption, and the subsequent lack of growth was likely due to starvation. While maintained in the laboratory, the paralarvae exhausted their yolk reserves and, despite offerings of zooplankton and phytoplankton, at no time did they exhibit obvious feeding behaviors. Ingested material was not found in their guts upon post-mortem examination.

A.4.5. Swimming kinematics (Jar 1)

After hatching from their eggs, the wild paralarvae swam easily within the large egg mass, maintaining their position by jetting up, then sinking down. Eventually they escaped from the mass and began to move actively within the water column, where they sank quickly (-0.46 ± 0.02 cm/s, n=3) upon cessation of swimming activity. Some jetted powerfully towards the surface and maintained height, but most sank to the bottom, where they remained oriented with the posterior mantle pointing up, jetting frequently but gaining no altitude.

Swimming direction was always vertical or nearly so. Swimming speed in 3-6 day old paralarvae varied from simply maintaining position in the water column (a net velocity of 0 cm/s, generated by the animal's swimming velocity counteracting its sinking velocity) to 0.51 cm/s, the fastest net upward swimming speed maintained over several seconds. Rates of mantle contraction ranged from 2.2-4.2 Hz, and the magnitude of mantle contraction varied from 28.17%-39.54%.

A.4.6. Other behavioral observations

A commonly observed behavior in 3-6 day old paralarvae was extension of the proboscis (Figure A-5). The proboscis stretched to 252±38% of its original length in 375±77 ms (n=12). Retraction to the original length was considerably slower and more variable. Although it is tempting to interpret proboscis extensions in the context of feeding attempts, their occurrence appeared to be spontaneous and independent of the presence of potential food items in the water.

Chromatophore activity, on the other hand, was often stimulated by external disturbance. Of the 27 instances of chromatophore activity observed during a 10 min video sample, 5 occurred when a paralarva bumped into the surface of the water, 8 occurred when it touched the bottom of the aquarium, and the remainder appeared to occur spontaneously during normal swimming. Chromatophore activity generally involved all of the chromatophores more or less at once. They expanded, remained that way for a variable length of time, usually less than one second, and then contracted again (Figure A-6). Occasionally, the chromatophores expanded and contracted sequentially at this rate for two or three cycles.

A less common response to disturbance was a dramatic cessation of normal vertical swimming and commencement of jetting in a tight circle, one to several times, before resuming the usual jetting up and sinking down. Even more rarely, paralarvae were observed retracting their heads into the mantle cavity. This only occurred when paralarvae were resting on the bottom, never while swimming in the water column.

A.5. Discussion

A.5.1. Considerations of spawning and reproductive behavior

Previously reported diameters of ommastrephid egg masses ranged from 0.4-1.0 m in *Illex illecebrosus* (Durward et al. 1980, Balch et al. 1985) and *Todarodes pacificus* (Bower and Sakurai 1996) to 1.0-2.0 m for *Nototodarus gouldi* (O'Shea et al. 2004). The major diameter of the ellipsoid *D. gigas* egg mass was estimated to be 3-4 m, making it by far the largest of any squid yet reported.

Our estimate of the number of eggs in the natural egg mass ranges from 0.6 million to 2 million, which is consistent with estimates of up to 1.2 million eggs from full oviducts of large-sized females (Nigmatullin et al. 1999, Nigmatullin and Markaida 2002). This is nearly an order of magnitude more eggs than have been found in any ommastrephid (or any squid) egg mass to date (*Illex illecebrosus*: 100,000 eggs (Durward et al. 1980) and *Todarodes pacificus*: 21,000-200,000 eggs (Bower and Sakurai 1996)). As a multiple spawner (Rocha et al. 2001), with a potential fecundity ranging from 5 to 32 million oocytes (Nigmatullin and Markaida 2002), the reproductive output of a single *D. gigas* female could be between 3 and 20 egg masses, each of a size comparable to the one discussed here.

The ecological consequences of this enormous quantity of offspring are noteworthy. Presumably the tiny hatchlings suffer high mortality early in life, and they are undoubtedly an important food source for a variety of small predators, just as adults provide crucial sustenance for oceanic megafauna. Furthermore, as a short-lived, highly fecund species, *D. gigas* can be extremely responsive to environmental variation (Gilly and Markaida 2007). When growth conditions are good and predation is low, *D. gigas* has the potential for explosive population growth. But when conditions are poor, affected populations may crash. This susceptibility is attested to by the highly variable fishery in the Gulf of California in relation to El Niño events (Bazzino et al. 2007).

Given the high population density and abundance of adult *D. gigas* (Nigmatullin et al. 2001), it is surprising that only one egg mass of this species has ever been reported. As a comparison, the most frequently encountered oceanic squid egg masses belong to a non-ommastrephid oegopsid, *Thysanoteuthis rhombus* (Young et al. 1985a). Over 30 of this species' egg masses have been reported over the last 20 years (Sabirov et al. 1987, Guerra and Rocha 1997, Watanabe et al. 1998, Guerra et al. 2002, Miyahara et al. 2006), although the adults are only sparsely distributed throughout their range (Nigmatullin and Arkhipkin 1998). What could account for the difference? The cylindrical egg masses of *T. rhombus* can reach 1.8 m in length, but diameters do not exceed 0.3 m and they contain only 32,000-76,000 eggs (Nigmatullin

et al. 1995), making them considerably smaller than the egg mass of *D. gigas*. Development to hatching occurs in 5-7 days (Sabirov et al. 1987), only two days longer than *D. gigas*. As the egg masses of *T. rhombus* are neither larger nor longer-lived, what could make them more easily discovered?

T. rhombus eggs are found in superficial surface waters (Nigmatullin and Arkhipkin 1998) and apparently float at the surface until hatching (Miyahara et al. 2006). Such floating egg masses should be visible from a ship, which is in fact how the discoveries have generally been made (Guerra et al. 2002). The few reported ommastrephid egg masses have all occurred at depths too great to permit discovery through surface observations (Laptikhovsky and Murzov 1990, O'Shea et al. 2004, this study). Given the difficulty of systematic exploration of a three-dimensional volume rather than a two-dimensional sea surface, and the limited visibility in water compared with air, it is likely that ommastrephid egg masses, though large, will remain rare finds.

Egg masses for experimental work may be more reliably obtained in captivity. In two consecutive years' field work during May/June, we found only one natural egg mass from 30 blue-water dives, but five females spawned in captivity (of about twice that many maintained overnight). The small size of these captive-spawned masses (1-2 l) relative to the wild egg mass (3,130 l) suggests they may have been "incomplete" egg masses (Bower and Sakurai 1996).

Although these captive spawning events were unnatural and probably stress-induced, they impart valuable information. Our morphological study of the post-spawning females raises an important question concerning identification of post-spawning animals taken from the wild. As no ripe eggs were visible in the ovary or oviducts, these post-spawning females could easily have been classified as "maturing" stage IV, even though they had already spawned at least once (in captivity). Accordingly, it may be necessary to reconsider the meaning of the established maturity stages (Lipiński and Underhill 1995) within the context of intermittent spawning. It has been previously suggested that 20% of eggs remain in the oviducts after spawning (Nigmatullin and Markaida 2002), but our observations of empty oviducts indicate

that all eggs may be evacuated in a single spawning event, at least in captivity. If a similar phenomenon were to occur in the wild, an adult female might repeatedly pass through the final maturity stages (IV and V) during the reproductively active part of her life (IV-V-spawning-IV-V-spawning, etc.). The present scheme of maturity stages does not recognize this possibility, since functional maturity and active spawning are assigned to stage V alone. This could lead to underestimating the fraction of actively spawning females in a sampled population.

A.5.2. Nature of the egg mass

Eggs within the wild egg mass as well as those expelled in captivity were surrounded by a diffuse, gelatinous matrix that was not present when eggs were artificially fertilized. There was no indication of microbial infection of the wild egg mass, or of the eggs sampled from it, but infection was clearly a problem with captive spawning and artificial fertilization. Although the holding tanks onboard the ship undoubtedly supported a different microbial community than that in the open ocean, it is likely that susceptibility to infection increases greatly if the egg mass is incomplete or damaged (captive spawned eggs) or absent (artificially fertilized eggs). An intact matrix around the eggs probably serves to prevent microbial infection. This idea is supported by previous studies of captive-spawned ommastrephid eggs that were more susceptible to microbial infection if the surface of an egg mass was physically damaged (Durward et al. 1980, Bower and Sakurai 1996). Egg capsules of other squid species are also known to be resistant to infection and predation, but the mechanisms involved are not well known (Atkinson 1973, Biggs and Epel 1991).

Each individual egg in a spawned egg mass of *D. gigas* was surrounded by a distinct envelope that was external to the chorion, but no such structure was evident in artificially fertilized eggs. Although the envelope was of a similar overall diameter in both wild- and captive-spawned eggs, chorion expansion was greater in wild eggs, and the thickness of the surrounding envelope layer was correspondingly less. At present the structural nature of the envelope is unknown, and we are not aware of any explicit description of a similar structure for other species of squid.

Chorion expansion was much greater in the eggs from the naturally deposited mass than in the artificially fertilized eggs (Table A-1). Chorion expansion in artificially fertilized eggs requires the addition of powdered oviducal gland (Ikeda et al. 1993b) but clearly this is less effective than the oviducal gland jelly produced naturally by a spawning female. Even natural jelly, however, may not be sufficient for full expansion if produced under stressed conditions, or with an incomplete egg mass, as can be seen from the lesser chorion expansion of the captive-spawned masses when compared to the wild egg mass (Table A-1).

The exact mechanism of egg mass formation and the origins of the gelatinous matrix and individual envelopes remain unclear. Bower and Sakurai (1996) speculated on the origin of the jelly in captive-spawned egg masses of *Todarodes pacificus*: *"Externally, the masses were covered with a jellylike secretion, presumably from the nidamental gland, and the interior of the masses, which contained the eggs, consisted of a jelly presumably secreted by the oviducal gland."* Unfortunately, it is not clear how these components correspond to the matrix and envelopes described in the present study. Although the natural egg mass from *D. gigas* was viewed only underwater by divers, no external skin or barrier of any type was noted. Moreover, following withdrawal of the sample jar, the matrix material appeared to immediately coalesce around the exit point and show no sign of having been penetrated by a hand and collecting vessel.

Following the suggestion by Bower and Sakurai (1996), we propose that each egg within the *D. gigas* egg mass is indeed coated with material from the oviducal gland as it passes through, and that this material forms the individual envelopes and acts to support fertilization and chorion expansion. Following passage through the oviducal gland, the coated eggs are then mixed with concentrated jelly from the nidamental glands, which eventually forms the gelatinous matrix in which the eggs are suspended. This entire mass is then extruded out the siphon, and presumably transferred by the arms to the buccal area, where it is mixed with sperm from spermatangia. Reaction with seawater then leads to an overall expansion of the egg

mass that probably continues as the embryos develop, eventually leading to the observed watery consistency of the wild egg mass.

A.5.3. Location of the natural egg mass in the water column

The egg mass may have been extruded by the female at the depth of discovery, or it may have risen or sunk to that depth. The rapidly decreasing salinity at this depth supports the assertion of O'Dor et al. (1982a) that oegopsid egg masses normally accumulate at mid-water pycnoclines. The resting depth of the egg mass is determined by its density, which is influenced by the physical and chemical properties of the jelly and the amount of seawater that it absorbs. Over time, evolutionary pressures have probably influenced the density of pelagic egg masses so that they float in an environment that is favorable for embryonic development and hatching. Although the peak in oxygen occurs below the depth of the egg mass, near-surface waters still provide a reasonably well-oxygenated environment, which may be important for proper embryonic development (Strathmann and Strathmann 1995).

The temperature at this depth was 25-27°C, just above the range of temperatures reported to result in successful development of artificially fertilized eggs of *Ommastrephes bartramii* and *Sthenoteuthis oualaniensis* (Sakurai et al. 1995). Because CTD data in the present study were not obtained from precisely the location of the egg mass, the exact temperature of natural incubation cannot be given, but it is unlikely that it was substantially higher than the range stated above.

Several analyses have addressed the rate of egg development in cephalopods as a function of egg size and temperature (Laptikhovsky 1991, Boletzky 1994, Laptikhovsky 1999). Small eggs at warm temperatures tend to develop to hatching in only a few days, a trend which is consistent with our observations here, and with other studies of ommastrephid development. *Todarodes pacificus* eggs (0.83 mm) hatched after almost 4 days at 23°C, (Watanabe 1996), and *D. gigas* eggs (1.3 mm) kept at 18°C began hatching after 6 days (Yatsu et al. 1999). Rapid development at warm temperatures may be advantageous due to a variety of factors, including reduced maternal investment in yolk.

Colder temperatures, on the other hand, may not be favorable for development. For example, some ommastrephid paralarvae are unable to tolerate temperatures below 18°C (O'Dor et al. 1982b, Miyanaga and Sakurai 2006). This characteristic could be shared by *D. gigas* paralarvae, as the egg mass was found in water well above this lower limit. Although *D. gigas* adults regularly undergo rapid vertical migrations, moving quickly from extremely warm temperatures (>26°C) to much colder temperatures (5-6°C) (Gilly et al. 2006b), the ability to withstand such large changes in temperature may be absent in hatchlings and arise later in development.

A.5.4. Paralarval development and behavior

Growth rates observed in hatchlings from the wild egg mass were comparable to those described for the hatchlings of artificially fertilized eggs (Yatsu et al. 1999), which showed "considerable variation within and among ages." Positive growth in wild hatchlings ceased between 3 and 6 days (Table A-2), but Yatsu et al. (1999) found that growth of artificially fertilized hatchlings appeared to continue through Day 7, and the yolk of these hatchlings was not exhausted until 8 days after hatching. The disparity could potentially be a result of the fact that artificially fertilized eggs tend to hatch two stages earlier than eggs in an egg mass (Watanabe et al. 1996), and so growth characterized as "hatchling growth" in artificially fertilized hatchlings may occur while wild embryos are still embryos. In addition, wild hatchlings in this study were maintained at slightly elevated temperatures (up to 20 °C) when compared to the hatchlings of Yatsu et al. (18 °C). This may have accelerated metabolism and yolk utilization.

Like other ommastrephids, *D. gigas* development time is short (3 days) and hatchlings are small (1 mm) when compared to myopsids (25-75 days and 1.6-7 mm, summary in Watanabe et al. 1996) and even other oegopsids such as *Gonatus onyx* (up to 9 months and 3.2-3.5 mm, Seibel et al. 2000). As one might expect based on these features, ommastrephid hatchlings are less developmentally advanced, with development of digestive and respiratory organs delayed until after hatching (Watanabe et al. 1996, Yatsu et al. 1999, Shigeno et al. 2001).

In particular, the eyes of ommastrephid hatchlings are not as morphologically developed as those of squid that hatch at larger sizes (Shigeno et al. 2001, pers. obs.). Laboratory studies of the myopsid *Doryteuthis opalescens* have revealed that hatchlings are active visual predators (Hurley 1976, Chen et al. 1996). It is possible that *D. gigas* hatchlings are not capable of similar visually guided prey capture simply because their eyes are insufficiently developed. This feature may be relevant to the fact that feeding of ommastrephid paralarvae has never been successful. Due to the unusual rhynchoteuthion morphology, it has been suggested that ommastrephid hatchlings are not immediately raptorial feeders, as are many other cephalopod paralarvae, and instead go through an initial dependence on particulates or dissolved organic material (O'Dor et al. 1985, Vidal and Haimovici 1998).

However, *D. gigas* paralarvae displayed swimming (jetting) abilities comparable to those reported for *Doryteuthis opalescens* (Preuss et al. 1997), consistent with the recent finding that loliginid and ommastrephid squids have similar metabolic rates throughout their common size range (Seibel 2007). If the swimming abilities of newly hatched *D. gigas* paralarvae are not used initially for prey capture, they may instead serve to avoid predation. The warm, well-lit and well-oxygenated surface waters where the egg mass was discovered may be good for development, but leave hatchlings vulnerable to visual predators, particularly during daylight.

One solution would be to sink to slightly greater depths during the day and return to the near-surface environment during the night. Evidence exists for a diel migration in the paralarvae of at least one ommastrephid, *Sthenoteuthis oualaniensis*. Piatkowski et al. (1993) found that paralarvae of this species were concentrated between 30-75 m depth during the day, whereas at night they were distributed fairly evenly between these depths and the surface. A migration of 15 m, from the egg mass depth of 16 m into a slightly deeper daytime zone, would take less than 1 hour at 0.5 cm/s. As the hatchling squid grew, the extent of this diel migration could gradually increase to the large distance seen in adults.

A.6. Acknowledgements

Thanks first and foremost to the co-authors of this study: Susana Camarillo-Coop, Steve Haddock, Al Nyack, John Payne, Cesar Salinas-Zavala, Brad Seibel, Lloyd Trueblood, Chad Widmer, and William Gilly. We are especially grateful to the crew of the R/V New Horizon and all cruise participants, especially champion squid fisherman Raul Ramirez-Rojo. We would also like to thank Alison Sweeney and Rui Rosa for their participation in the dive. Louis Zeidberg generously provided lyophilized oviducal gland for artificial fertilization, and Ashley Booth kindly made the map. Special thanks are due to Zora Lebaric and Carl Elliger, who used molecular techniques to positively identify the wild embryos as *Dosidicus gigas*. The manuscript was greatly improved by comments from Unai Markaida, Louis Zeidberg, and two anonymous reviewers. This research was supported by NSF grant # OCE-0526493 to B.A.S. and # OCE-0526640 to W.F.G.

A.7. Tables

Table A-1. Ratio of chorion diameter (CD) to embryo total length (TL) for eggs from artificial fertilization, captive-spawned egg mass and naturally deposited wild egg mass at different developmental stages (Stage after Watanabe et al. 1996). Values of mean ± standard deviation are indicated. N indicates number of embryos measured.

Embryo source	Stage	N	CD:TL
artificial fertilization 2006	21-23	4	1.06 ± 0.03
artificial fertilization 2007	1	5	1.05 ± 0.02
	5	5	1.15 ± 0.05
	10	5	1.08 ± 0.06
	15	5	1.16 ± 0.04
	20	5	1.17 ± 0.11
	25	5	1.08 ± 0.09
captive-spawned 2006	21-23	4	1.20 ± 0.18
captive-spawned 2007	19-20	4	1.25 ± 0.12
wild egg mass	25	10	2.08 ± 0.13

Table A-2. Wild egg mass paralarval dimensions (in mm) through development. Mean ± standard deviation. Age is given in days post-hatching. N indicates number of paralarvae measured.

Age	N	DML	Mantle width	Proboscis length	Head width
0	10	1.02 ± 0.08	0.80 ± 0.04	0.0	0.60 ± 0.05
3	4	1.55 ± 0.17	1.29 ± 0.13	0.55 ± 0.06	0.79 ± 0.06
6	4	1.36 ± 0.08	1.27 ± 0.05	0.55 ± 0.08	0.75 ± 0.09

A.8. Figures

Figure A-1. Location of CTD casts and egg mass in the Guaymas Basin. Inset locates the region in the Gulf of California. Depth contours are every 100 m; 1700 m and 1800 m contours are labeled. Bathymetry data from U.S. Department of Commerce, National Oceanic and Atmospheric Administration, National Geophysical Data Center, 2006. *2-minute Gridded Global Relief Data (ETOPO2v2)* http://www.ngdc.noaa.gov/mgg/fliers/06mgg01.html

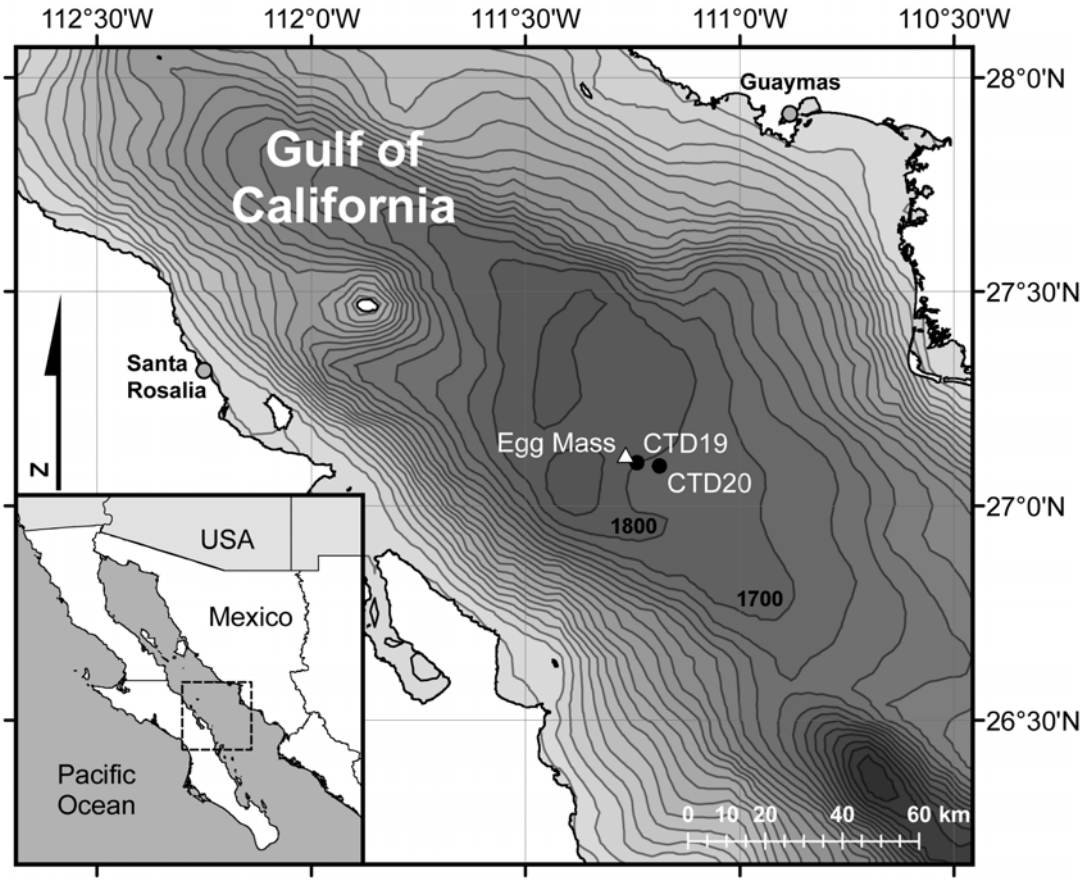

Figure A-2. Oceanographic features revealed by CTD casts (salinity: dotted line, temperature: solid line, oxygen: filled gray) near the site where the egg mass was found. A line is drawn across both casts at 16 m, the depth of the egg mass discovery.

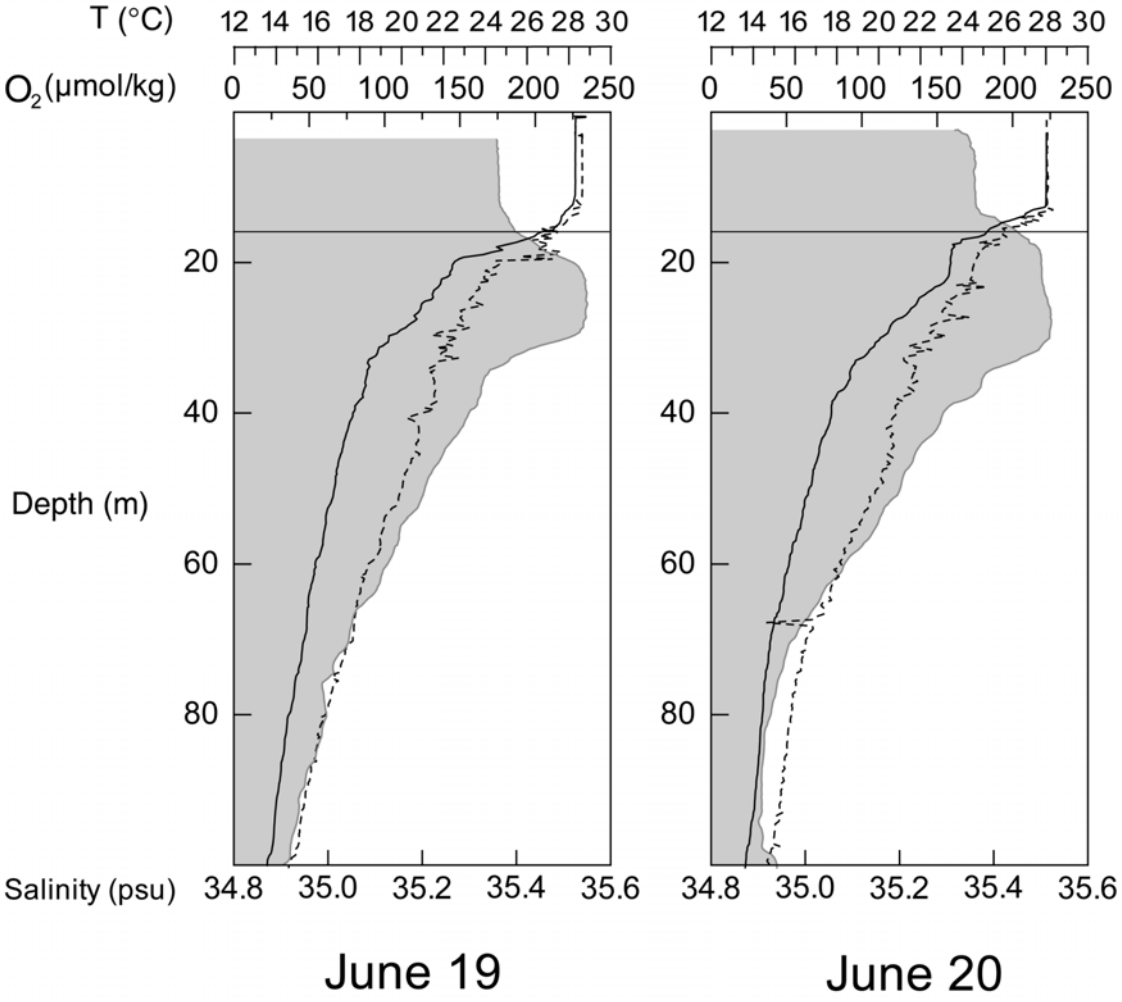

Figure A-3. Part of the naturally deposited egg mass with a portion of a diver and the blue-water safety-line visible. The diver is behind the semi-transparent egg mass. This was a frame grab from video taken at a 29.97 Hz frame rate.

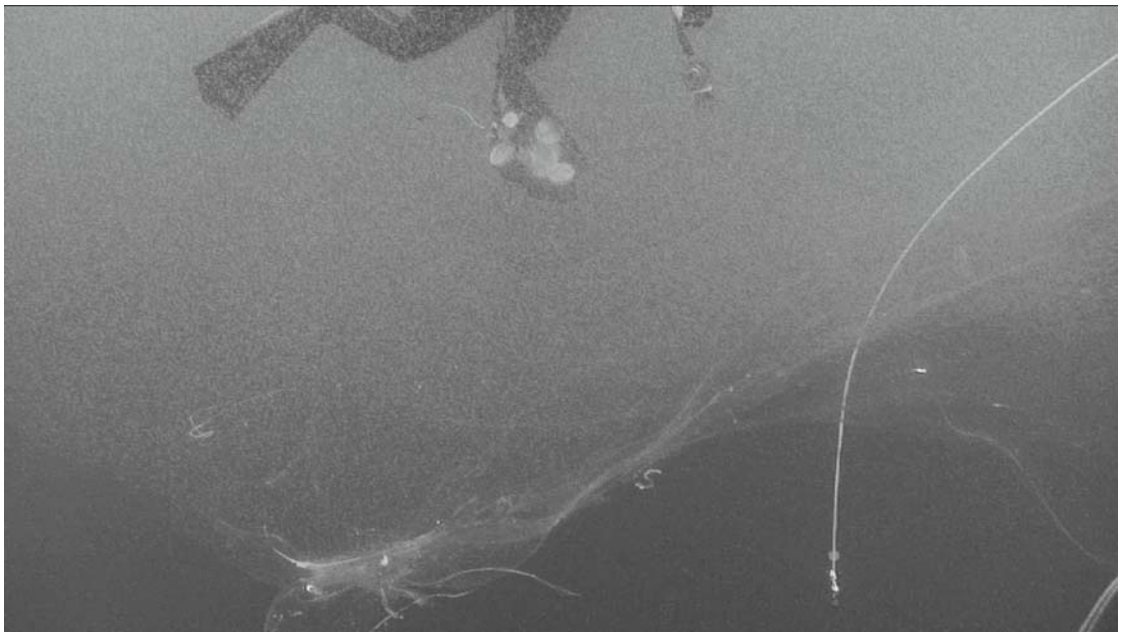

Figure A-4. Developing embryo (Stage 25) from the wild egg mass (A) and an unfertilized egg deposited in captivity (B). The unusual envelope surrounding the chorion is similarly sized, although the chorion of the wild egg is much more expanded. Scale bars are approximately 1 mm.

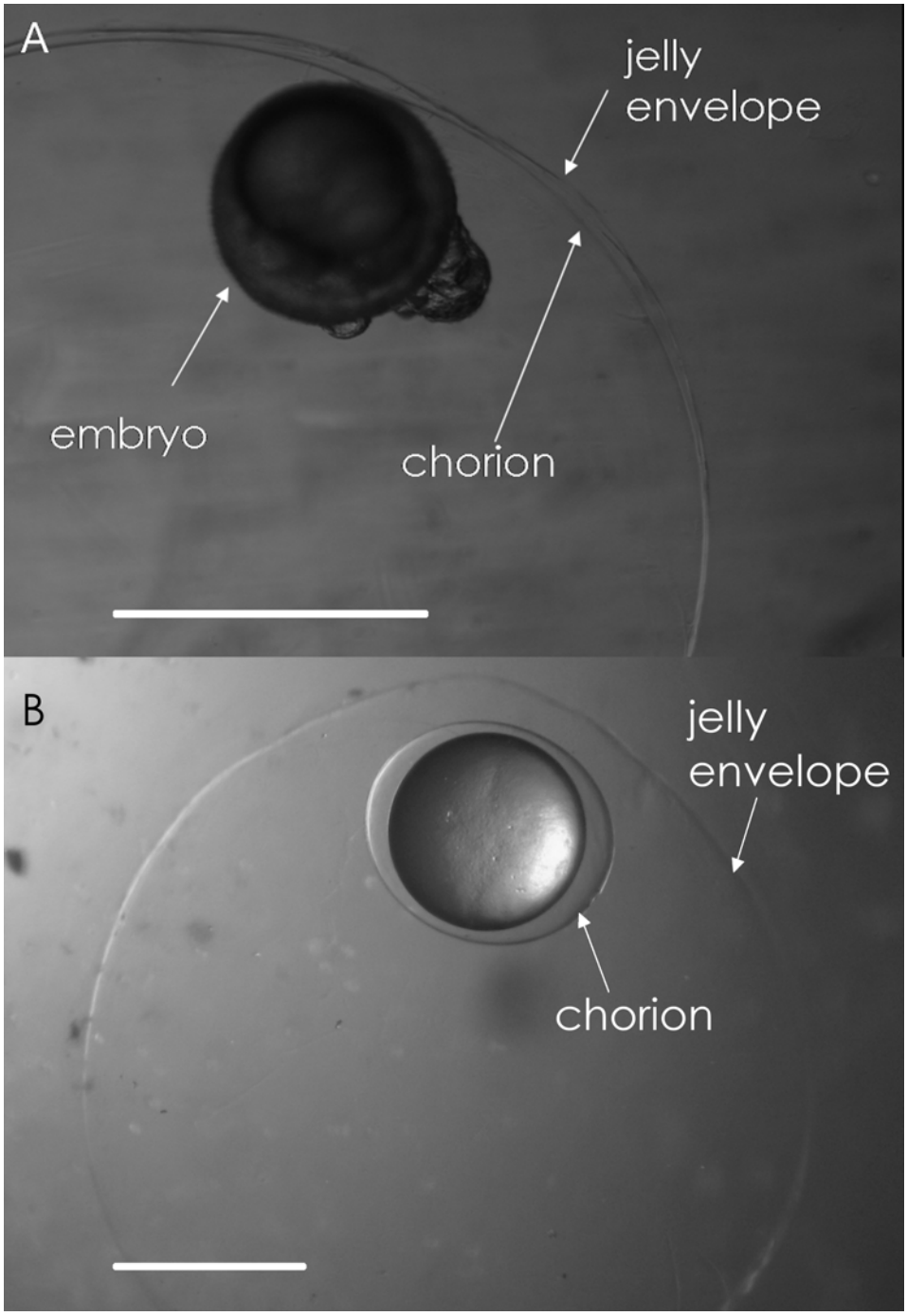

Figure A-5. Representative proboscis extension derived from a video clip (29.97 Hz frame rate). Inset frames are before extension, at the peak of extension, and during retraction. Scale bar in first frame is approximately 1 mm.

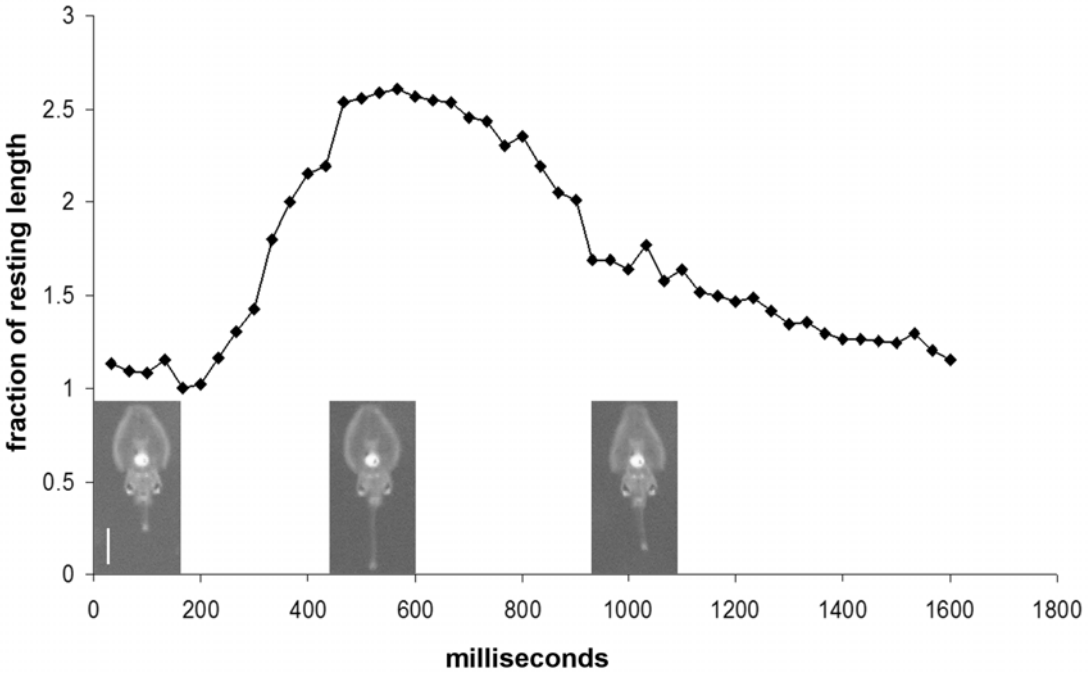

Figure A-6. Drawings from video frames (29.97 Hz frame rate) illustrating roughly synchronous activity of chromatophores on the dorsal mantle surface which occurred when the paralarva touched the water surface.

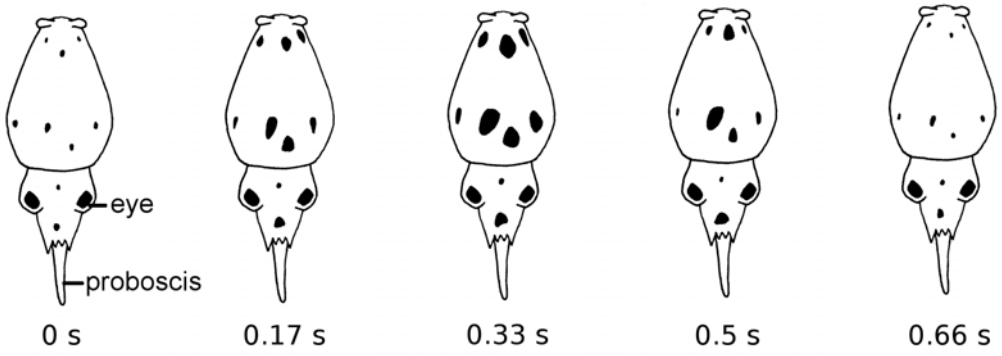

References

Abitía-Cárdenas L, Muhlia-Melo A, Cruz-Escalona V, Galván-Magaña F (2002) Trophic dynamics and seasonal energetics of striped marlin *Tetrapturus audax* in the southern Gulf of California, Mexico. Fish Res 57:287-295

Anderson C, Rodhouse PG (2001) Life cycles, oceanography and variability: ommastrephid squid in variable oceanographic environments. Fish Res 54: 133-143

Anderson EJ, DeMont ME (2000). The mechanics of locomotion in the squid *Loligo pealei*: locomotory function and unsteady hydrodynamics of the jet and intramantle pressure. J Exp Biol 203:2851-2863

Anderson EJ, Grosenbaugh MA (2005) Jet flow in steadily swimming adult squid. J Exp Biol 208:1125-1146

Arnold JM (1965) Normal embryonic stages of the squid, *Loligo pealii* (Lesueur). Biol Bull 128:24-32

Arnold JM, O'Dor RK (1990) In vitro fertilization and embryonic development of oceanic squid. J Cephalopod Biol 1:21-36

Arnold JM, Williams-Arnold LD (1976) The egg cortex problem as seen through the squid eye. Am Zool 16:421-446

Atkinson B (1973) Squid nidamental gland extract: isolation of a factor inhibiting ciliary activity. J Exp Zool 184:335-340

Bailey KM, Francis RC, Stevens PR (1982) The life history and fishery of Pacific whiting, *Merluccius productus*. Calif Coop Oceanic Fish Invest Rep 23:81-98

Balch N, O'Dor RK, Helm P (1985) Laboratory rearing of rhynchoteuthions of the ommastrephid squid *Illex illecebrosus* (Mollusca: Cephalopoda). Vie Milieu 35:243–246

Barlow J, Forney KA (2007) Abundance and population density of cetaceans in the California Current ecosystem. Fish Bull 105:509-526

Bartol IK, Patterson MR, Mann R (2001). Swimming mechanics and behavior of the negatively buoyant shallow-water brief squid *Lolliguncula brevis*. J Exp Biol 204:3655-3682

Bartol IK, Krueger PS, Thompson JT, Stewart WJ (2008) Swimming dynamics and propulsive efficiency of squids throughout ontogeny. Integr Comp Biol 48:720-733

Bartol IK, Krueger PS, Stewart WJ, Thompson JT (2009). Pulsed jet dynamics of squid hatchlings at intermediate Reynolds numbers. J Exp Biol 212:1506-1518.

Bazzino G, Salinas-Zavala C, Markaida U (2007) Variability in the population structure of jumbo squid (*Dosidicus gigas*) in Santa Rosalía, central Gulf of California. Cienc Mar 33:173-186

Bennet-Clark HC (1975) The energetics of the jump of the locust *Schistocerca gregaria*. J Exp Biol 47:53-83

Biggs J, Epel D (1991) Egg capsule sheath of *Loligo opalescens* Berry: structure and association with bacteria. J Exp Zool 259:263-267

Boletzky Sv (1974) The "larvae" of cephalopoda: a review. Thalassia Jugosl 10:45-76

Boletzky Sv (1994) Embryonic development of cephalopods at low temperatures. Antarctic Sci 6:139-142

Boletzky Sv (2003) Biology of early life stages in cephalopod molluscs. Adv Mar Biol 44:143-293

Bower JR, Sakurai Y (1996) Laboratory observations on *Todarodes pacificus* (Cephalopoda: Ommastrephidae) egg masses. Am Malacol Bull 13:65–71

Boyle PR (1991) The UFAW Handbook on the care and management of cephalopods in the laboratory. Universities Federation for Animal Welfare

Boyle PR, Rodhouse P (2005) Cephalopods: Ecology and Fisheries. Oxford: Blackwell Science

Brierley AS, Rodhouse PG, Thorpe JP, Clarke MR (1993) Genetic evidence of population heterogeneity and cryptic speciation in the ommastrephid squid *Martialia hyadesi* from the Patagonia Shelf and Antarctic Polar Frontal Zone. Mar Biol 116:593-602

Brown DM, Cheng L (1981) New net for sampling the ocean surface. Mar Ecol Prog Ser 5:225-227

Brunetti NE (1990) Description of rhynchoteuthion larvae of *Illex argentinus* from the summer spawning subpopulation. J Plank Res 12:1045-1057

Caddy JF, Rodhouse PGD (1998) Cephalopod and groundfish landings: evidence for ecological change in global fisheries? Rev Fish Biol Fish 8:431-444

Caley M, Carr M, Hixon M, Hughes T, Jones G, Menge B (1996) Recruitment and the local dynamics of open marine populations. Annu Rev Ecol Syst 27:477-500

Camarillo-Coop S, De Silva-Dávila R, Hernández-Rivas ME, Durazo-Arvizu R (2006) Distribution of *Dosidicus gigas* paralarvae off the west coast of the Baja California peninsula, Mexico. GLOBEC: The role of squid in open ocean ecosystems, 16-17 November, Hawaii, USA

Camarillo-Coop S, Salinas Zavala C (2008) New distribution areas of *Dosidicus gigas* paralarvae and juveniles in the Gulf of California. 4th International Symposium on Pacific Squids, 28 November - 2 December, Coquimbo, Chile

Camarillo-Coop S, Salinas-Zavala C, Manzano-Sarabia M, Aragón-Noriego EA. Presence of *Dosidicus gigas* paralarvae (Cephalopoda: Ommastrephidae) in the central Gulf of California, Mexico relates to oceanographic conditions. J Mar Biol Assoc UK in press

Carlini DB, Kunkle LK, Vecchione M (2006) A molecular systematic evaluation of the squid genus *Illex* (Cephalopoda: Ommastrephidae) in the North Atlantic Ocean and Mediterranean Sea. Mol Phy Evol 41:496-502

Carvalho GR, Thompson A, Stoner AL (1992) Genetic diversity and population differentiation in the shortfin squid (*Illex argentinus*) in the south-west Atlantic. J Exp Mar Biol Ecol 158:105-121

Chen DS, Van Dykhuizen G, Hodge J, Gilly WF (1996) Ontogeny of Copepod Predation in Juvenile Squid (*Loligo opalescens*). Biol Bull 190:69-81

Clarke M (1965) Large light organs on the dorsal surfaces of the squids *Ommastrephes pteropus*, "*Symplectoteuthis oualaniensis*," and "*Dosidicus gigas*." Proc Malacol Soc London 36:319-321

Clarke M (1966) A review of the systematic and ecology of oceanic squids. Adv Mar Biol 4:147-187

Clarke R, Paliza O (2000) The Humboldt current squid *Dosidicus gigas* (Orbigny, 1835). Rev Biol Mar Oceanog 35:1-38

Clement M, Posada D, Crandall K (2000) TCS: a computer program to estimate gene genealogies. Mol Ecol 9:1657-1660

Cosgrove JA (2005) The first specimens of Humboldt squid in British Columbia. PICES Press 13:30-31

Crawford K (2002) Culture method for *in vitro* fertilization to hatching of the squid, *Loligo pealii*. Biol Bull 203:216-217

Davis RW, Jaquet N, Gendron D, Markaida U, Bazzino G, Gilly W (2007) Diving behavior of sperm whales in relation to behavior of a major prey species, the jumbo squid, in the Gulf of California, Mexico. Mar Ecol Prog Ser 333:291–302

Donald KM, Kennedy M, Spencer HG (2005) Cladogenesis as the result of long-distance rafting events in South Pacific topshells (Gastropoda, Trochidae). Evolution 59:1701-1711

Dunlap CR (1970) A reconnaissance of the deep scattering layers in the eastern tropical Pacific and the Gulf of California. In: Farquhar GB (ed) Proc Int Symp on Biological Sound Scattering in the Ocean, Airlie House Conference Center, Warrenton, VA, 31 March – 2 April. Maury Center for Ocean Science, Report 005, Washington, DC, pp. 395-408

Dunning M (1998) A review of the systematics, distribution and biology of the arrow squid genera *Ommastrephes* Orbigny, 1835, *Sthenoteuthis* Verrill, 1880, and *Ornithoteuthis* Okada, 1927 (Cephalopoda, Ommastrephidae). In: Voss NA, Vecchione M, Toll RB, Sweeney MJ (eds) Systematics and Biogeography of Cephalopods. Smith Contr Zool 586:425-433

Durward RD, Vessey E, O'Dor RK, Amaratunga T (1980) Reproduction in the squid, *Illex illecebrosus*: first observations in captivity and implications for the life cycle.

International Commission for the Northwest Atlantic Fisheries Selected Papers 6, 7–13

Ersts PJ [Internet] Geographic Distance Matrix Generator (version 1.2.3). American Museum of Natural History, Center for Biodiversity and Conservation. Available from http://biodiversityinformatics.amnh.org/open_source/gdmg. Accessed on 2009-12-4

Excoffier L, Laval G, Schneider S (2005) Arlequin (version 3.0): An integrated software package for population genetics data analysis. Evol Bioinform Online 1:47-50

Fernandez-Alamo MA and Farber-Lorda J (2006) Zooplankton and the oceanography of the eastern tropical Pacific: A review. Prog Oceanogr 69:318-359

Fiedler PC, Talley LD (2006) Hydrography of the eastern tropical Pacific: A review. Prog Oceanogr 69:143-180

Field JC, Baltz K, Phillips AJ, Walker WA (2007) Range expansion and trophic interactions of the jumbo squid, *Dosidicus gigas*, in the California Current. Calif Coop Oceanic Fish Invest Rep 48:131-144

Fisher R, Bellwood DR, Job SD (2000) Development of swimming abilities in reef fish larvae. Mar Ecol Prog Ser 202:163-173

Folmer O, Black M, Hoeh W, Lutz R, Vrijenhoek R (1994) DNA primers for amplification of mitochondrial cytochrome c oxidase subunit I from diverse metazoan invertebrates. Mol Mar Bio Biotech 3:294-299

Gilbert DL, Adelman WJ, Arnold JM, eds. (1990). Squid as Experimental Animals. New York: Plenum Press

Gilly WF, Markaida U (2007) Perspectives on *Dosidicus gigas* in a changing world. In: Olson RW and Young J (eds), GLOBEC Report: The ecological role of squids in pelagic ecosystems, CLIOTOP workshop, 16-17 November, 2006, Honolulu, HI. In press

Gilly WF, Hopkins B, Mackie GO (1991) Development of giant motor axons and neural control of escape responses in squid embryos and hatchlings. Biol Bull 180:209–220

Gilly WF, Elliger CA, Salinas-Zavala CA, Camarillo-Coop S, Bazzino G, Beman M (2006a) Spawning by jumbo squid *Dosidicus gigas* in the San Pedro Mártir Basin, Gulf of California, Mexico. Mar Ecol Prog Ser 313:125–133

Gilly WF, Markaida U, Baxter CH, Block BA, Boustany A, Zeidberg L, Reisenbichler K, Robison B, Bazzino G, Salinas C (2006b) Vertical and horizontal migrations by the jumbo squid *Dosidicus gigas* revealed by electronic tagging. Mar Ecol Prog Ser 324:1-17

Gosline JM, Demont ME (1985) Jet-propelled swimming in squids. Sci Am 252:96-103

Gosline JM, Shadwick RE (1983) The role of elastic energy storage mechanisms in swimming: an analysis of mantle elasticity in escape jetting in the squid, *Loligo opalescens*. Can J Zool 61:1421-1431

Gosline JM, Steeves JD, Harman AD, DeMont ME (1983) Patterns of circular and radial mantle activity in respiration and jetting in the squid *Loligo opalescens*. J Exp Biol 104:97-109

Guerra A, González AF, Rocha FJ, Sagarminaga R, Cañadas A (2002) Planktonic egg masses of the diamond-shaped squid *Thysanoteuthis rhombus* in the eastern Atlantic and the Mediterranean Sea. J Plank Res 24:333-338

Guerra A, Rocha F (1997) On a floating egg mass of the diamond shaped squid *Thysanoteuthis rhombus* (Cephalopoda: Thysanoteuthidae) in the western Mediterranean. Iberus 15:125-130

Guindon S, Gascuel O (2003) PhyML - A simple, fast, and accurate algorithm to estimate large phylogenies by maximum likelihood. Syst Biology 52:696-704

Haddock SHD, Heine JN (2005) Scientific blue-water diving. California Sea Grant, La Jolla

Happel J, Brenner H (1965) Low Reynolds number hydrodynamics. New Jersey: Prentice Hall

Harman RF, Young RE (1985) The larvae of ommastrephid squids (Cephalopoda, Teuthoidea) from Hawaiian waters. Vie Milieu 35:211-222

Harman RF, Young RE, Mangold KM, Suzuki T, Hixon RF (1989) Evidence of multiple spawning in the tropical oceanic squid *Sthenoteuthis oualaniensis* (Teuthoidea: Ommastrephidae). Mar Biol 101:513-519

Haury L, Weihs D (1976) Energetically efficient swimming behavior of negatively buoyant zooplankton. Limnol Oceanog 21:797-803

Hellberg ME, Vacquier VD (1999) Rapid evolution of fertilization selectivity and lysin cDNA sequences in teguline gastropods. Mol Biol Evol 16:839-848

Hernández-Rivas ME, De Silva-Dávila R, Camarillo-Coop S, Granadores-Amores J, Durazo R (2007) Ommastrephid paralarvae during 1997-1999 IMECOCAL cruises. Calif Coop Oceanic Fish Invest Conference, 26-28 November, San Diego, California, USA

Hey J, Nielsen R (2004) Multilocus methods for estimating population sizes, migration rates and divergence time, with applications to the divergence of *Drosophila pseudoobscura* and *D. persimilis*. Genetics 167:747–760

Hoar JA, Sim E, Webber DM, O'Dor RK (1994) The role of fins in the competition between squid and fish. In: Maddock L, Bone Q, Rayner JMC (eds) Mechanics and Physiology of Animal Swimming. Cambridge: Cambridge University Press, pp. 27-33

Hoelzel AR (1998) Genetic structure of cetacean populations in sympatry, parapatry, and mixed assemblages: implications for conservation policy. J Hered 89:451-458

Hoerner SF (1965) *Fluid-Dynamic Drag*. Bricktown, NJ, USA: Hoerner Fluid Dynamics

Holmes J, Cooke K, Cronkite G (2008) Interactions between jumbo squid (*Dosidicus gigas*) and Pacific hake (*Merluccius productus*) in the northern California Current in 2007. Calif Coop Oceanic Fish Invest Rep 49:86-89

Huffard CL, Buck K, Robison B (2007) Assessment of *Dosidicus gigas* sperm logevity using fluorescence microscopy. Calif Coop Oceanic Fish Invest Rep 48:65

Hunt JC, Zeidberg LD, Hamner WM, Robison BH (2000) The behavior of *Loligo opalescens* (Mollusca: Cephalopoda) as observed by a remotely operated vehicle (ROV). J Mar Biol Assoc UK 80:873-883

Hurley AC (1976) Feeding behavior, food consumption, growth, and respiration of the squid *Loligo opalescens* raised in the laboratory. Fish Bull 74:176-l 82

Huyer A (1982) Coastal upwelling in the California Current system. Prog Oceanogr 12:259-284

Ichii T, Mahapatra K, Watanabe T, Yatsu A, Inagake D, and Okada Y (2002) Occurrence of jumbo flying squid *Dosidicus gigas* aggregations associated with the counter current ridge off the Costa Rica Dome during 1997 El Niño and 1999 La Niña. Mar Ecol Prog Ser 231:151-166

Ikeda Y, Sakurai Y, Shimazaki K (1993a) Maturation process of the Japanese common squid *Todarodes pacificus* in captivity. In: Okutani T, O'Dor RK, Kubodera T (eds) Recent Advances in Cephalopod Fisheries Biology. Tokyo: Tokai University Press, pp. 27-33

Ikeda Y, Sakurai Y, Shimazaki K (1993b) Fertilizing capacity of squid (*Todarodes pacificus*) spermatozoa collected from various sperm storage sites, with special reference to the role of gelatinous substance from oviducal gland in fertilization and embryonic development. Invertebr Repr Dev 23:39-44

Jameson A, Schmidt W, Turkel E (1981) Numerical solutions of the Euler equations by finite-volume methods using Runge-Kutta timestepping. AIAA Pap 81-1259.

Kagan BM (1935) The fertilizable period of the eggs of *Fundulus heteroclitus* and some associated phenomena. Biol Bull 69:185-201

Keyl F, Argüelles J, Mariátegui, L, Tafur R, Wolff M, Yamashiro C (2008) A hypothesis on range expansion and spatio-temporal shifts in size-at-maturity of jumbo squid (*Dosidicus gigas*) in the Eastern Pacific Ocean. Calif Coop Oceanic Fish Invest Rep 49:119-128

Kimura M (1980) A simple method for estimating evolutionary rate of base substitutions through comparative studies of nucleotide sequences. J Mol Evol 16:111-120

Klein K, Jaffe LA (1984) Development of *in vitro* fertilized eggs of the squid *Loligo pealii*, and techniques for dechorionation and artifical activation. Biol Bull 167:518

Klimley AP, Caberera-Mancilla I, Castillo-Geniz JL (1993) Horizontal and vertical movements of the scalloped hammerhead shark, *Sphyrna lewini*, in the southern Gulf of California, Mexico. Cienc Mar 19:95-115

Laptikhovsky VV (1991) Mathematical model for the study of duration of embryogenesis in cephalopods. Biologicheskiye Nauki 3:37-48 (In Russian, English summary)

Laptikhovsky VV (1999) Improved mathematical model to study the duration of embryogenesis in cephalopod molluscs. Ruthenica 9:141-146

Laptikhovsky VV, Murzov SA (1990) A catch of the epipelagic egg mass of the squid *Stenoteuthis pteropus* in Eastern Tropical Atlantic. Biologiya Morya 3:62-63 (In Russian, English summary).

Laptikhovsky VV, Nigmatullin CM (1993) Egg size, fecundity, and spawning in females of the genus *Illex* (Cephalopoda: Ommastrephidae). ICES J Mar Sci 50:393-403

Lipiński MR, Underhill LG (1995) Sexual maturation in squid: Quantum or continuum? South African J Mar Sci 15:207-223

Mantel N (1967) The detection of disease clustering and a generalized regression approach. Cancer Res 27:209-220

Markaida U (2006) Population structure and reproductive biology of jumbo squid *Dosidicus gigas* from the Gulf of California after the 1997–1998 El Niño event. Fish Res 79:28-37

Markaida U, Sosa-Nishizaki O (2001) Reproductive biology of jumbo squid *Dosidicus gigas* in the Gulf of California, 1995-1997. Fish Res 54:63-82

Markaida U, Sosa-Nishizaki O (2003) Food and feeding habits of jumbo squid *Dosidicus gigas* (Cephalopoda: Ommastrephidae) from the Gulf of California, Mexico. J Mar Biol Assoc UK 83:507-522

Markaida U, Quiñonez-Velazquez C, Sosa-Nishizaki O (2004) Age, growth and maturation of jumbo squid *Dosidicus gigas* (Cephalopoda: Ommastrephidae) from the Gulf of California, Mexico. Fish Res 66:31–47

Markaida U, Rosenthal JJ, Gilly WF (2005). Tagging studies on the jumbo squid (*Dosidicus gigas*) in the Gulf of California, Mexico. Fish Bull 103:219-226

Markaida U, Gilly W, Salinas-Zavala CA, Rosas-Luis R, Booth JAT (2007) Food and feeding of jumbo squid *Dosidicus gigas* in the central Gulf of California during 2005-2007. Calif Coop Oceanic Fish Invest Rep 49:90-103

Marko PB (2002) Fossil calibration of molecular clocks and the divergence times of geminate species pairs separated by the isthmus of Panama. Mol Biol Evol 18:2005-2021

Masuda S, Yokawa K, Yatsu A, Kawahara S (1996) Growth and population structure of *Dosidicus gigas* in the southeastern Pacific Ocean.). In: Okutani T (ed), Large Pelagic Squids. Tokyo: Japan Marine Fishery Resource Research Center, pp. 107-118.

McGowan JA, Brown DM (1966) A new opening-closed paired zooplankton net. Univ Calif: Scripps Inst Oceanogr Ref 66-23, pp. 1-56

McHenry MJ, Jed J (2003) The ontogenetic scaling of hydrodynamics and swimming performance in jellyfish (*Aurelia aurita*). J Exp Biol 206:4125-4137

Mileikovsky SA (1973) Speed of active movement of pelagic larvae of marine bottom invertebrates and their ability to regulate their vertical position. Mar Biol 23:11-17

Milligan BJ, Curtin NA, Bone Q (1997) Contractile properties of obliquely striated muscle from the mantle of squid (*Alloteuthis subulata*) and cuttlefish (*Sepia officinalis*). J Exp Biol 200:2425-2436

Miyahara K, Fukui K, Ota T, Minami T (2006) Laboratory observations on the early life stages of the diamond squid *Thysanoteuthis rhombus*. J Moll Studies 72:199-205

Miyanaga S, Sakurai Y (2006) Effect of temperature on the swimming behavior of Japanese common squid (Todarodes pacificus) paralarvae. In: Proceedings of the Cephalopod International Advisory Council Symposium 2006, Cephalopod Life Cycles, 6-10 February, Hotel Grand Chancellor, Hobart, Tasmania, p. 89

Moltschaniwskyj NA, Hall K, Lipinski M, Marian JEAR, Nishiguchi M, Sakai M, Shulman DJ, Sinclair B, Sinn DL, Staudinger M, Van Gelderen R, Villanueva R, Warnke K (2007) Ethical considerations when using cephalopods as experimental animals. Rev Fish Biol Fish 17:455-476

Moreno A, Dos Santos A, Piatkowski U, Pantos AMP, Cabral H (2009) Distribution of cephalopod paralarvae in relation to the regional oceanography of the western Iberia. J Plank Res 31:73-91

Nesis KN (1977) Population structure of the squid *Sthenoteuthis oualaniensis* (Lesson 1930) (Ommastrephidae) in the Tropical Western Pacific. Trud Inst Ocean 107: 15-29 [In Russian]

Nesis KN (1983) *Dosidicus gigas*. In: Boyle PR (ed) Cephalopod Life Cycles Vol 1 Species Accounts. London: Academic Press, pp. 216-231

Nesis KN (1993) Population structure of oceanic ommastrephids, with particular reference to *Sthenoteuthis oualaniensis*: a review. In: Okutani K, O'Dor RK, Kubodera T (eds) Recent Advances in Cephalopod Fisheries Biology. Tokyo: Tokai University Press, pp. 293-312

Nigmatullin CM, Arkhipkin AI (1998) A review of the biology of the diamondback squid, *Thysanoteuthis rhombus* (Oegopsida: Thysanoteuthidae). In: Okutani T (ed), Large Pelagic Squids. Tokyo: Japan Marine Fishery Resource Research Center, pp. 155-181

Nigmatullin CM, Laptikhovsky VV (1994) Reproductive strategies in the squids of the family Ommastrephidae (preliminary report). Ruthenica 4:79-82

Nigmatullin CM, Markaida U (2002) Oocyte development, egg size, and fecundity of the large size females of jumbo squid *Dosidicus gigas*. Second International Symposium on Pacific Squid (November 25-29, 2002), La Paz, Baja California Sur, Mexico. Abstracts book, IPN-CICIMAR, La Paz, p. 9

Nigmatullin CM, Tsygankov VYu, Sabirov RM (1983a) On the taxonomic status of the early-maturing and late-maturing forms of the squid *Sthenoteuthis oualaniensis* (Lesson). Starobogatov Ya.I. and Nesis K.N. (eds). *Taxonomy and ecology of cephalopods*. Leningrad: Zoological Institute of Academy of Sciences USSR Publ. pp 94-96 (In Russian)

Nigmatullin CM, Sabirov RM, Tsygankov VYu, Schetinnikov SA (1983b) Reproductive biology of squids *Sthenoteuthis oualaniensis* (Lesson) and *Dosidicus gigas* (d'Orbigny) in the eastern tropical Pacific. Starobogatov Ya.I. and Nesis K.N. (eds). *Taxonomy and ecology of cephalopods*. Leningrad: Zoological Institute of Academy of Sciences USSR Publ. pp 122-124 (In Russian)

Nigmatullin CM, Arkhipkin AI, Sabirov RM (1995) Age, growth and reproductive biology of diamond-shaped squid *Thysanoteuthis rhombus* (Oegopsida: Thysanoteuthidae). Mar Ecol Prog Ser 124:73–87

Nigmatullin CM, Laptikhovsky VV, Mokrin N, Sabirov R, Markaida U (1999) On life history traits of the jumbo squid *Dosidicus gigas*. In: Tresierra Aguilar AE and Culquichicon ZG (eds), VIII Congreso Latinoamericano sobre Ciencias del Mar (COLACMAR), Trujillo, Peru, 17-21 October. Libro de Resúmenes Ampliados, Tomo I, p. 291

Nigmatullin CM, Nesis KN, Arkhipkin AI (2001) Biology of the jumbo squid *Dosidicus gigas* (Cephalopoda: Ommastrephidae). Fish Res 54:9-19

Norris, RD (2000) Pelagic species diversity, biogeography, and evolution. Paleobiology 26(4) Supplement (Autumn, 2000): 236-258

O'Dor RK (1988a) Forces acting on swimming squid. J Exp Biol 137:421-442

O'Dor RK (1988b) Limitations on locomotor performance in squid. J Appl Physiol 64:128-134

O'Dor RK, Balch N (1985) Properties of *Illex illecebrosus* egg masses potentially influencing larval oceanographic distribution. Northwest Atlantic Fisheries Organization Scientific Council Studies 9:69-76

O'Dor RK, Hoar JA (2000) Does geometry limit squid growth? J Mar Sci 57:8-14

O'Dor RK, Webber DM (1991) Invertebrate athletes: trade-offs between transport efficiency and power density in cephalopod evolution. J Exp Biol 160:93-112

O'Dor RK, Balch N, Amaratunga T (1982a) Laboratory observations of midwater spawning by *Illex illecebrosus*. Sci Counc Stud NAFO 6:5-8

O'Dor RK, Balch N, Foy EA, Hirtle RWM, Johnston DA, Amaratunga T (1982b) Embryonic development of the squid, *Illex illecebrosus*, and effect of temperature on developmental rates. J Northwest Atl Fish Sci 3:41–45

O'Dor RK, Helm P, Balch N (1985) Can rhynchoteuthions suspension feed? (Mollusca: Cephalopoda). Vie Milieu 35:267-271

O'Dor RK, Balch N, Foy EA, Helm PL (1986) The locomotion and energetics of hatchling squid, *Illex illecebrosus*. Am Malacol Bull 4:55-60

O'Shea S, Bolstad KS, Ritchie PA (2004) First records of egg masses of *Nototodarus gouldi* McCoy, 1888 (Mollusca: Cephalopoda: Ommastrephidae), with comments on egg-mass susceptibility to damage by fisheries trawl. New Zealand J Zool 31:161-166

Okada S (1961) On the uninseminated egg and the egg with dead embryo of dog-salmon, *Oncorhynchus keta* (Walbaum). J Fac Agric Hokkaido Univ 51:551-558

Okutani T (1974) Epipelagic decapod cephalopods collected by micronekton tows during the EASTROPAC expeditions, 1967-1968 (systematic part). Bull Tokai Reg Fish Res Lab 80:29-118

Okutani T, McGowan JA (1969) Systematics, distribution, and abundance of the epiplanktonic squid (Cephalopoda, Decapoda) larvae of the California Current, April 1954 - March 1957. Bull Scripps Inst Oceanogr 14. University of California, San Diego, La Jolla

Okutani T, Tung I (1978) Reviews of biology of commercially important squids in Japanese and adjacent waters. Veliger 21:87-94

Packard A (1969) Jet propulsion and the giant fibre response of *Loligo*. Nature 221:875-877

Palomares-García R, De Silva-Dávila R, Avendaño-Ibarra R (2007) Predation of the copepod *Oncaea mediterranea* upon ommastrephid paralarvae in the mouth of the Gulf of California. Proc 1st CLIOTOP Symposium, 3-7 December, La Paz, México

Pastene LA, Goto M, Kanda N, Zerbini AN, Kerem D, Watanabe K, Bessho Y, Hasegawa M, Nielsen R, Larsen F, Palsbøll PJ (2007) Radiation and speciation of pelagic organisms during periods of global warming: the case of the common minke whale, *Balaenoptera acutorostrata*. Mol Ecol 16:1481-1495

Pennington JT, Mahoney KL, Kuwahara VS, Kolber DD, Calienes D, Chaves FP (2006) Primary production in the eastern tropical Pacific: A review. Prog Oceanogr 69:285-317

Piatkowski U, Welsch W, Röpke A (1993) Distribution patterns of the early life stages of pelagic cephalopods in three geographically different regions of the Arabian Sea. In: Okutani T, O'Dor RK, Kubodera T (eds), Recent Advances in Cephalopod Fisheries Biology. Tokyo: Tokai University Press, pp. 417-431

Posada D (2008) jModelTest: Phylogenetic Model Averaging. Mol Biol Evol 25: 1253-1256

Preti A, Kohin S, Dewar H, Ramon DA (2008) Feeding habits of the bigeye thresher shark (*Alopias superciliosus*) sampled from the California-based drift gillnet fishery. Calif Coop Oceanic Fish Invest Rep 49:202–211

Preuss T, Lebaric ZN, Gilly WF (1997) Post-hatching development of circular mantle muscles in the squid *Loligo opalescens*. Biol Bull 192:375-387

Ramos-Castillejos JE, Salinas-Zavala CA, Camarillo-Coop S, Enriquez-Paredes LM (2010) Paralarvae of the jumbo squid, *Dosidicus gigas*. Invertebr Biol 129:172-183

Redfern JV, Ferguson MC, Becker EA, Hyrenbach KD and others (2006) Techniques for cetacean-habitat modelling. Mar Ecol Prog Ser 310:271–295

Rocha F, Guerra A, González AF (2001) A review of reproductive strategies in cephalopods. Biol Rev 76:291-304

Rodríguez F, Oliver JF, Marín A, Medina JR (1990) The general stochastic model of nucleotide substitution. J Theor Biol 142:485-501

Roper CFE, Sweeny MJ, Nauen CE (1984) Cephalopods of the world: an annotated and illustrated catalogue of species of interest to fisheries. FAO Species Catalogue Vol. 3, FAO Species Synopses, 125

Rosa R, Seibel BA (2010) Metabolic physiology of the Humboldt squid, *Dosidicus gigas*: Implications for vertical migration in a pronounced oxygen minimum zone. Prog Ocean 86:72-80

Rosa R, Seibel BA (2010) Slow pace of life of the Antarctic colossal squid. J Mar Biol Assoc UK doi:10.1017/S0025315409991494

Rosas-Aloya J, Hernández-Herrera A, Galván-Magaña F, Abitía-Cárdenas L, Muhlia-Melo A (2002) Diet composition of sailfish (*Istiophorus platypterus*) from the southern Gulf of California, Mexico. Fish Res 57:185-195

Ruegg JC (1968) Contractile mechanisms of smooth muscle. Symp Soc Exp Biol 22:45-66

Ruiz-Cooley RI, Gendron D, Aguíñiga S, Mesnick S, Carriquiry JD (2004) Trophic relationships between sperm whales and jumbo squid using stable isotopes of C and N. Mar Ecol Prog Ser 277:275–283

Sabirov RM, Arkhipkin AI, Tsygankov VY, Schetinnikov AS (1987) Egg laying and embryonal development of diamond-shaped squid, *Thysanoteuthis rhombus* (Oegopsida. Thysanoteuthidae). Zool Zhurnal 66:1155-1163

Saito H and Kubodera T (1993), Distribution of ommastrephid rhynchoteuthion paralarvae (Mollusca, Cephalopoda) in the Kuroshio Region. In: Okutani T, O'Dor RK, Kubodera T (eds), Recent Advances in Cephalopod Fisheries Biology. Tokyo: Tokai University Press, pp. 457-466

Sakai M, Mariátegui L, Wakabayashi T, Yamashiro C, Tuchiya K (2008) Distribution and abundance of jumbo flying squid paralarvae (*Dosidicus gigas*) off Perú and in waters west of the Costa Rica Dome during the 2007 La Niña. 4th International Symposium on Pacific Squids, 28 November - 2 December, Coquimbo, Chile

Sakurai Y, Ikeda Y (1994) Laboratory rearing methods of *Todarodes pacificus* for the ecological study of life cycle. Report of 1992 Annual Meeting on Resources and

Fisheries of Squids. National Institute for Far Sea Research, 51-69 (In Japanese, with English title and abstract)

Sakurai Y, Young RE, Hirota J, Mangold K (1995) Artificial fertilization and development through hatching in the oceanic squids *Ommastrephes bartramii* and *Sthenoteuthis oulaniensis* (Cephalopod: Ommastrephidae). Veliger 38:185-191

Sandoval-Castellanos E, Uribe-Alcocer M, Díaz-Jaimes P (2007) Population genetic structure of jumbo squid (*Dosidicus gigas*) evaluated by RAPD analysis. Fish Res 83:113-118

Sandoval-Castellanos E, Uribe-Alcocer M, Díaz-Jaimes P (2010) Population genetic structure of the Humboldt squid (*Dosidicus gigas* d'Orbigny, 1835) inferred by mitochondrial DNA analysis. J Exp Mar Biol Ecol.

Sato T (1976) Results of exploratory fishing for *Dosidicus gigas* (d'Orbigny) off California and Mexico. FAO Fish Rep 170:61-67

Seibel BA (2007) On the depth and scale of metabolic rate variation: scaling of oxygen consumption and enzymatic activity in the Class Cephalopoda (Mollusca). J Exp Biol 210:1-11

Seibel BA, Hochberg FG, Carlini DB (2000). Life history of *Gonatus onyx* (Cephalopoda: Teuthoidea): deep-sea spawning and post-spawning egg care. Mar Biol 137:519-526

Shea EK (2005) Ontogeny of the fused tentacles in three species of ommastrephid squids (Cephalopoda, Ommastrephidae). Invertebr Biol 124:25-38

Shigeno S, Kidokoro H, Goto T, Tsuchiya K, Segawa S (2001) Early ontogeny of the Japanese common squid *Todarodes pacificus* (Cephalopoda, Ommastrephidae) with special reference to its characteristic morphology and ecological significance. Zool Sci 18:1011-1026

Shukhgalter OA, Nigmatullin CM (2001) Parasitic helminths of the jumbo squid *Dosidicus gigas* (Cephalopoda: Ommastrephidae) in open waters of the central east Pacific. Fish Res 54: 95-110.

Slatkin M (1995) A measure of population subdivision based on microsatellite allele frequencies. Genetics 139:457-462

Smith PE, SL Richardson (1977) Standard techniques for pelagic fish egg and larva surveys. FAO Fisheries Technical Paper No. 175.

Snÿder R (1998) Aspects of the biology of the giant form of *Sthenoteuthis oualaniensis* Cephalopoda: Ommastrephidae) from the Arabian Sea. J Moll Stud 64: 21-34

Sokal R, Rohlf FJ (1995) Biometry. WH Freeman and Co, New York.

Staaf DJ, Camarillo-Coop S, Haddock SHD, Nyack AC, Payne J, Salinas-Zavala CA, Seibel BA, Trueblood L, Widmer C, Gilly WF (2008) Natural egg mass deposition by the Humboldt squid (*Dosidicus gigas*) in the Gulf of California and characteristics of hatchlings and paralarvae. J Mar Biol Assoc UK 88:759-770

Stevenson D (1996) Squid locomotion: size limitations on effective and efficient swimming. Honors Thesis, Stanford University.

Strathmann RR, Strathmann MF (1995) Oxygen supply and limits on aggregation of embryos. J Mar Biol Assoc UK 75:413-428

Tafur R, Villegas P, Rabí M, Yamashiro C (2001) Dynamics of maturation, seasonality of reproduction and spawning grounds of the jumbo squid *Dosidicus gigas* (Cephalopoda: Ommastrephidae) in Peruvian waters. Fish Res 54:33-50

Tamura K, Nei M (1993) Estimation of the number of nucleotide substitutions in the control region of mitochondrial DNA in humans and chimpanzees. Mol Biol Evol 10: 512–526

Thompson JT, Kier WM (2001) Ontogenetic changes in mantle kinematics during escape-jet locomotion in the oval squid, *Sepioteuthis lessoniana* Lesson, 1830. Biol Bull 201:154-166

Thompson JT, Kier WM (2002) Ontogeny of squid mantle function: changes in the mechanics of escape-jet locomotion in the oval squid, *Sepioteuthis lessoniana* Lesson, 1830. Biol Bull 203:14-26

Thompson JT, Kier WM (2006) Ontogeny of mantle musculature and implications for jet locomotion in oval squid *Sepioteuthis lessoniana*. J Exp Biol 209:433-443

Thompson JT, Szczepanski JA, Brody J (2008) Mechanical specialization of the obliquely striated circular mantle muscle fibres of the long-finned squid *Doryteuthis pealeii*. J Exp Biol 211:1463-1474

Thorpe JP, Havenhand JN, Patterson K (1986) Report of the University of Liverpool (Department of Marine Biology) to the Falkland Islands Developmental Corporation. Stock and species identity of the Patagonian Shelf *Illex*. Falkland Islands Developmental Corporation, Port Stanley, Falkland Islands.

Trueman ER (1980) Swimming by jet propulsion. In Elder HY and Trueman ER (eds) Aspects of Animal Movement. Cambridge: Cambridge University Press, pp. 93-105

Trueman ER, Packard A (1968) Motor performance of some cephalopods. J Exp Biol 49:495-507

Ueynagi S and Nonaka H (1993) Distribution of ommastrephid paralarvae in the central-eastern Pacific Ocean. In: Okutani T, O'Dor RK, Kubodera T (eds), Recent Advances in Cephalopod Fisheries Biology. Tokyo: Tokai University Press, pp. 587-589

Vecchione M (1999) Extraordinary abundance of squid paralarvae in the tropical eastern Pacific Ocean during El Niño of 1987. Fish Bull 97:1025-1030

Vetter R, Kohin S, Preti A, McClatchie S, and Dewar H (2008) Predatory interactions and niche overlap between mako shark, *Isurus oxyrinchus*, and jumbo squid, *Dosidicus gigas*, in the California Current. Calif Coop Oceanic Fish Invest Rep 49:142-156

Vidal EAG, Haimovici M (1998) Feeding and the possible role of the proboscis and mucus cover in the ingestion of microorganisms by rhynchoteuthion paralarvae (Cephalopod: Ommastrephidae). Bull Mar Sci 63:305-316

Vilchis LI, Ballance LT, Watson W (2009) Temporal variability of neustonic ichthyoplankton assemblages of the eastern Pacific warm pool: Can community structure be linked to climate variability? Deep Sea Res I 56:125-140

Wakabayashi T, Yanagimoto T, Sakai M, Ichii T, Kobayashi T (2008) Identification of *Dosidicus gigas* and *Sthenoteuthis oualaniensis* paralarvae using SSPPCR analysis

onboard a ship. 4th International Symposium on Pacific Squids, 28 November - 2 December, Coquimbo, Chile

Waluda C, Rodhouse P (2006) Remotely sensed mesoscale oceanography of the Central Eastern Pacific and recruitment variability in *Dosidicus gigas*. Mar Ecol Prog Ser 310:25-32

Watanabe K, Ando K, Tsuchiya K, Segawa S (1998) Late embryos and paralarvae of diamondback squid *Thysanoteuthis rhombus* Troschel, 1857. Venus 57:291-301

Watanabe K, Sakurai Y, Segawa S, Okutani T (1996) Development of the ommastrephid squid *Todarodes pacificus*, from fertilized egg through to rhynchoteuthion paralarva. Am Malacol Bull 13:73–88

Watase S (1891) Studies on Cephalopods. i. Cleavage of the Ovum. J Morphol iv:3

Webber DM, O'Dor RK (1986) Monitoring the metabolic rate and activity of free-swimming squid with telemetered jet pressure. J Exp Biol 126:205-224

Weihs D (1980) Energetic significance of changes in swimming modes during growth of larval anchovy, *Engraulis mordax*. Fish Bull 77:597-604

Weir BS (1996) Disequilibrium. Genetic data analysis II: methods for discrete population genetic data. Sunderland, MA: Sinaur Associates, pp. 91-139

Weir BS, Cockerham CC (1984) Estimating F-statistics for the analysis of population structure. Evolution 38:1358-1370

Wing BL (2006) Unusual invertebrates and fish observed in the Gulf of Alaska, 2004-2005. PICES Press 14:26-28

Wormuth JH (1976) The biogeography and numerical taxonomy of the oegopsid squid family Ommastrephidae in the Pacific Ocean. Bull Scripps Inst Oceanogr 23:1-90

Wormuth JH (1998) Workshop deliberations on the Ommastrephidae: A brief history of their systematics and a review of the systematics, distribution and biology of the genera *Martialia* Rochebrune and Mabille, 1889, *Todaropsis* Girard, 1890, *Dosidicus* Steenstrup, 1857, *Hyaloteuthis* Gray, 1849 and *Eucleoteuthis* Berry, 1916. In: Voss NA, Vecchione M, Toll RB, Sweeney MJ (eds) Systematics and Biogeography of Cephalopods. Smith Contr Zool 586:373-383

Wormuth JH, O'Dor RK, Balch N, Dunning MC, Forch EC, Harman RF, Rowell TW (1992) Ommastrephidae. In: Sweeney MJ, Roper FE, Mangold KM, Clarke MR, Boletsky SV (eds) Larval and Juvenile Cephalopods: A Manual for their Identification. Washington, DC: Smithsonian Institution Press, pp.105-120

Xinjun C, Bilin L, Siquan T, Weiguo Q, Xiaohu Z (2007) Fishery biology of purpleback squid, *Sthenoteuthis oualaniensis*, in the northwest Indian Ocean. Fish Res 83:98-104

Yamamoto J, Masuda S, Miyashita K, Uji R, Sakurai Y (2002) Investigation on the early stages of the ommastrephid squid *Todarodes pacificus* near the Oki Islands (Sea of Japan). Bull Mar Sci 73:987-992.

Yamamoto J, Shimura T, Uji R, Masuda S, Watanabe S, Sakurai Y (2007) Vertical distribution of *Todarodes pacificus* (Cephalopoda: Ommastrephidae) paralarvae near the Oki Islands, southwestern Sea of Japan. Mar Biol 153:7-13

Yang WT, Hixon RF, Turk PE, Krejci ME, Hulet WH, Hanlon RT (1986) Growth, behavior and sexual maturation of the market squid, *Loligo opalescens*, cultured throughou the life cycle. Fish Bull 84:771-798

Yatsu A (1999) Morphological and distribution of rhynchoteuthion paralarvae of two ommastrephid squids, *Dosidicus gigas* and *Sthenoteuthis oualaniensis*, collected from eastern tropical Pacific Ocean during 1997 - preliminary report. Report of the Kaiyo Maru cruise for study on the resources of two ommastrephid squids, *Dosidicus gigas* and *Ommastrephes bartramii*, in the Pacific Ocean, during September 11 - December 24. Fisheries Agency of Japan, pp.193-206

Yatsu A, Tafur R, Maravi C (1999) Embryos and rhynchoteuthion paralarvae of the jumbo flying squid *Dosidicus gigas* (Cephalopoda) obtained through artificial fertilization from Peruvian waters. Fish Sci 65:904

Yokawa K (1995) Isozyme comparison of large, medium and small size specimens of *Dosidicus gigas*. Proc Res Conf Squid Resourc Fish Cond Hachinohe, f. y. 1993, 48–52 (in Japanese)

Yokawa K, Jerez B (1999) Estudios preliminares en la estructura genética bioquímica del calamar púrpura (*Sthenoteuthis oualaniensis*) en el Indico norte y el océano

Pacífico sur. In Avances en métodos y tecnología aplicados a la investigación pesquera. Seminario final del proyecto INIDEP-JICA sobre evaluación y monitoreo de recursos pesqueros (1994-1999). Instituto Nacional de Investigación y Desarrollo Pesquero, Mar del Plata, Argentina, pp. 185-187 (In Spanish with English abstract)

Yokobori S, Fukuda N, Nakamura M, Aoyama T, Oshima T (2004) Long term conservation of six duplicated structural genes in cephalopod mitochondrial genomes. Mol Biol Evol 21:2034-2046.

Young RE, Hirota J (1990) Description of *Ommastrephes bartramii* (Cephalopoda: Ommastrephidae) paralarvae with evidence for spawning in Hawaiian waters. Pac Sci 44:71-80

Young RE, Harman RF (1988) 'Larva', 'paralarva', and 'sub-adult' in cephalopod terminology. Malacologia 29:201-207

Young RE, Hirota J (1998) Review of the ecology of *Sthenoteuthis oualaniensis* near the Hawaiian Archipelago. In: Okutani T (ed) Contributed papers to international symposium on large pelagic squids. Tokyo: Japan Marine Fishery Resources Research Center, pp. 131-143

Young RE, Harman RF, Mangold KM (1985a) The common occurrence of oegopsid squid eggs in near-surface oceanic waters. Pac Sci 39:359-366

Young RE, Harman RF, Mangold KM (1985b) The eggs and larvae of *Brachioteuthis* sp. (Cephalopoda: Teuthoidea) from Hawaiian waters. Vie Milieu 35:203-209

Zeidberg LD, Hamner WM (2002) Distribution of squid paralarvae, *Loligo opalescens* (Cephalopoda: Myopsida), in the southern California Bight in the three years following the 1997-1998 El Nino. Mar Biol 141:111-122

Zeidberg LD, Robison BH (2007) Invasive range expansion by the Humboldt squid, *Dosidicus gigas*, in the eastern North Pacific. Proc Nat Acad Sci USA 104:12948–12950

Zuyev G, Nigmatullin C, Chesalin M, Nesis K (2002) Main results of long-term worldwide studies on tropical nektonic oceanic squid genus *Sthenoteuthis*: An overview of the Soviet investigations. Bull Mar Sci 71:1019-1060